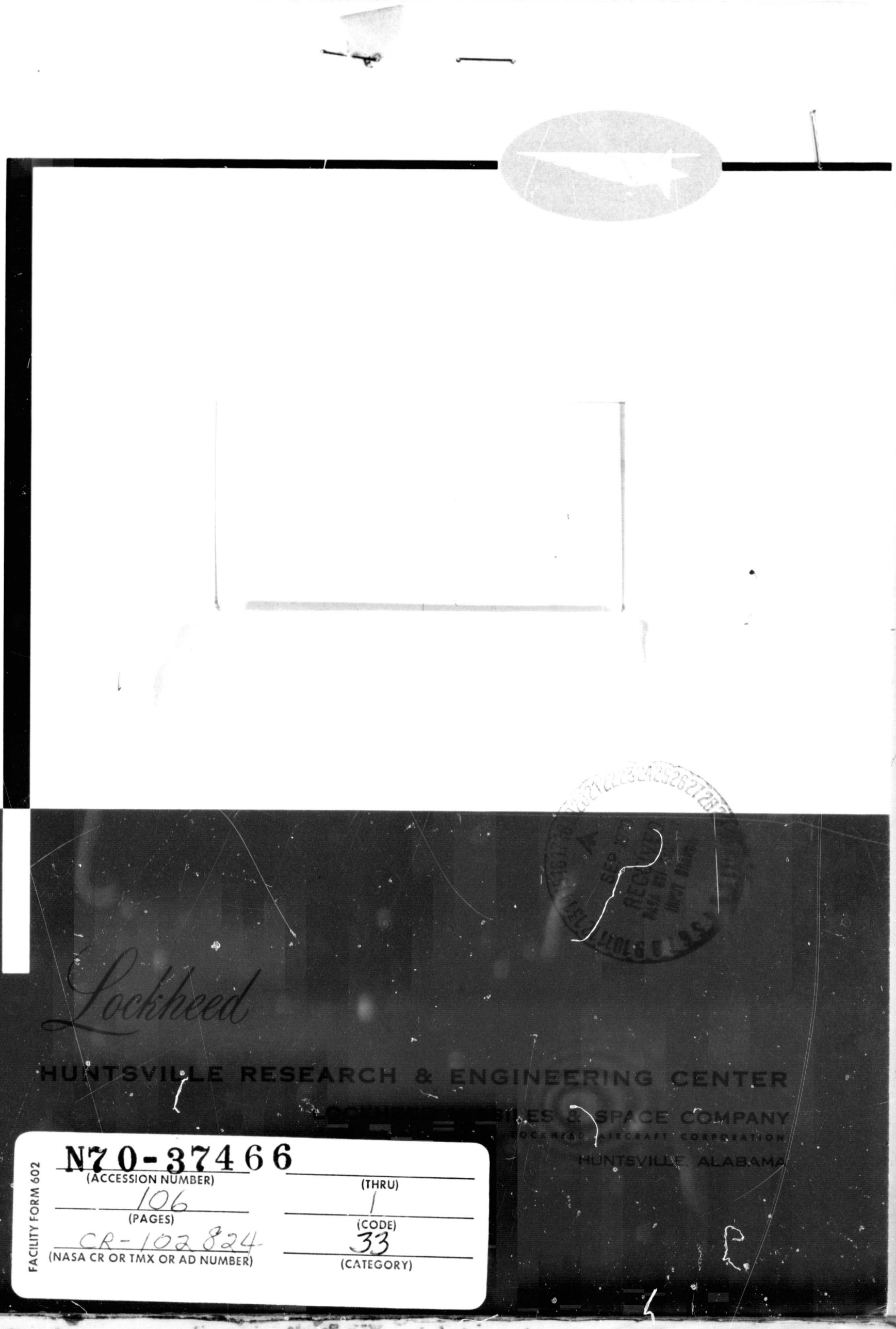

Lockheed

HUNTSVILLE RESEARCH & ENGINEERING CENTER

MISSILES & SPACE COMPANY

LOCKHEED AIRCRAFT CORPORATION

HUNTSVILLE, ALABAMA

HREC-4535-1
LMSC/HREC D162315

LOCKHEED MISSILES & SPACE COMPANY
HUNTSVILLE RESEARCH & ENGINEERING CENTER
HUNTSVILLE RESEARCH PARK
4800 BRADFORD DRIVE, HUNTSVILLE, ALABAMA

STUDY OF CONVECTIVE HEAT TRANSFER TO CONES AND CYLINDERS AT ANGLE OF ATTACK

FINAL REPORT

May 1970

Contract NAS8-24535

Prepared for National Aeronautics and Space Administration
Marshall Space Flight Center, Alabama

by

W. G. Dean
C. J. Wojciechowski
A. G. Bhadsavle

APPROVED: F. K. Lovin

J. K. Lovin, Supervisor
Thermal Environment Section

George D. Reny

G. D. Reny, Manager
Aeromechanics Dept.

George D. Reny
for

J. S. Farrior
Resident Director

FOREWORD

This document presents results of work performed by Lockheed's Huntsville Research & Engineering Center under Contract NAS8-24535, "Angle of Attack Computer Program," for the Aero-Astrodynamics Laboratory of Marshall Space Flight Center. The NASA-Marshall Space Flight Center technical monitors for this contract were Mr. Alan Forney and Mr. Homer B. Wilson, Jr., S&E-AERO-AT.

ACKNOWLEDGEMENT

Acknowledgement is given to Mr. R. J. Prozan of Lockheed/Huntsville for his contribution to this work in the form of the conical flow solution by characteristic theory.

SUMMARY

This report summarizes a study effort directed toward developing handbook-type methods for predicting, without undue conservatism, aerodynamic heating rates to cones and cylinders at angle of attack. Applicability of these isolated body methods to composite body geometries consisting of cones and cylinders is also discussed. Approximate methods for compression and expansion corner regions are also given.

In general, the test data trends were predicted well by several theories. Laminar convective heating rates to cylinders at zero-degree angle of attack were well predicted by flat plate theory. For cylinders at angle of attack, yawed infinite cylinder theory applied. The laminar stagnation line heating rates were well predicted by the method of Kemp, Rose and Detra at the angles of attack less than 30 degrees. The turbulent stagnation line heating rates were well predicted by the method of Beckwith and Gallagher. For cones at angle of attack, the laminar and turbulent heating rates were well predicted by streamline divergence theory. Heating rate distributions off the stagnation line for cones and cylinders are also presented based on available experimental data. Then, using the heat transfer theories that correlated best with the test data, extrapolations to typical boost trajectory flight conditions were made and the results are presented in the form of graphs that can be used for rapid estimates of aerodynamic heating rates. To aid in the calculation of aerodynamic heating rates, the local flowfield properties for cones and cylinders are also presented. Finally two example calculations are made to illustrate the use of the graphs presented.

CONTENTS

NOMENCLATURE

Symbols

CP	pressure coefficient
C_p	specific heat
D	diameter
$\bar{E}$	crossflow momentum thickness ratio
$\bar{E}_L$	defined by Eq. (2.7)
$\bar{E}_T$	defined by Eq. (2.18)
g	gravitational constant
H	total enthalpy
h	static enthalpy
h_c	heat transfer coefficient
k	thermal conductivity
M	Mach number
M_{wt}	molecular weight
N	defined by Eq. (2.5)
Nu	Nusselt number
P	pressure
Pr	Pranti number
q	velocity used in Section 2.3.2
$\dot{q}$	convection heating rate
R	radius of cylinder
r, x	position coordinates used in Section 2.3.2
Re	Reynolds number
St	Stanton number
T	temperature (^oR)
T_r	recovery temperature
u_l	normal component of freestream velocity

NOMENCLATURE (Continued)

Symbols

V	velocity
v_l	tangential component of freestream velocity
X_L	transformed characteristic length (laminar flow)
X_T	transformed characteristic length (turbulent flow)
x	running length; measured along surface
Z	compressibility factor

Greek

α	angle of attack
γ	ratio of specific heats
δ, β	defined in Section 2.3.2
Δ	$\sin^{-1}\left(\frac{1}{M}\right)$, Mach angle
ϵ	attached shock angle
ξ	flow angle
ρ	density
ϕ	angle measured perpendicular to the body axis (ϕ is zero at the stagnation line)
θ	cone half-angle

Subscripts

c	crossflow pressure gradient effects
d	downstream of corner
D	based on diameter
e	boundary layer edge values
L	local conditions
m, c	evaluation at local pressure and mean boundary layer enthalpy
o	evaluated at zero Mach number
R	recovery value
r	Hanks Rho Mu Reference condition (simplified method)
s	stagnation conditions

NOMENCLATURE (Continued)

Subscripts

SL	stagnation line
u	upstream of corner
w	wall conditions
x	based on x
∞	freestream condition ahead of shock
-	right characteristic
+	left characteristic
1	property upstream of shock
2	property downstream of shock

Superscript

*	Eckert Reference Enthalpy condition

Section 1
INTRODUCTION

Plans are being considered to launch several Saturn vehicles into polar orbit from the East Coast. This calls for launch maneuvers which require the vehicle to fly at angles of attack of up to approximately 50 degrees. Because Saturn vehicles were not originally analyzed for the thermal environment created by these maneuvers, a reevaluation of the ascent phase heating must be made. There are at present, however, no completely effective means to predict induced aerodynamic heating at these large angles of attack. As a result, extremely conservative assumptions must be made which will result in excessive weight and cost penalties. It is therefore expedient that techniques be developed to predict these heating rates as accurately as possible at large angles of attack.

In addition to flying the Saturn vehicle, NASA is currently involved with the development of a reusable Space Shuttle vehicle. The results of the efforts presented herein are also directly applicable to determining heating to various areas of the Shuttle vehicle. These areas include: (1) swept wing leading edges; (2) swept fin leading edges; (3) centerline of round bottom delta wings at angle of attack; and (4) bottom centerline of cylindrical fuselages.

The following sections present a technical discussion of the work done under this contract. First, a discussion of the acquisition, reduction, and correlation of the test data is given. Next, results of the reductions and correlations are given. This is followed with the design curves for application of these results to flight heating calculations.

Section 2
TECHNICAL DISCUSSION

Discussed in this section are the sources of test data and methods used in the data correlations, the theoretical methods used for comparision with test data, and the methods used to calculate the local flowfield properties.

It is evident that many sources of data exist in the literature. However, when conducting data correlations one has to be very selective in the choice of data used in order to isolate the various effects on heat transfer such as Reynolds number, Mach number, nose bluntness, angle of attack, wall temperature, compression and expansion corners, and other pressure gradient effects such as might exist in some test facilities. One also has to look at the accuracy of the instrumentation used to obtain the test data.

To provide meaningful insight into the effects of some of the above variables on heat transfer, several convective heat transfer theories were investigated. Some of the theories were programmed and their results were compared with the data. The theories that correlated best were then used to provide extrapolations of the existing data to provide the "best" estimate of the aerodynamic heating environment expected during a typical boost trajectory. The theories were applied only to the stagnation line. The heating rate distributions off the stagnation line were obtained from actual test data and as such are limited in their applicability to conditions other than the test conditions.

The local flowfield properties were needed to perform the data correlations. The method used in the literature for presenting the test data in many cases varied from source to source even for the same type bodies. It was decided in the course of this work to use two standard methods, one for

cones and another for cylinders. The flowfield methods used in this work are documented in Section 2.3 and flowfield results for a variety of flight conditions are presented in Section 4.

2.1 ACQUISITION OF TEST DATA

Data were obtained from numerous sources (Refs. 1 through 11). Cylinder test data correlations were made using both local and freestream flow properties for yawed cylinders. The method used to obtain the local flow properties for cylinders is discussed in Section 2.3. Since there was no apparent gain in accuracy and elimination of data scatter to be gained using local flow properties all the cylinder data correlations are presented in Section 3.1 using freestream properties.

Data correlations for cones were also reduced using both local and freestream properties. Since much less data scatter was evident using the local flow properties, the results are presented in this form. For cones at angle of attack the equivalent cone concept was used to obtain local flow properties along the most windward (stagnation) streamline. The numerical solution used for obtaining the conical flow properties is presented in Section 2.3.

Numerous other reports contained test data that were reviewed but were rejected for various reasons. Some of the reasons for rejecting them were: (1) insufficient data on test conditions; (2) uncertainty in methods used to obtain local flow properties in reducing data presentation; (3) abscence of other pertinent parameters needed for data correlations; (4) uncertainty in air properties used, i.e., conductivity and viscosity; (5) data were not applicable (not isolated body data); and (6) data were not clearly laminar or turbulent, but apparently transitional.

2.2 THEORETICAL CONVECTIVE HEAT TRANSFER METHODS

The boundary layer on axisymmetric bodies at angle of attack is three-dimensional. Solution of the general three-dimensional boundary layer equations was not within the scope of this contract and, therefore, approximate techniques were used to provide first-order corrections for the effects of crossflow.

2.2.1 Cones

Several methods were tried and the method ultimately selected to calculate the convective heating rates along the most windward streamline on cones was based on Streamline Divergence theory as first proposed by Vaglio-Laurin in Refs. 12 and 13. Since Vaglio-Laurin's initial work, many engineers have used the Streamline Divergence method with numerous modifications. The method used here is still another modification. The modification was necessary only for the laminar boundary layer case in order to obtain good correlations at angle of attack.

The basic idea of the Streamline Divergence method is relatively straightforward and is a natural continuation of the axisymmetric flat plate analysis. As is known, axisymmetric bodies at zero-degree angle of attack have been analyzed successfully by two-dimensional methods with the introduction of various characteristic length transformations. In these transformations, the local normal radius of curvature of the body is the major contributing factor to the "stretched" characteristic length used in the heating equations. This arises from the momentum change in the boundary layer due to the spreading effect as it moves around the axisymmetric body. When the non-axisymmetric body is considered, or vehicle at an angle of attack in this case, the momentum change is no longer about the normal curvature of the axisymmetric surface, but is along the curvature of the local fluid streamline. The corresponding length transformation was calculated in this work for both laminar and turbulent flow along the stagnation (most windward) streamlines.

The Streamline Divergence method used to evaluate this transform is explained in the following sections.

- Laminar Cones

The basic task of the Streamline Divergence method is to provide a transformed characteristic length along the streamlines which will modify the familiar zero pressure gradient (flat plate) heating rate equations into relationships that will handle flows with both circumferential and longitudinal pressure gradients. To do this we start with the following equation for zero pressure gradient flow fields:

$$\dot{q} = 0.332 (H_r - h_w) Pr^{*-2/3} \left(\frac{V_e}{X_L}\right)^{1/2} (\rho^* \mu^*)^{1/2} \qquad (2.1)$$

This is the Blasius incompressible solution modified for compressible flow by the introduction of Eckert reference condition fluid properties, denoted by the asterisk (*).

In addition, for comparison purposes, the following flat plate heating rate equation was also used,

$$\dot{q} = 0.332 (H_r - h_w) Pr_r^{-2/3} \left(\frac{V_e}{X_L}\right)^{1/2} (\rho_r \mu_r)^{1/2} \qquad (2.2)$$

This again is the Blasius incompressible solution modified for compressible flow by the introduction of reference conditions based on Hanks Rho-Mu method (Ref. 14).

For an unyawed sharp cone in laminar flow, the solution for the characteristic length X_L is

$$X_L = \frac{x}{3} \tag{2.3}$$

For the stagnation line of a yawed sharp cone (negligible streamwise pressure gradients), the solution for the transformed characteristic length X_L is

$$X_L = \frac{x}{1+2(1+N\,\bar{E}_L)} \tag{2.4}$$

where the parameters N and $\bar{E}_L$ are calculated as follows (Ref. 14). The solution for the parameter N was obtained from the solution of the cross-flow momentum equation for inviscid flow along with certain simplifying assumptions which appear valid along the stagnation line. The result is,

$$N = \frac{1}{2}\left[1 + \sqrt{1 - \frac{4}{\sin^2\theta}\,\frac{d^2P}{d\phi}}\,\right] \tag{2.5}$$

where

$$\frac{d^2P}{d\phi} = -2\,\frac{P_e}{\rho_e V_e^{\,2}}\left[\frac{\sin\alpha\cos\theta}{\sin(\alpha+\theta)}\right]\left(1 - \frac{P_\infty}{P_e}\right) \tag{2.6}$$

The quantity $\bar{E}_L$ is defined as

$$\bar{E}_L = 1 + 0.718\,(\sqrt{1+F_{\Sigma,c}} - 1)\,(2\,\Sigma_c)^{\exp K} \tag{2.7}$$

where

$$\exp K = 0 \text{ when } N \leq 0.05 \text{ and } 0.99 \leq N \leq 1.01$$

$$\exp K = -0.194 \exp \left[- 2/3\ N(N-1) \right] \text{ when } 0.05 < N < 0.99$$

$$\exp K = 0.194 \exp \left[- 2/3\ (N-1) \right] \text{ when } N > 1.01$$

and

$$F_{\Sigma, c} = \frac{\Sigma_c - 0.294}{0.402}\ Pr_r^{0.355} \tag{2.8}$$

$$\Sigma_c = \frac{(ZT)_{m,c}}{(ZT)_{e,SL}} \tag{2.9}$$

The quantity $(ZT)_{m,c}$ is evaluated at the local pressure and mean boundary layer enthalpy. Equations (2.7) through (2.9) were developed in Ref. 14 on the basis of providing the best fit to exact similiar solutions.

- Turbulent Yawed Cones

For turbulent flow over cones, three heating rate methods were selected for comparison with test data. They are: (1) the Eckert Reference Enthalpy method using the Blasius skin friction law, i.e.,

$$\dot{q} = \frac{0.0296}{Pr^{*0.6667}}\ (\rho^* V_e)^{0.8} \left(\frac{\mu^*}{X_T} \right)^{0.2} (H_r - h_w) \tag{2.10}$$

(2) the Eckert Reference Enthalpy method using the Shultz-Grunow skin friction law, i.e.,

$$\dot{q} = \frac{0.185\ \rho^* V_e}{Pr^{*0.6667} \left[A\log(Re^*) \right]^{2.584}} (H_r - h_w) \tag{2.11}$$

where

$$Re^* = \frac{\rho^* V_e X_T}{\mu^*} \tag{2.12}$$

and finally (3) the Hanks Rho-Mu method, also using the Shultz-Grunow skin friction law, i.e.,

$$\dot{q} = \frac{0.185\,\rho_r V_e}{Pr_r^{0.6667}\left[\text{Alog}\,(Re_r + 3000)\right]^{2.584}}\left(\frac{\mu_r}{\mu_o}\right)(H_R - h_w) \tag{2.13}$$

where,

$$Re_r = \frac{\rho_r \mu_r V_e X_T}{\mu_o^2} \tag{2.14}$$

and

$$\mu_o = \mu_r\left(\frac{H_e}{h_r}\right)^{3/2}\frac{\left|(ZT)_r + 200\right|}{\left[(ZT)_T\left(\frac{H_e}{h_r}\right) + 200\right]} \tag{2.15}$$

For the stagnation line of an unyawed sharp cone in turbulent flow, the solution for the transformed characteristic length X_T is,

$$X_T = \left(\frac{4}{9}\right) x \tag{2.16}$$

For the stagnation line of a yawed sharp cone in turbulent flow, the solution for the transformed characteristic length X_T is

$$X_T = \frac{x}{1 + \frac{5}{4}(1 + \bar{E}_T N)} \tag{2.17}$$

where N is evaluated using Eq. (2.5). The parameter $\bar{E}_T$ is evaluated in Ref. 14 as follows,

$$\bar{E}_T = 1 + 0.55 \left(\sqrt{1 + F_{\Sigma, c, o}} - 1\right) (2 \Sigma_{c, o})^{\exp K}$$

$$\left[\frac{\bar{E}_L}{1 + 0.718 \left(\sqrt{1 + F_{\Sigma, c, o}} - 1\right) (2 \Sigma_{c, o})^{\exp K}}\right]^4 \tag{2.18}$$

where the quantities $F_{\Sigma, c, o}$ and $\Sigma_{c, o}$ are evaluated using Eqs. (2.8) and (2.9), respectively, except that the Mach number is now zero, therefore the mean boundary layer enthalpy is now

$$h_{m, o} = 0.5 (h_e + h_w) \tag{2.19}$$

2.2.2 Cylinders

The methods used to calculate the three-dimensional boundary layer heat transfer on the stagnation line of yawed infinite cylinders are based on the Crossflow Approximation method. This method employs existing similiar solutions to the boundary layer equation.

- Laminar Yawed Cylinders

Two stagnation line laminar heat transfer methods were programmed for comparison with the test data. One method used the correlations of Kemp, Rose and Detra (Ref. 15), and the other used Beckwith's yawed cylinder method (Ref. 16). The stagnation line convective heating rates for equilibrium air was analyzed in Ref. 15 . The resulting heat transfer correlation obtained was

$$\dot{q} = \frac{0.565}{Pr_w^{0.6}} \sqrt{\rho_w \mu_w \frac{dV}{dR}} \left(\frac{\rho_e \mu_e}{\rho_w \mu_w}\right)^{0.44} (H_R - h_w) \qquad (2.20)$$

If the crossflow velocity component is supersonic, then the velocity gradient is computed from Newtonian theory, i.e.,

$$\frac{dV}{dR} = \frac{1}{R} \sqrt{2g\left(\frac{P_e - P_\infty}{\rho_e}\right)} \qquad (2.21)$$

If the crossflow velocity component is subsonic, then the velocity gradient is computed by the following equation from Ref. 16:

$$\frac{dV}{dR} = \frac{V_\infty \sin\alpha}{2R} \left[5.1 \cos(M_\infty \sin\alpha) - 1.6\right] \qquad (2.22)$$

The other laminar heat transfer solution for the stagnation line of a yawed infinite cylinder is that of Beckwith (Ref. 16), i.e.,

$$\dot{q} = 0.354 \sqrt{\frac{\rho_e \mu_e}{\sin\alpha} \frac{dV}{dR}} \left(\frac{\mu_w T_e}{\mu_e T_w}\right)^{0.06} \frac{k_\infty}{\mu_\infty} (T_R - t_w) \qquad (2.23)$$

Equation (2.23) is based on exact boundary layer solutions for constant specific heat and a constant Prandtl number equal to 0.7. The velocity gradient is calculated using either Eq. (2.21) or (2.22).

- Turbulent Yawed Cylinders

The turbulent yawed cylinder stagnation line heat transfer method used was that presented by Beckwith and Gallagher in Ref. 8, i.e.,

$$\dot{q} = 0.0288 \left(\frac{V_\infty \cos\alpha}{\mu_s}\right)^{0.6} \left(\frac{dV}{dR}\right)^{0.2} (\rho_w \mu_w)^{0.8} \frac{k_\infty}{\mu_\infty} (T_R - T_w) \qquad (2.24)$$

2.3 LOCAL FLOWFIELD CALCULATION METHODS

This section presents methods used to calculate the local flowfield properties on cones and cylinders. Inviscid analysis methods were used, and no boundary layer interactions were considered.

2.3.1 Yawed Cylinder Flow Fields

The local flowfield at the stagnation line of a yawed infinite cylinder is computed as the real gas stagnation conditions behind a normal shock wave. The real gas (equilibrium air) properties are computed using the method of Hansen (Ref. 17). The normal shock calculation used is similiar to that presented in Ref. 18. Basically the solution involves the solution of the continuity, momentum, and energy equations plus an equation of state which includes compressibility effects. The following sketch shows the flowfield geometry.

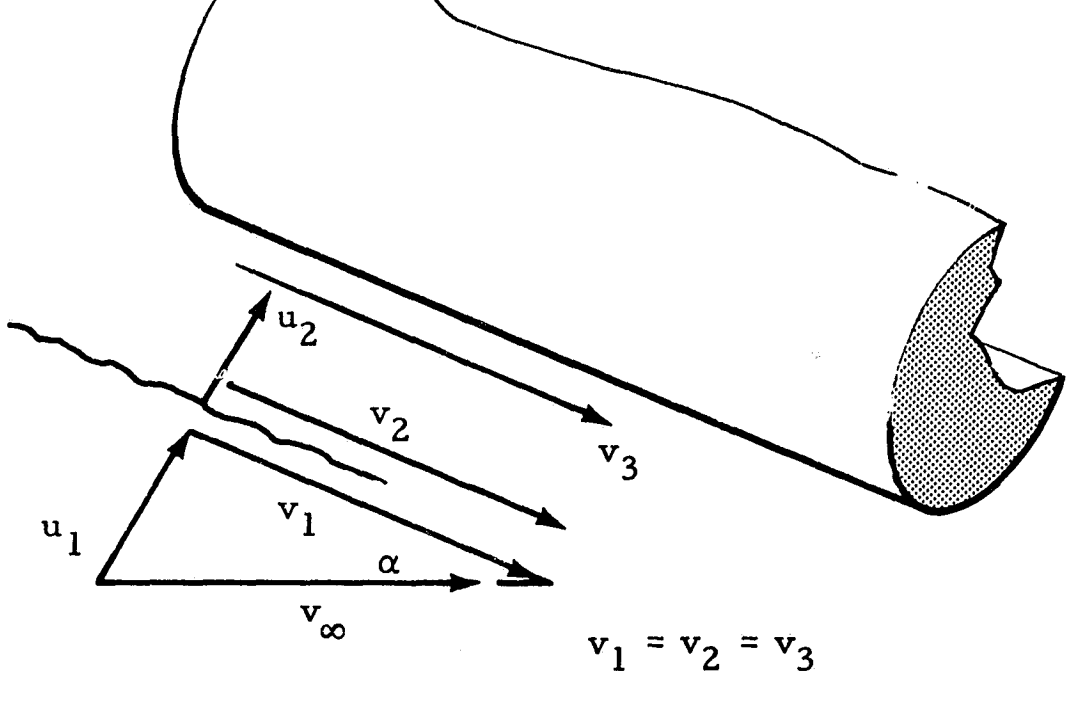

$$v_1 = v_2 = v_3 \qquad (2.25)$$

The pertinent equations are

$$\frac{P_2}{P_1} = 1 + \gamma_\infty M_1^2 \left[1 - \left(\frac{u_2}{u_1}\right)\right]^2 \qquad \text{Conservation of Momentum} \qquad (2.26)$$

$$\frac{h_2}{h_1} = 1 + \frac{\gamma_\infty - 1}{2} M_1^2 \left[1 - \left(\frac{u_2}{u_1}\right)^2\right] \qquad \text{Conservation of Energy} \qquad (2.27)$$

$$\rho_1 \mu_1 = \rho_2 \mu_2 \qquad \text{Continuity} \qquad (2.28)$$

$$P_2 = \frac{R}{M_{wt}} \rho_2 T_2 Z_2 \qquad \text{Equation of State} \qquad (2.29)$$

An iteration procedure is used to obtain the solution to the preceding set of equations. After the normal shock solution is obtained, the flow is isentropically decelerated such that u_2 equals zero with a corresponding increase in P_2 and T_2.

2.3.2 Cone Flow Fields

The method used to solve the conical flow field is the method of Ref. 19. For cones at angle of attack the equivalent cone concept was used to obtain conical flow solutions along the most windward streamline. The method is well suited to treat ideal, frozen, or equilibrium reacting gas mixtures. The resultant equations require a double-iterative solution rather than an iterative-integral solution such as the Taylor-Maccoll method.

Consider a right circular cone immersed in a supersonic flow (Fig. 2-1). The flow downstream of the shock wave is irrotational for conical flow. If the Mach number downstream of the shock wave is greater than unity, the characteristic equations are real. They are:

$$\frac{dr}{dx} = \tan(\xi \mp \Delta) \tag{2.30}$$

$$d\left(\xi \mp \cot\Delta \frac{dq}{q} \mp \frac{\sin\Delta \sin\xi}{\sin(\xi \mp \Delta)} \left(\frac{dr}{r}\right)\right) = 0 \tag{2.31}$$

Along the right (-) characteristic the finite difference analog of Eq. (2.32) is written;

$$\xi_2 - \theta + \cot\Delta \frac{(q_2 - q_w)}{\bar{q}} - \frac{\sin\bar{\Delta} \sin\bar{\xi}}{\sin(\bar{\xi}\,\bar{\Delta})} \left(\frac{dr}{r}\right)_- = 0 \tag{2.32}$$

while along the left (+) characteristic

$$\xi_2 - \theta - \cot\Delta \frac{(q_2 - q_w)}{\bar{q}} + \frac{\sin\bar{\Delta}\,\sin\bar{\xi}}{\sin(\bar{\xi} - \bar{\Delta})} \left(\frac{dr}{r}\right)_+ = 0 \qquad (2.33)$$

where the barred values are average between the shock and the cone surface. With the aid of the physical characteristic equation (2.30) and geometry the axisymmetric term is found;

$$\left(\frac{dr}{r}\right)_{\bar{+}} = 2\frac{(1-\delta)}{(1+\delta)} \qquad (2.34)$$

where $\delta = \dfrac{\cos(\epsilon+\beta)\,\sin\sigma}{\cos(\sigma+\beta)\,\sin\epsilon}$

and where $\beta\bar{+} = \tan^{-1}\left\{\cot(\bar{\xi}\ \bar{+}\ \bar{\Delta})\right\}$

The final relations necessary for the solution are provided by oblique shock theory. The relations define the properties behind the shock in terms of the shock angle (ϵ) for a given freestream condition. The solution is obtained by choosing a shock angle, solving the oblique shock relations, and, with this knowledge, finding q_w in Eq. (2.33). Eq. (2.34) must also be satisfied and is used to gauge the inaccuracy of the shock angle. An iterative solution driving the left-hand side of Eq. (2.33) to zero produces the desired result.

The distinction between ideal, frozen, or equilibrium solutions comes into play only in the oblique shock solution and the relationship between q and Δ.

To check the accuracy of the approximate treatment, a comparison was made against the conical flow tables given in Ref. 20. An examination of the results presented in Fig. 2-2 reveals excellent agreement over the entire range of approach Mach numbers and cone semi-vertex angles.

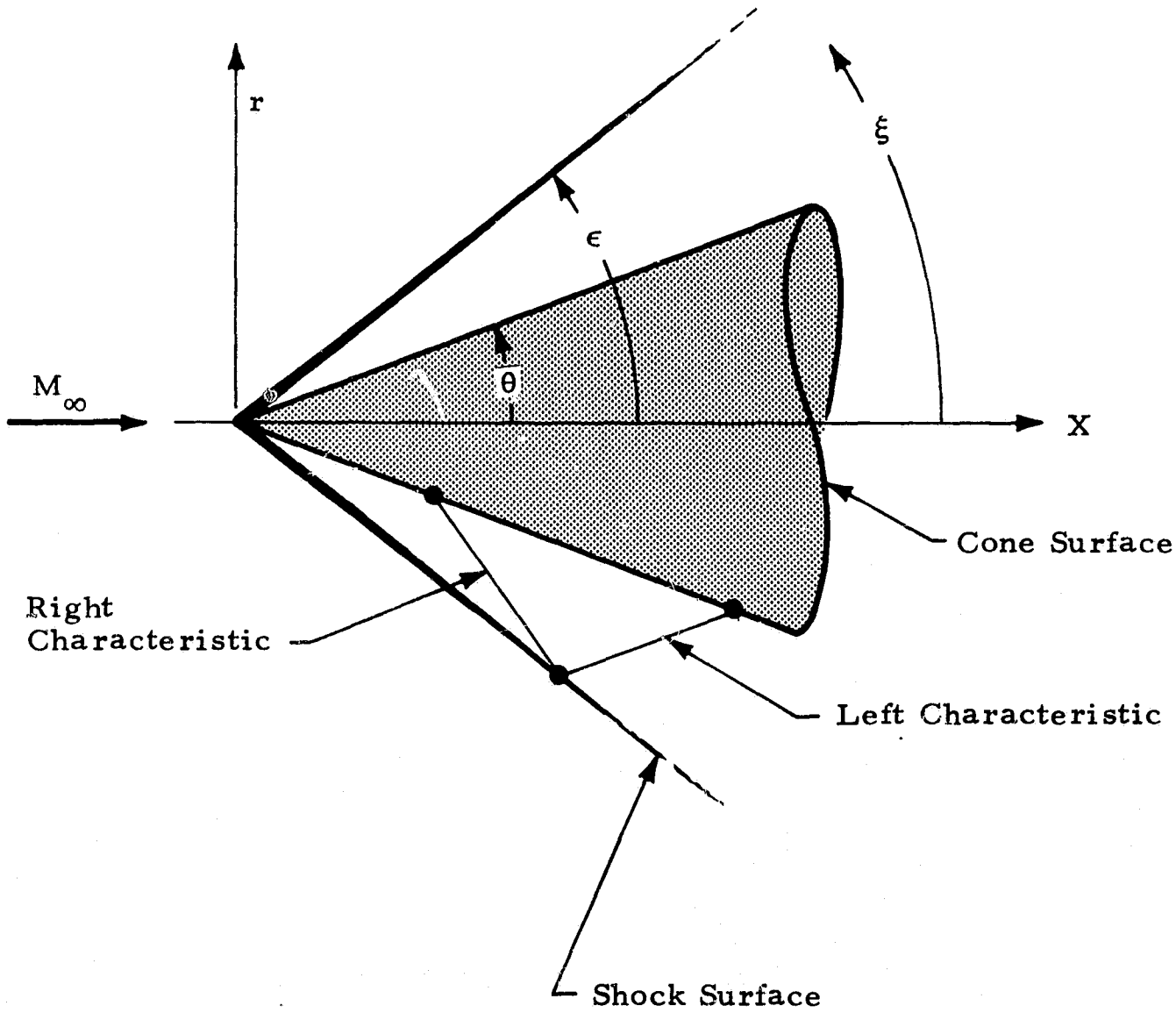

Fig. 2-1 - Right Circular Cone Immersed in a Supersonic Flow

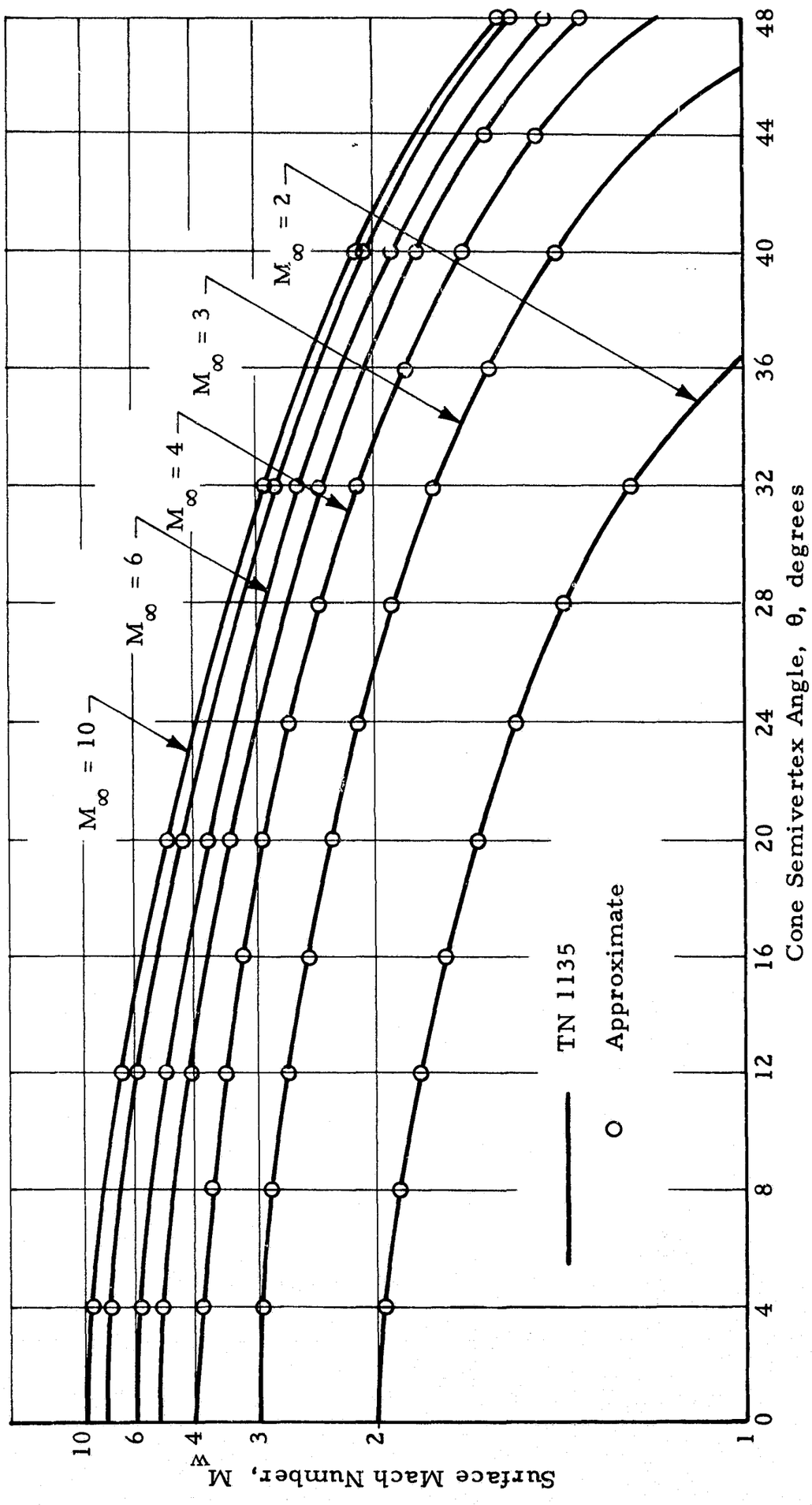

Fig. 2-2 - Variation of Mach Number at the Surface of a Cone with Cone Semivertex Angle for Various Upstream Mach Numbers

Section 3
RESULTS

Heating rate data correlations for cylinders and cones in laminar and turbulent flow are presented in this section. Also presented for comparison with the data are results of the theoretical investigations conducted to provide a meaningful extrapolation of the data to flight conditions.

3.1 YAWED AND UNYAWED CYLINDERS

Yawed cylinder data correlations were made using the following four methods, i.e.,

Nu_L versus Re_L

St_L versus Re_L

Nu_∞ versus Re_∞

St_∞ versus Re_∞

From the observed trends of the data, there was no advantage seen in correlating the data in forms other than Nu_∞ versus Re_∞; therefore, this is the only form presented. Cylinder test data were obtained from numerous sources for laminar flow. However, for turbulent flow, very little test data were available.

3.1.1 Laminar Results

The resulting data correlation for laminar flow over cylinders at zero degree angle of attack is shown in Fig. 3-1. Sources of the data are noted on the figure. As the figure shows, the data correlate well with the Blasuis flat plate results, namely

$$Nu = 0.332 \frac{\sqrt{Re}}{Pr^{0.4}} .$$

Figure 3-2 shows the Stanton number versus Reynolds number correlation for the same data. Fairly good agreement is also noted with the Blasius flat plate results. Figures 3-3 through 3-6 show the freestream Nusselt number versus freestream Reynolds number correlations for angles of attack of 10, 20, 30, 40 and 50 degrees. Again the sources of the selected data are noted on the figures. Also shown are two yawed infinite cylinder theories. Beckwith's laminar cylinder theory, Ref. 16 is shown as the dashed line, whereas the data correlation theory of Ref. 15-Kemp, Rose and Detra, is shown as the solid line. The theory of Kemp, Rose and Detra is shown to correlate best at all angles of attack except 50 degrees, where the difference between the two theories is small. Referring to the figures, Mach number effects are evident.

3.1.2 Turbulent Results

As mentioned earlier, the available test data for turbulent flow over yawed cylinders was very limited. Figure 3-7 shows the Nusselt number versus Reynolds number data correlation for angles of attack of 30 and 50 degrees. As is evident from the figure, Beckwith's turbulent infinite cylinder theory correlates well with the test data.

3.2 YAWED AND UNYAWED CONES

Cone test data correlations were made using local and freestream flow properties. The local flow properties were calculated using the equivalent cone method. Cone surface pressures predicted using this method for the stagnation line were compared with available test data, and in all cases good agreement was evident. Less data scatter was evident using the local flow properties, therefore only these results are presented.

3.2.1 Laminar Results

Figure 3-8 shows the local Nusselt number versus local Reynolds number data correlation for several cone half angles and Mach numbers, all at zero-degree angle of attack. Note that most of the data are grouped together in a line and correlated well when plotted in this form. The wall temperature-to-total-temperature ratios for the data ranged from 0.2 to 0.5. The Mach number effects (for the tunnel conditions used) were small. The Mach number varies from 2.49 to 10.1. The cone half angle varied from 5 to 25 degrees. However, from a plot such as this, where more than one parameter is changed between sets of data, it is difficult to isolate the individual effects. In Section 4 of this report it is shown that Mach number and cone half angle effects are present and should be considered.

Also shown in Fig. 3-8 are the theoretical results obtained using Eqs. (2.1) and (2.2). There is very little difference between the two theories although Eq. (2.1) tended to predict the data slightly better than Eq. (2.2). Figure 3-9 shows the local Stanton number versus local Reynolds number data correlation. Figures 3-10 through 3-20 shows the data correlations for cones in laminar flow at angles of attack from 5 to 45 degrees. Figures 3-10, 3-12, 3-14, 3-16, 3-18 and 3-20 show that the trend of the data with angle of attack is predicted quite well using Streamline Divergence theory. However, to obtain the theoretical variations of heating rates with angle of attack, Eq. (2.4) was not used per se. Using Eq. (2.4) per se, the theoretical results showed a huge increase in heating rate as the angle of attack

increased from zero degrees. This resulted in theoretical results approximately 70% higher than the data at all angles of attack. However, the theoretical results showed that the proper variation with angle of attack could be predicted by Eq. (2.4) if this initial discrepancy could be corrected. For this reason the following equation for X_L was used and showed good correlations with the data, i.e.,

$$X_{L_\alpha} = X_{L_{\alpha=0\ \mathrm{deg}}} \left(\frac{\dfrac{x}{1+2(1+N\bar{E}_L)_\alpha}}{\dfrac{x}{1+2(1+N\bar{E}_L)_{\alpha=0\ \mathrm{deg}}}} \right) \tag{2.35}$$

where

$$X_{L_{\alpha=0\ \mathrm{deg}}} = \frac{x}{3}$$

The data of Bushnell (Ref. 3) tend to fall below the theoretical results at all angles of attack. This is attributed to the data being taken on a blunt cone, and the method used (in Ref. 3) to obtain the local flow properties for use in reducing the heat transfer data was different than that used in this report. An estimation made to determine the magnitude of the flow property effects showed that the data should be about 15% lower than the theoretical sharp cone results.

3.2.2 Turbulent Results

Figures 3-21 through 3-26 show the turbulent cone data correlations. Turbulent cone data available in the literature were more scarce than laminar cone data. Shown in Fig. 3-21 along with the data correlations are the theoretical results obtained using Eqs. (2.10) and (2.13). The theoretical results obtained using Eq. (2.11) fell between the results obtained using Eqs. (2.10) and (2.13) and in most cases very small differences were observed between

the three theories for the flight conditions investigated. Figure 3-21 shows that the results obtained using Eq. (2.10) tend to correlate best with the test data. It can be seen that the Mach number effects are well predicted by the theories and they are more pronounced for turbulent flow than for laminar flow. The freeflight data of Ref. 7 was predicted well by Eq. (2.10) throughout the portions of the flight envelope where the flow was completely turbulent. From Figs. 3-23 and 3-25 it is evident that the Streamline Divergence theory, Eq. (2.17) predicts the data trend quite well at angle of attack. No problems were encountered using Eq. (2.17) per se as were encountered in the laminar case.

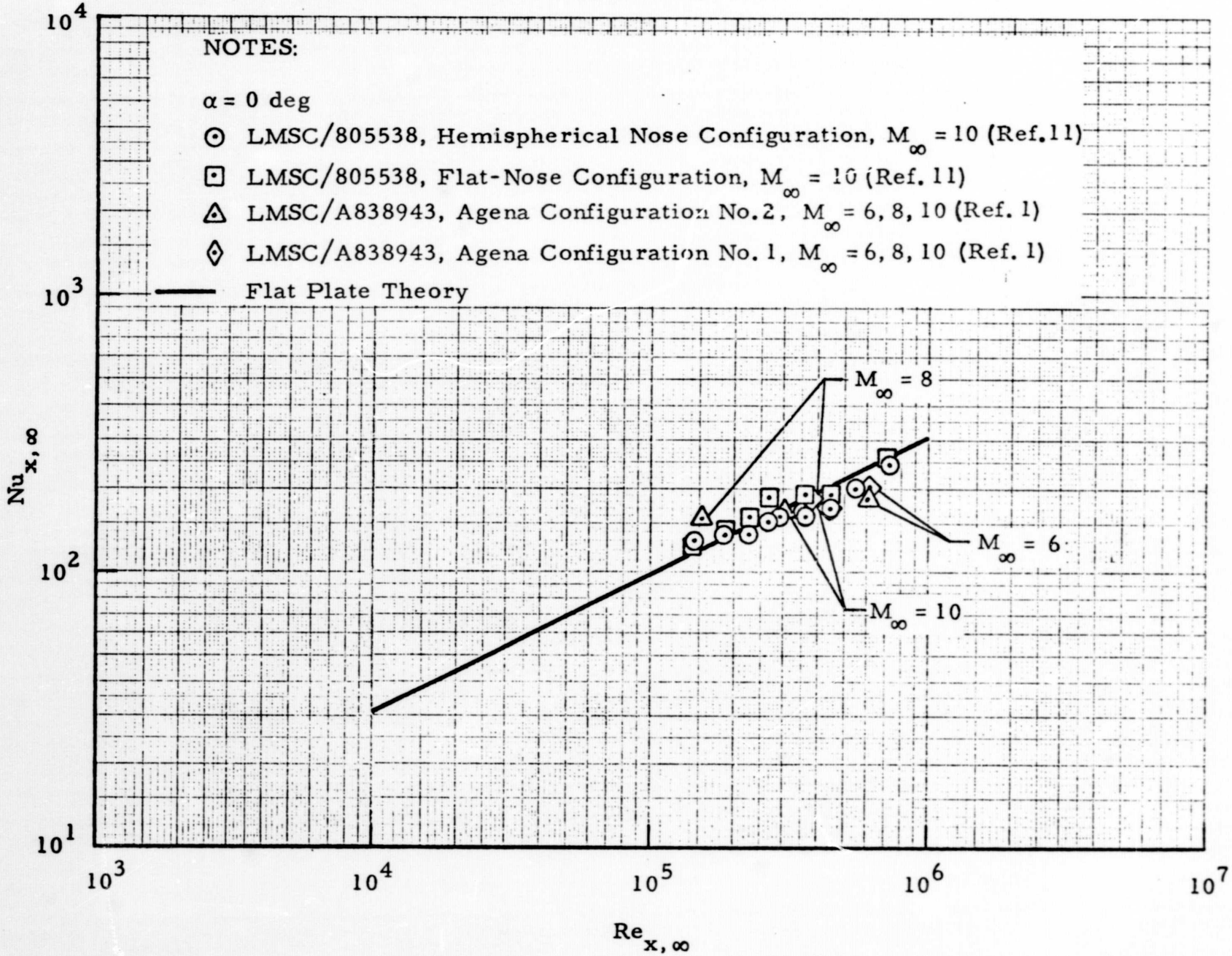

Fig. 3-1 - Freestream Nusselt Number vs Freestream Reynolds Number for Laminar Flow over Cylinder at α = 20 Degrees

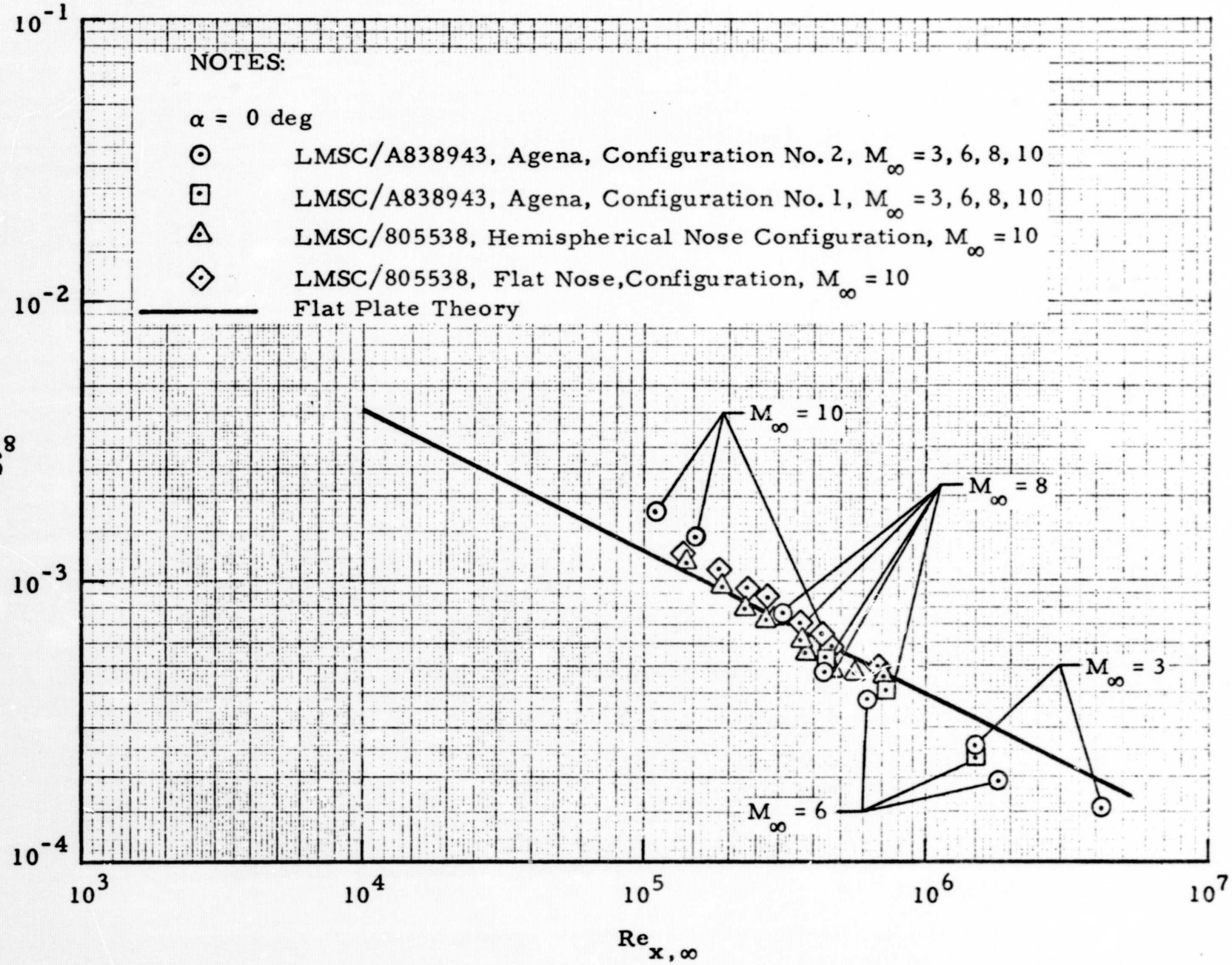

Fig. 3-2 - Freestream Stanton Number vs Freestream Reynolds Number for Laminar Flow over Cylinder at α = 0 Degrees

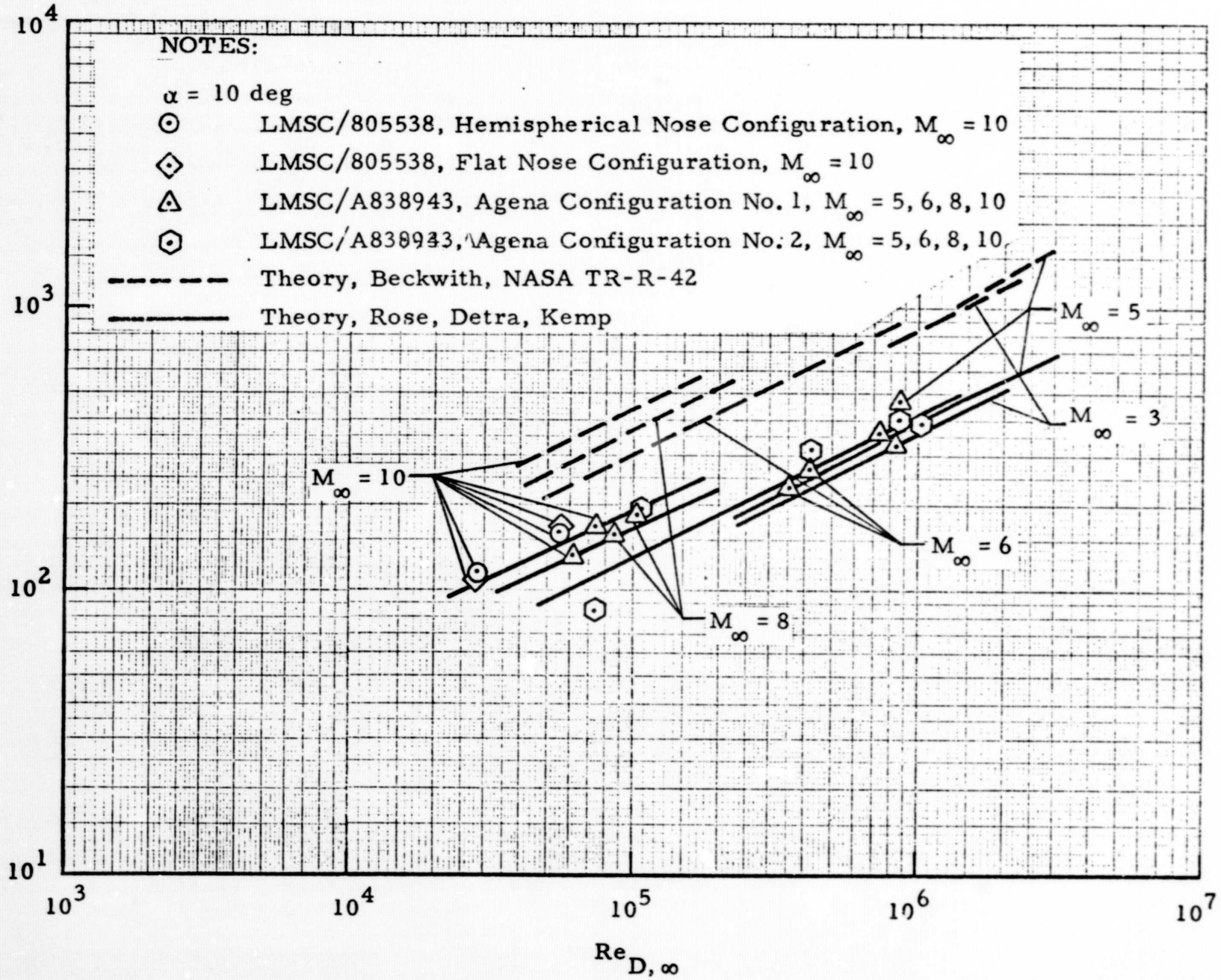

Fig. 3-3 - Freestream Nusselt Number vs Freestream Reynolds Number for Laminar Flow over Cylinders at α = 10 Degrees

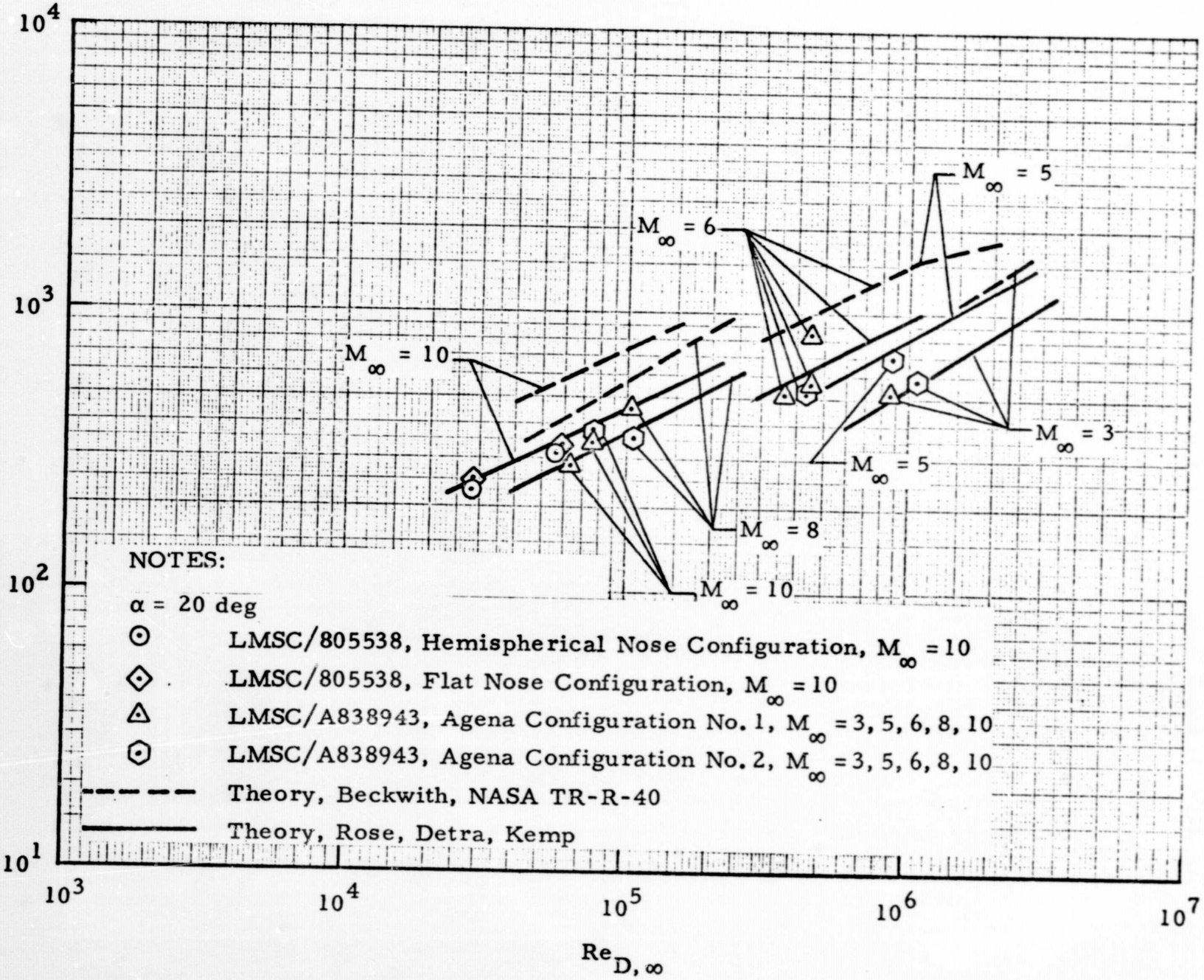

Fig. 3-4 - Freestream Nusselt Number vs Freestream Reynolds Number for Laminar Flow over Cylinders at α = 20 Degrees

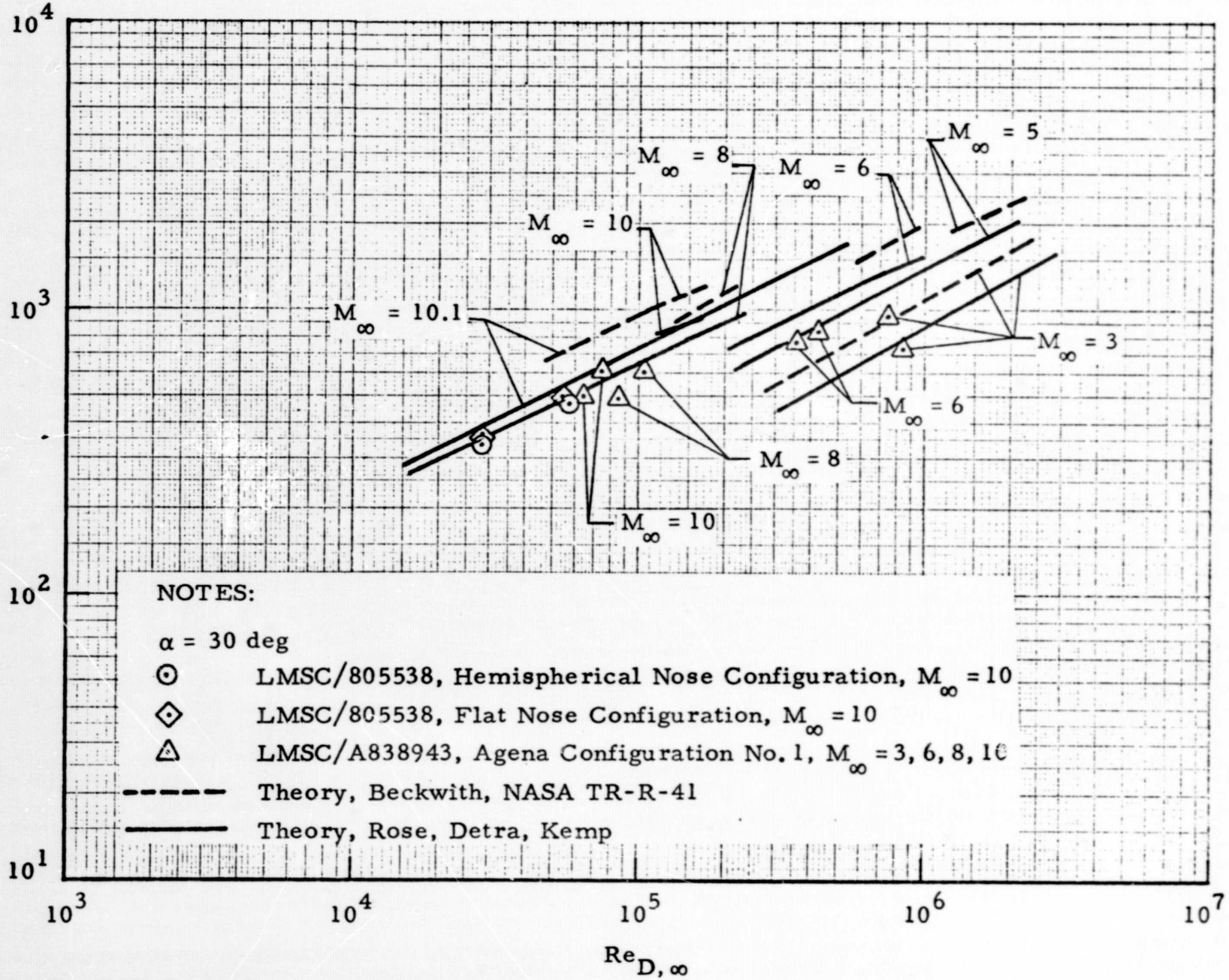

Fig. 3-5 - Freestream Nusselt Number vs Freestream Reynolds Number for Laminar Flow over Cylinders at α = 30 Degrees

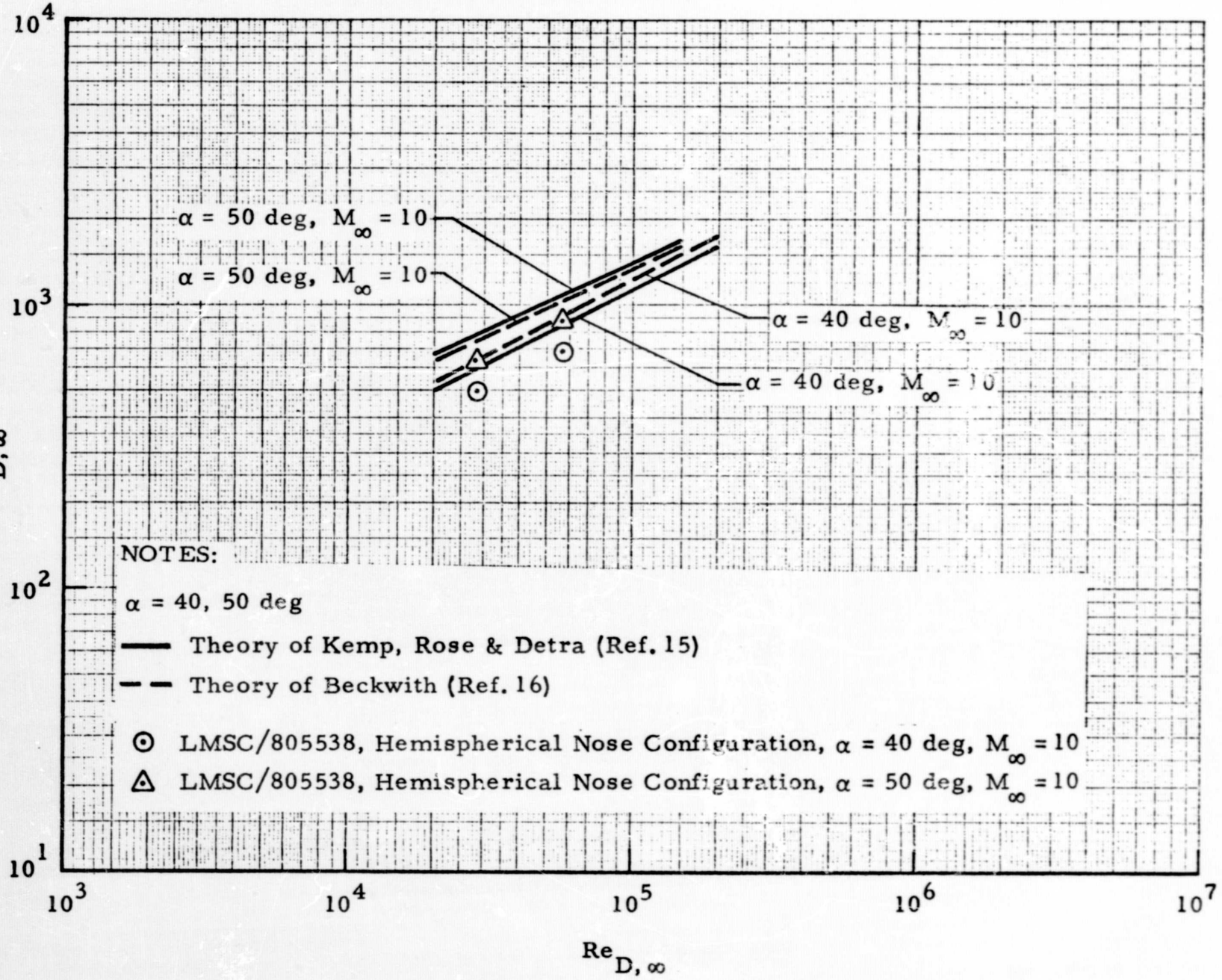

Fig. 3-6 - Freestream Nusselt Number vs Freestream Reynolds Number for Laminar Flow Over Cylinders at α = 40 and 50 Degrees

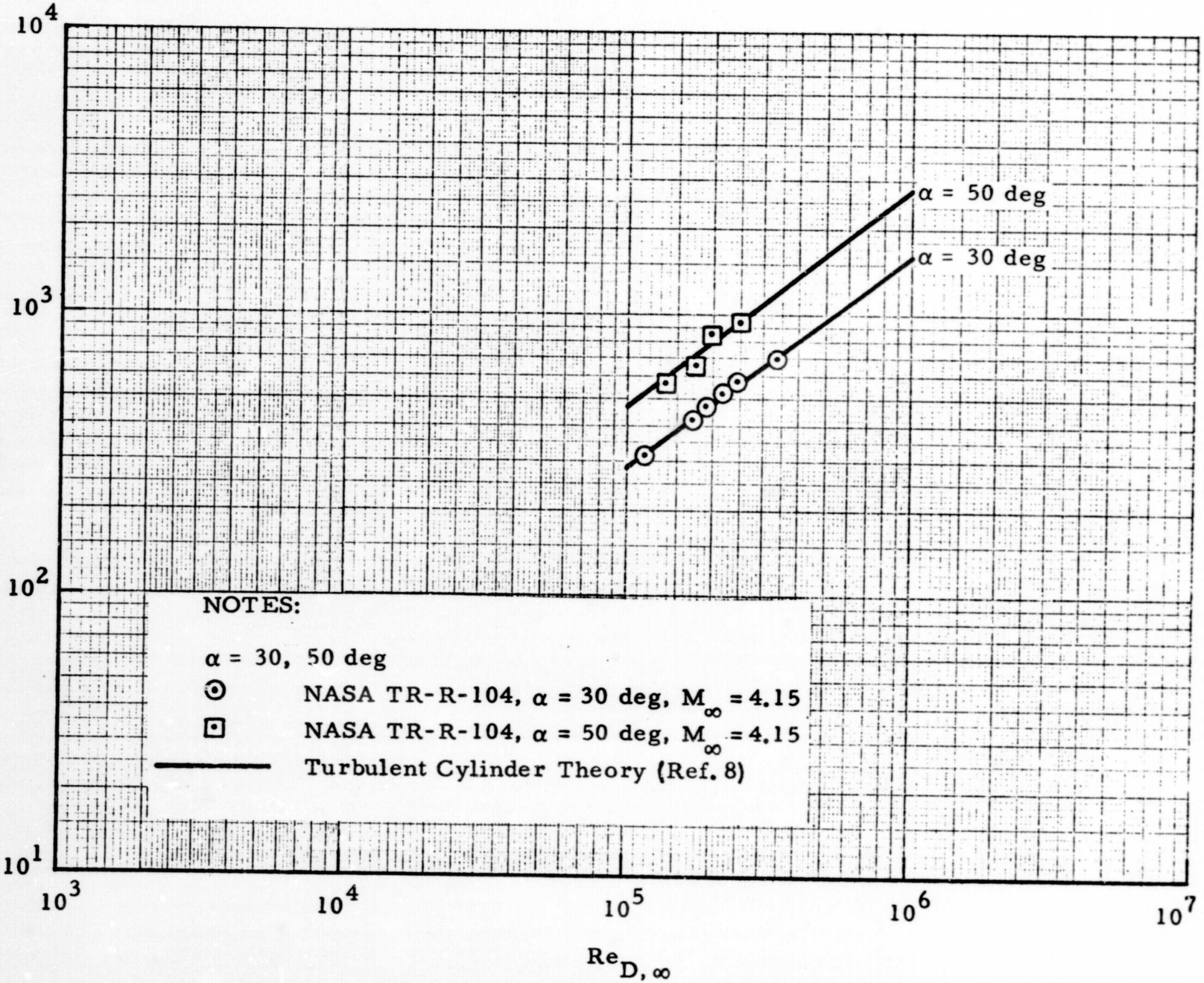

Fig. 3-7 - Freestream Nusselt Number vs Freestream Reynolds Number for Turbulent Flow over Cylinders at α = 30 and 50 Degrees

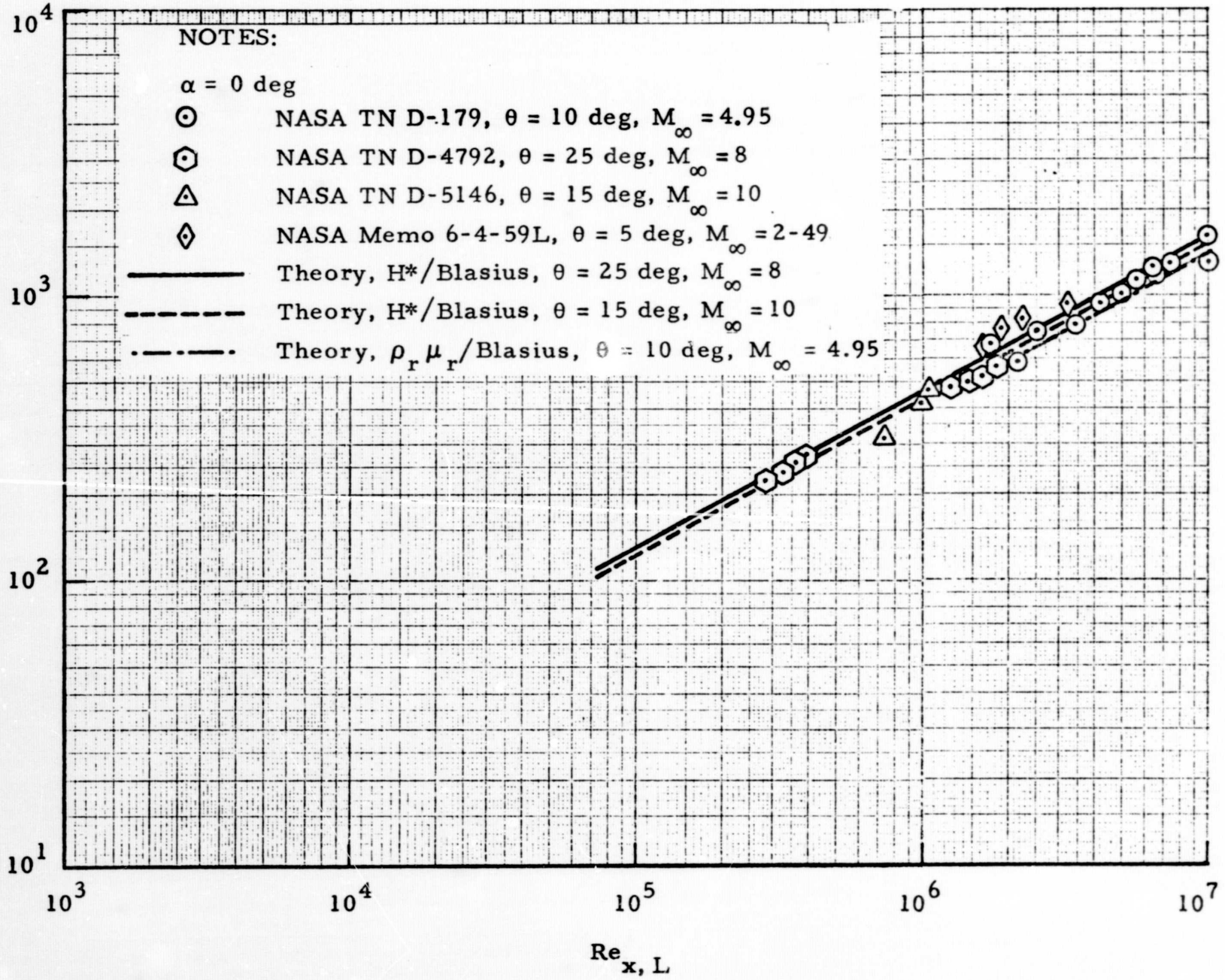

Fig. 3-8 - Local Nusselt Number vs Local Reynolds Number for Laminar Flow over Cones at α = 0 Degrees

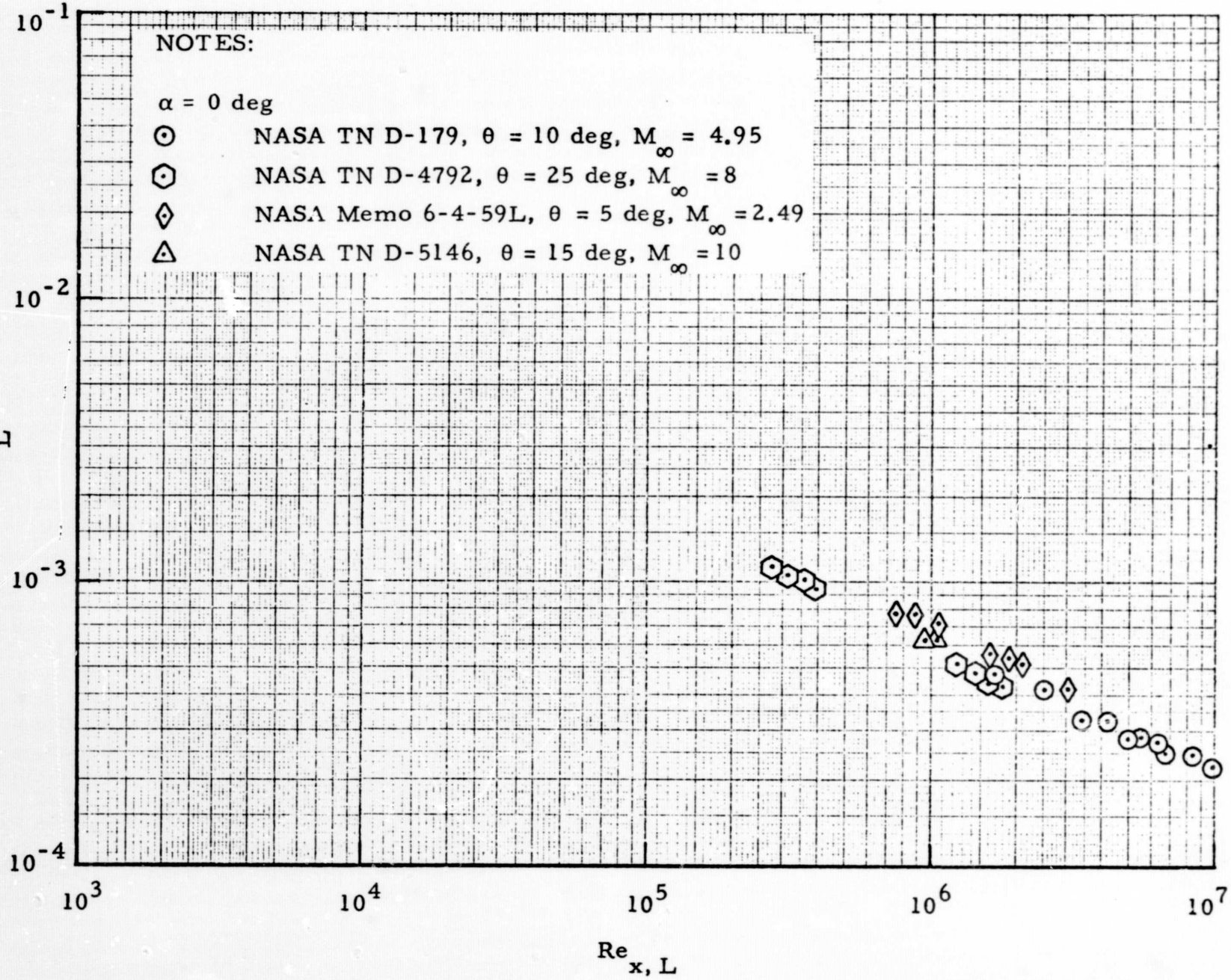

Fig. 3-9 - Local Stanton Number vs Local Reynolds Number for Laminar Flow over Cones at α = 0 Degrees

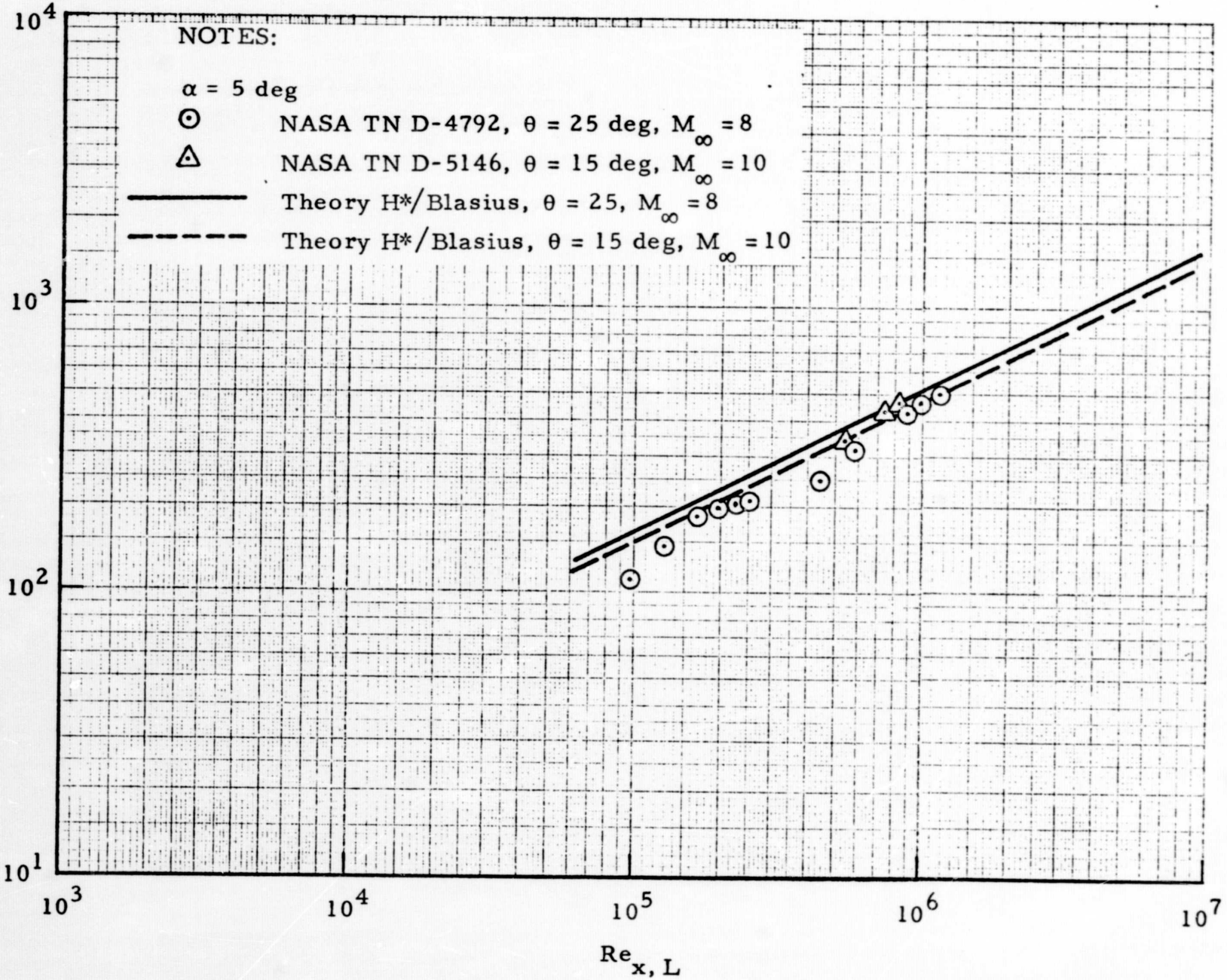

Fig. 3-10 - Local Nusselt Number vs Local Reynolds Number for Laminar Flow over Cones at α = 5 Degrees

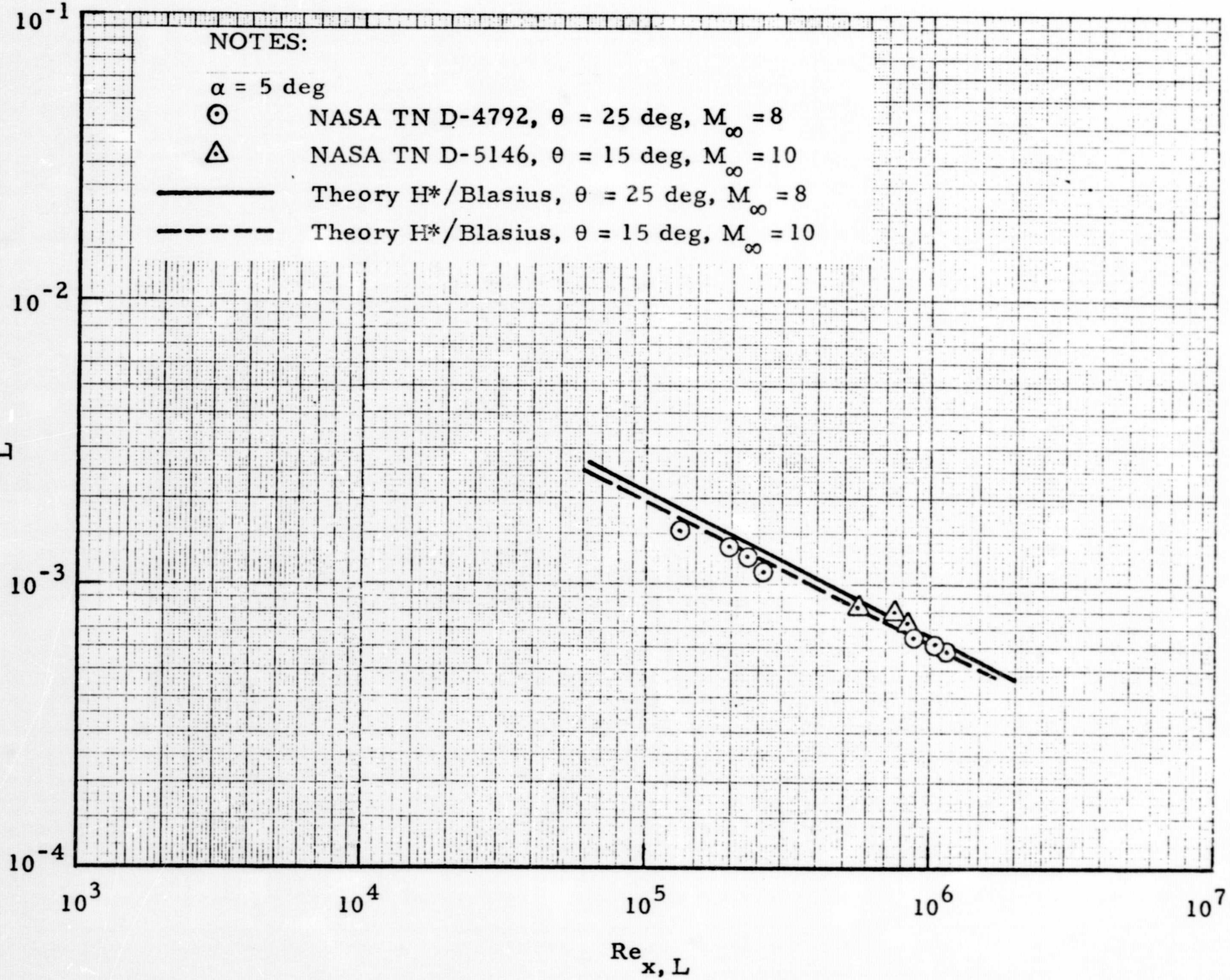

Fig. 3-11 - Local Stanton Number vs Local Reynolds Number for Laminar Flow over Cones at α = 5 Degrees

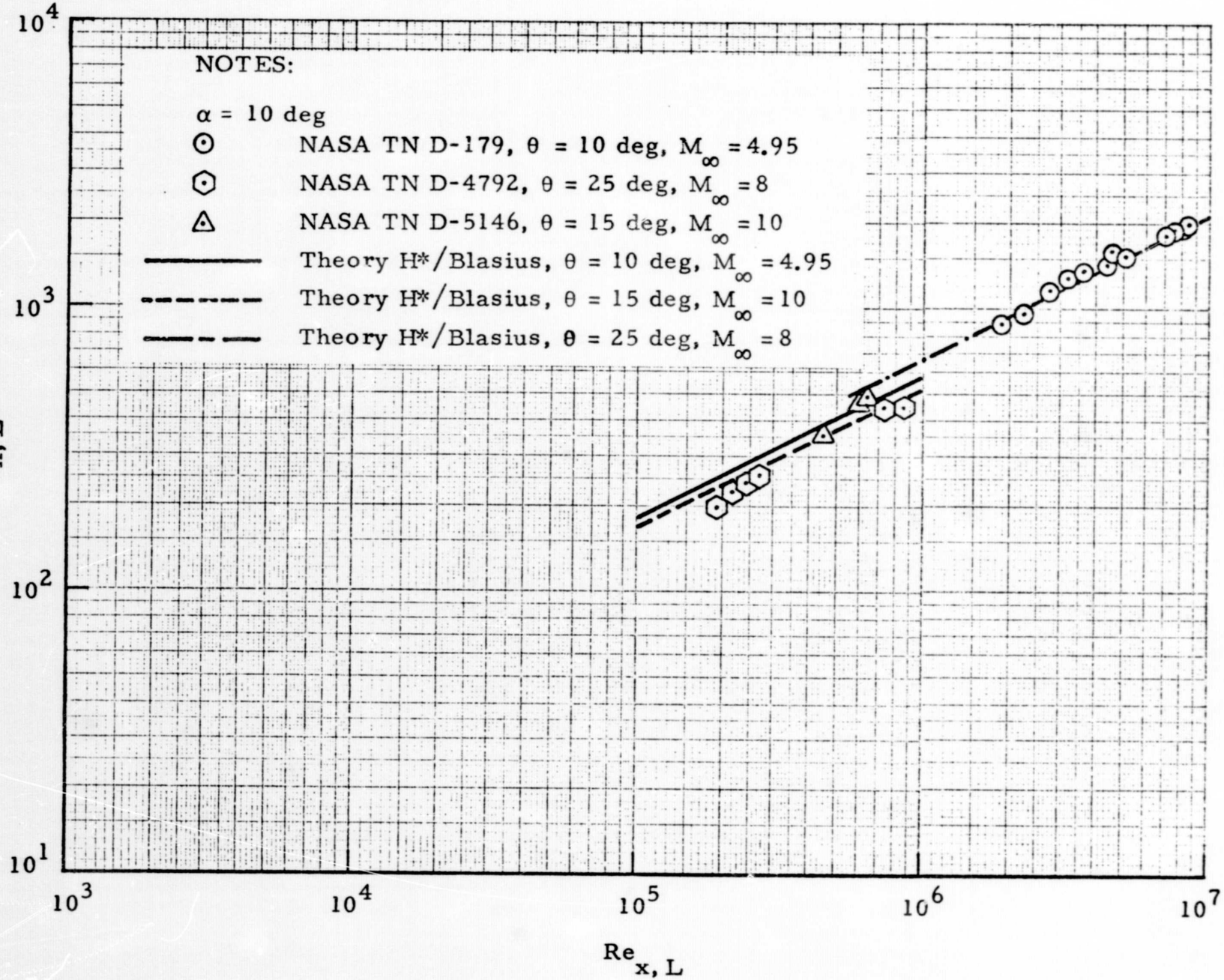

Fig. 3-12 - Local Nusselt Number vs Local Reynolds Number for Laminar Flow over Cones at α = 10 Degrees

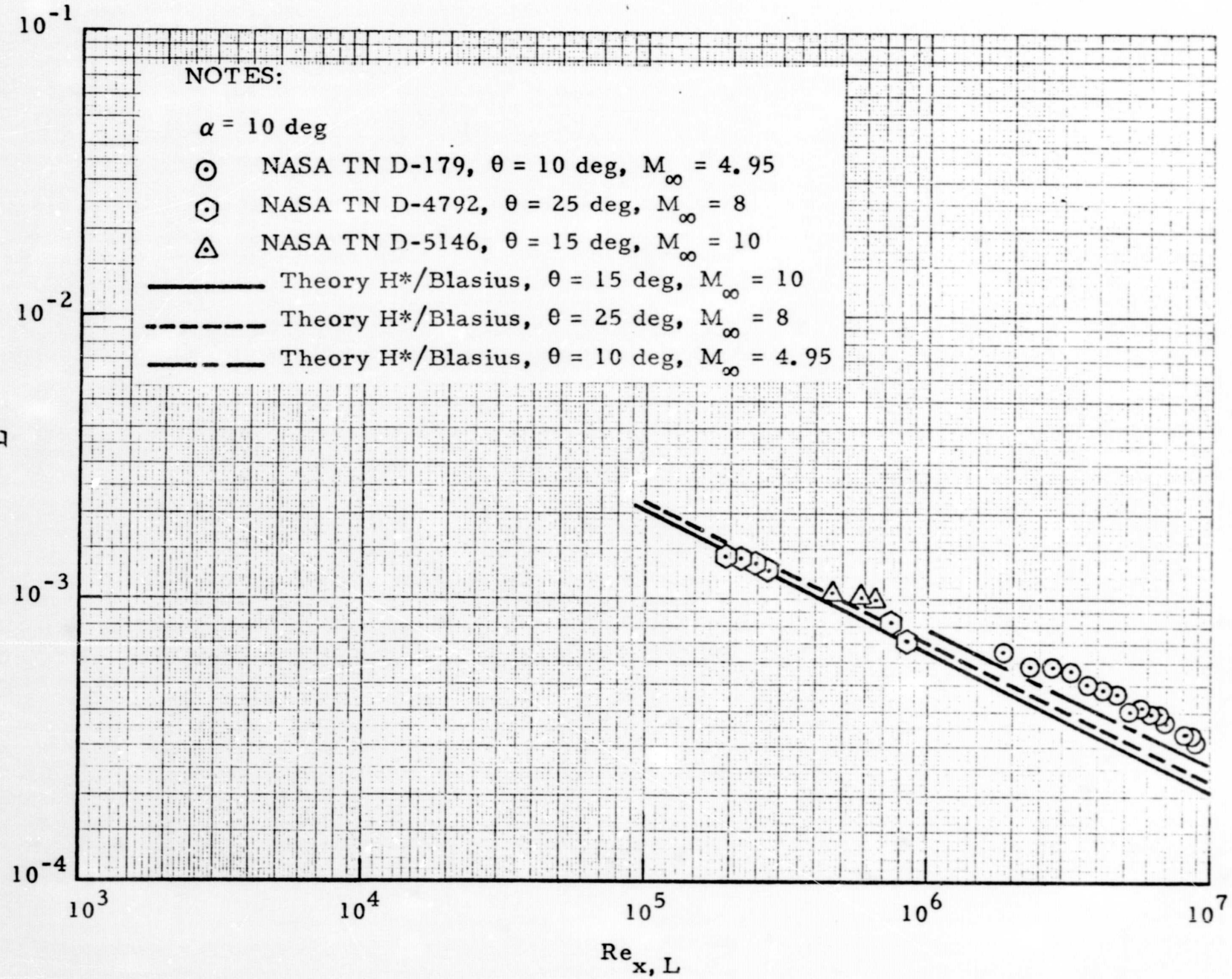

Fig. 3-13 - Local Stanton Number vs Local Reynolds Number for Laminar Flow over Cones at α = 10 Degrees

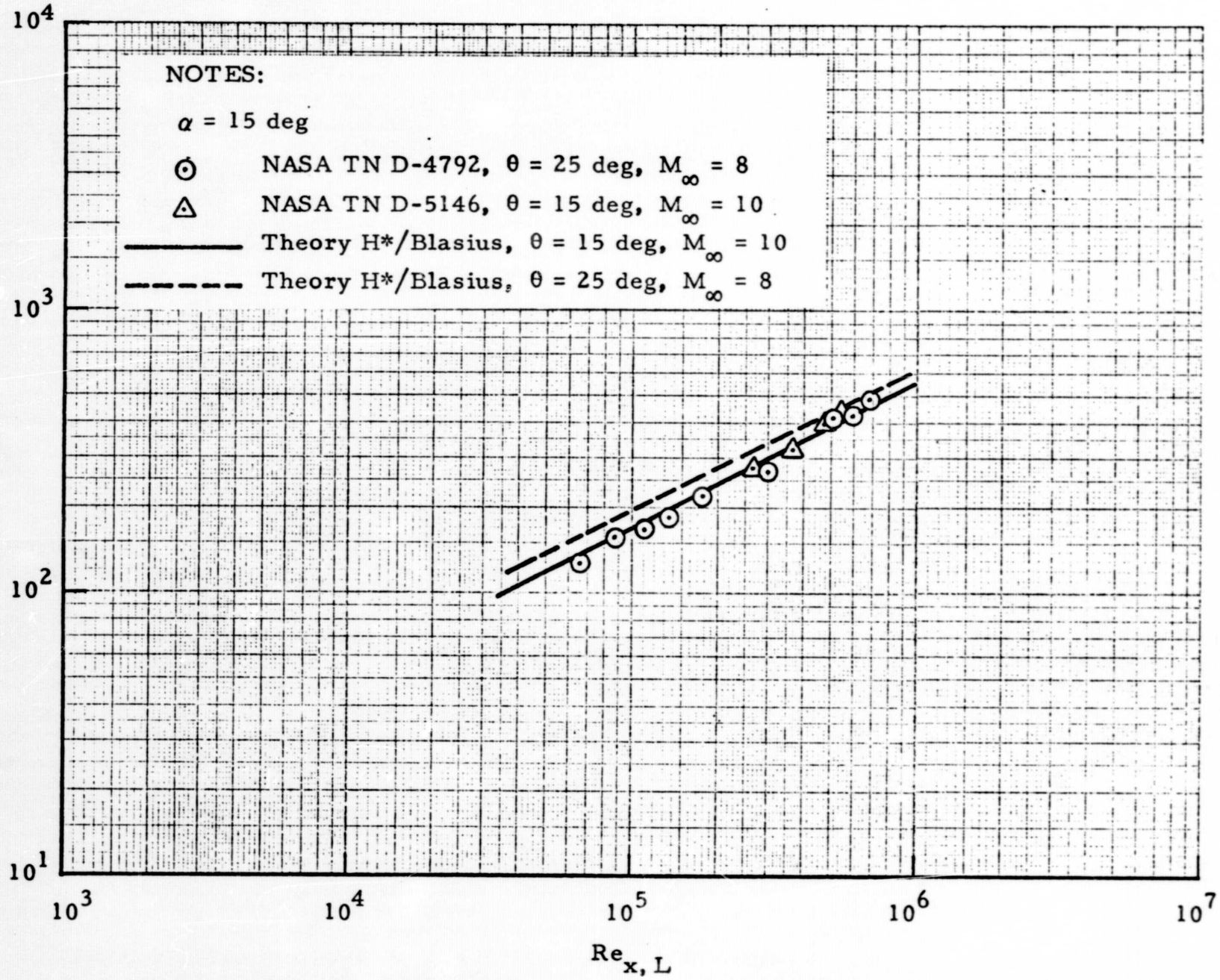

Fig. 3-14 - Local Nusselt Number vs Local Reynolds Number for Laminar Flow over Cones at α = 15 Degrees

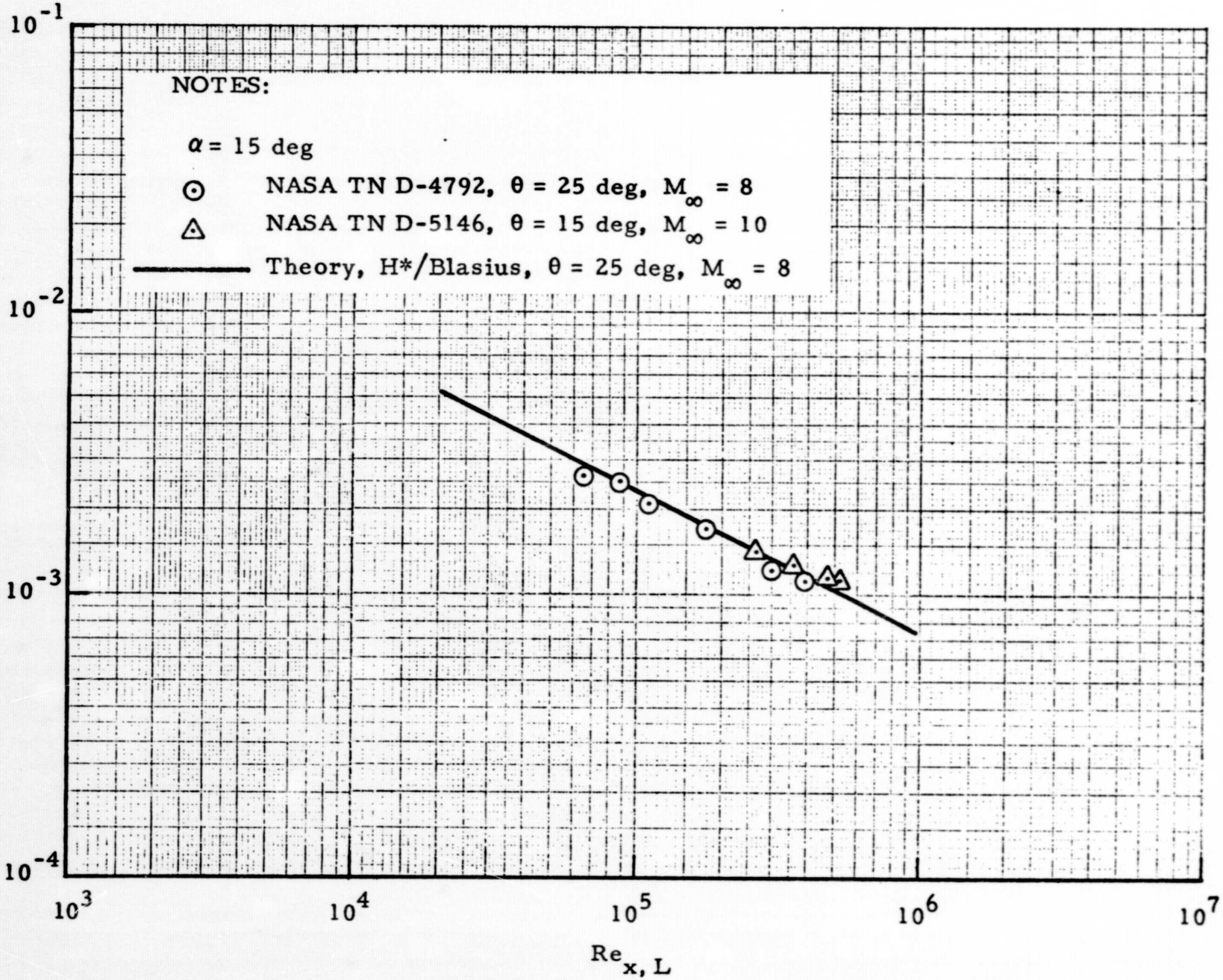

Fig. 3-15 - Local Stanton Number vs Local Reynolds Number for Laminar Flow over Cones at α = 15 Degrees

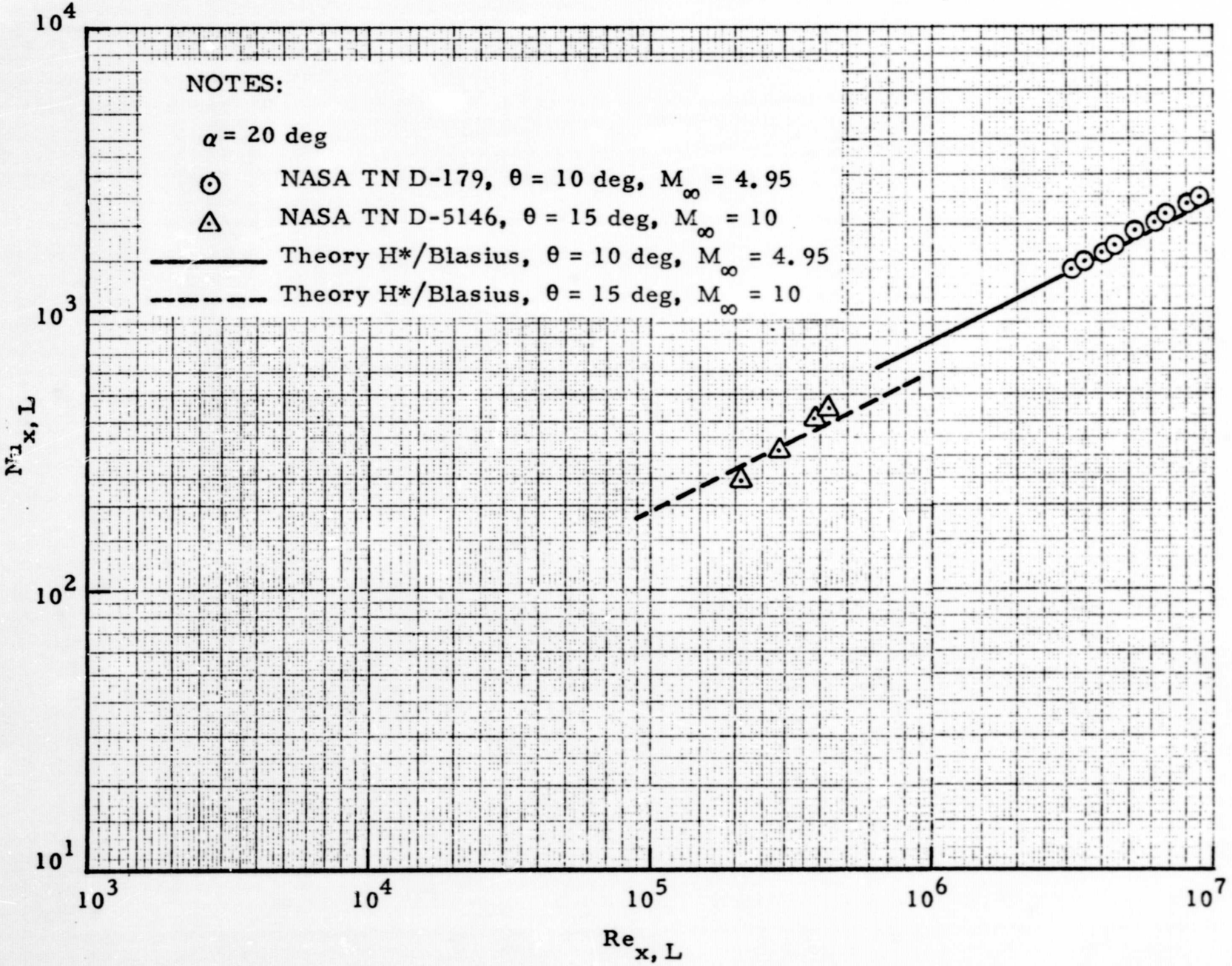

Fig. 3-16 - Local Nusselt Number vs Local Reynolds Number for Laminar Flow over Cones at α = 20 Degrees

Fig. 3-17 - Local Stanton Number vs Local Reynolds Number for Laminar Flow over Cones at α = 20 Degrees

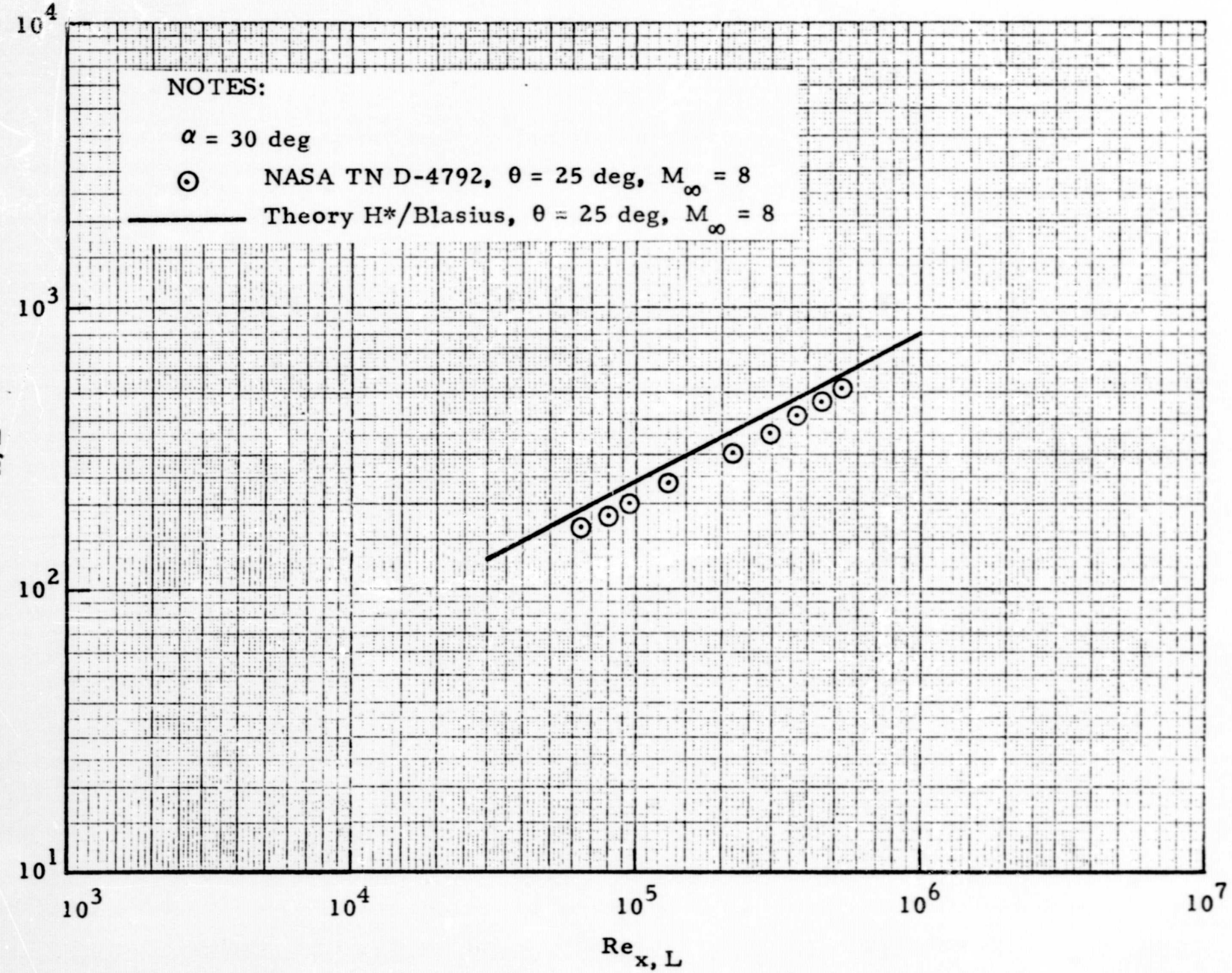

Fig. 3-18 - Local Nusselt Number vs Local Reynolds Number for Laminar Flow over Cones at α = 30 Degrees

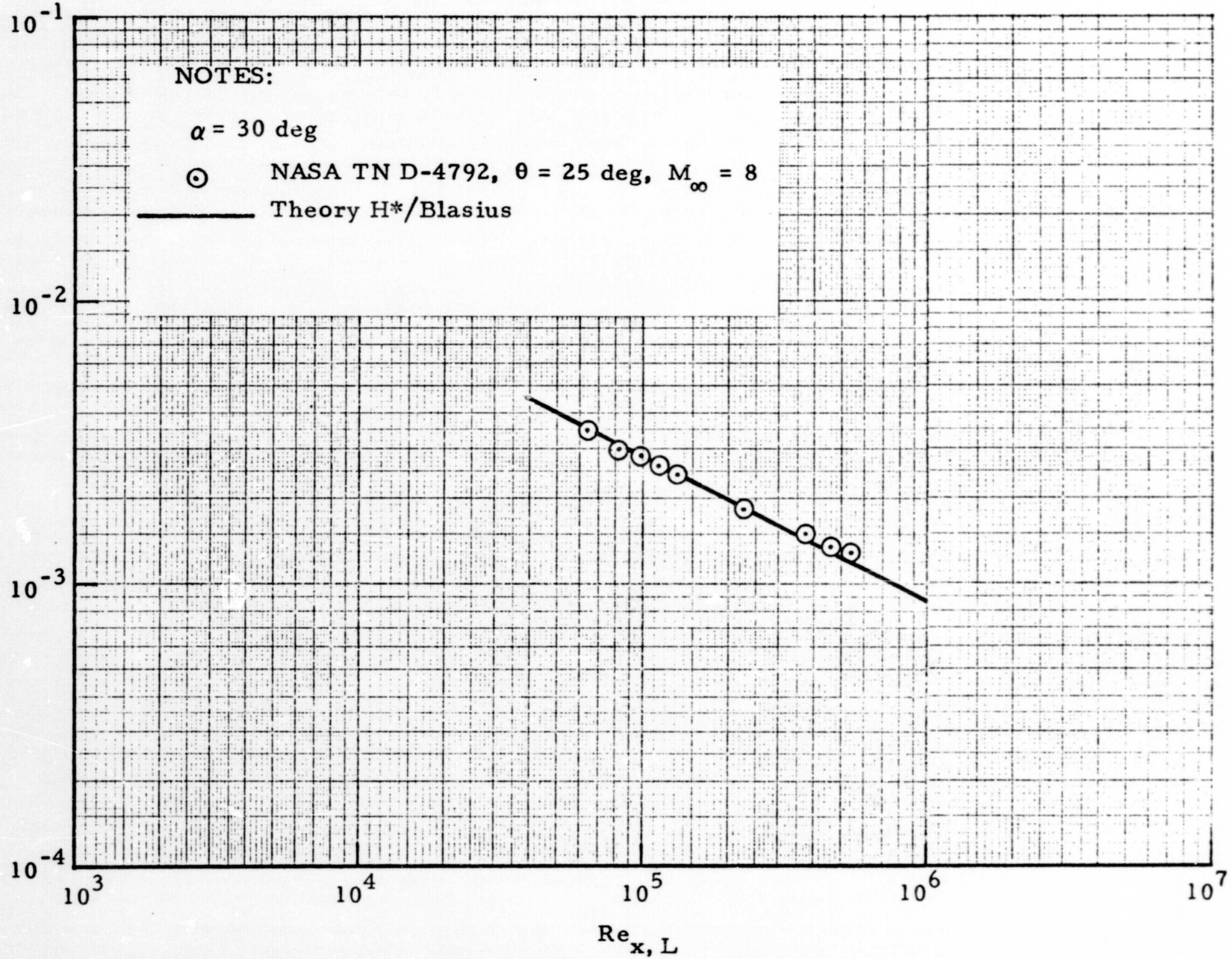

Fig. 3-19 - Local Stanton Number vs Local Reynolds Number for Laminar Flow over Cones at α = 30 Degrees

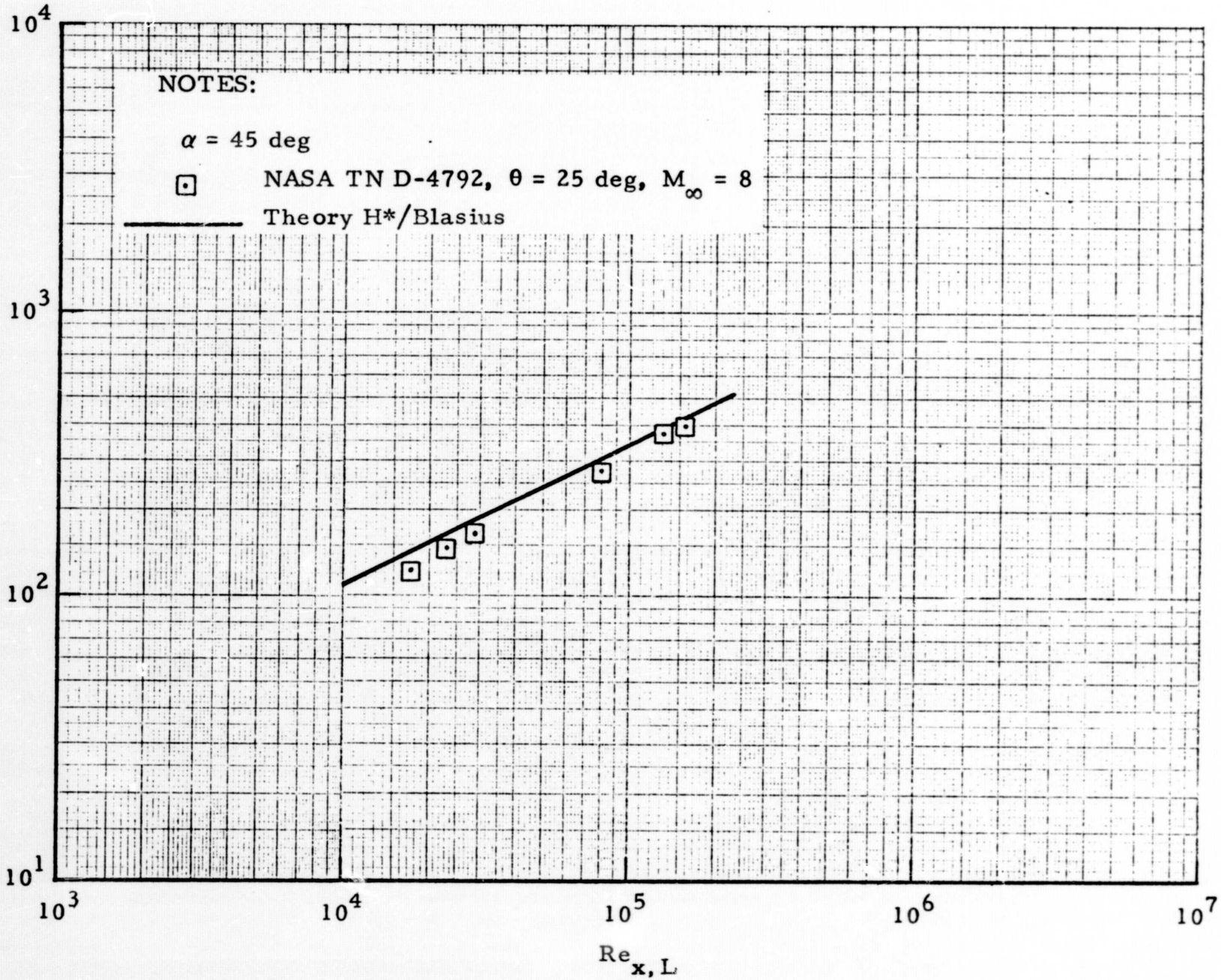

Fig. 3-20 - Local Nusselt Number vs Local Reynolds Number for Laminar Flow over Cones at α = 45 Degrees

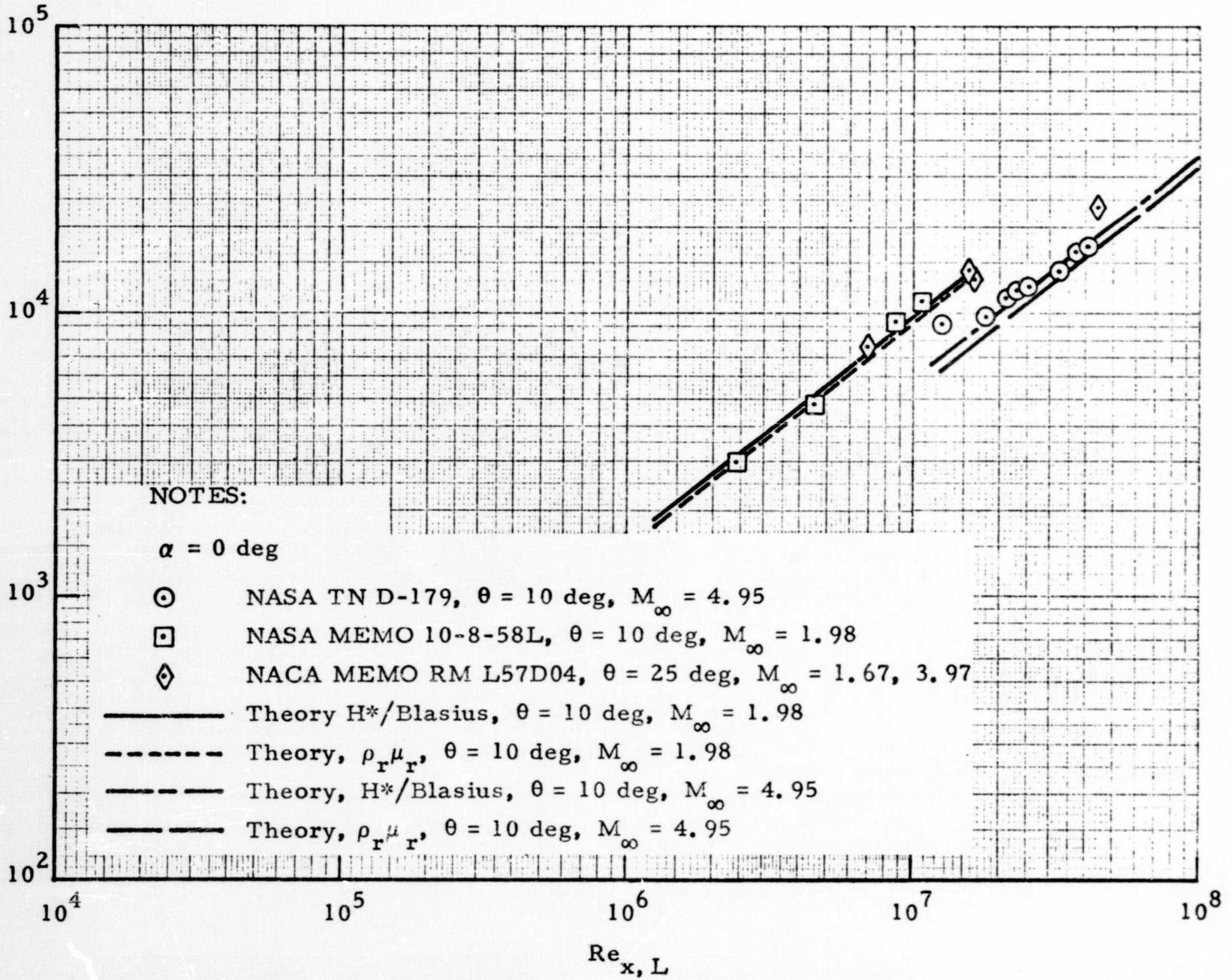

Fig. 3-21 - Local Nusselt Number vs Local Reynolds Number for Turbulent Flow over Cones at α = 0 Degrees

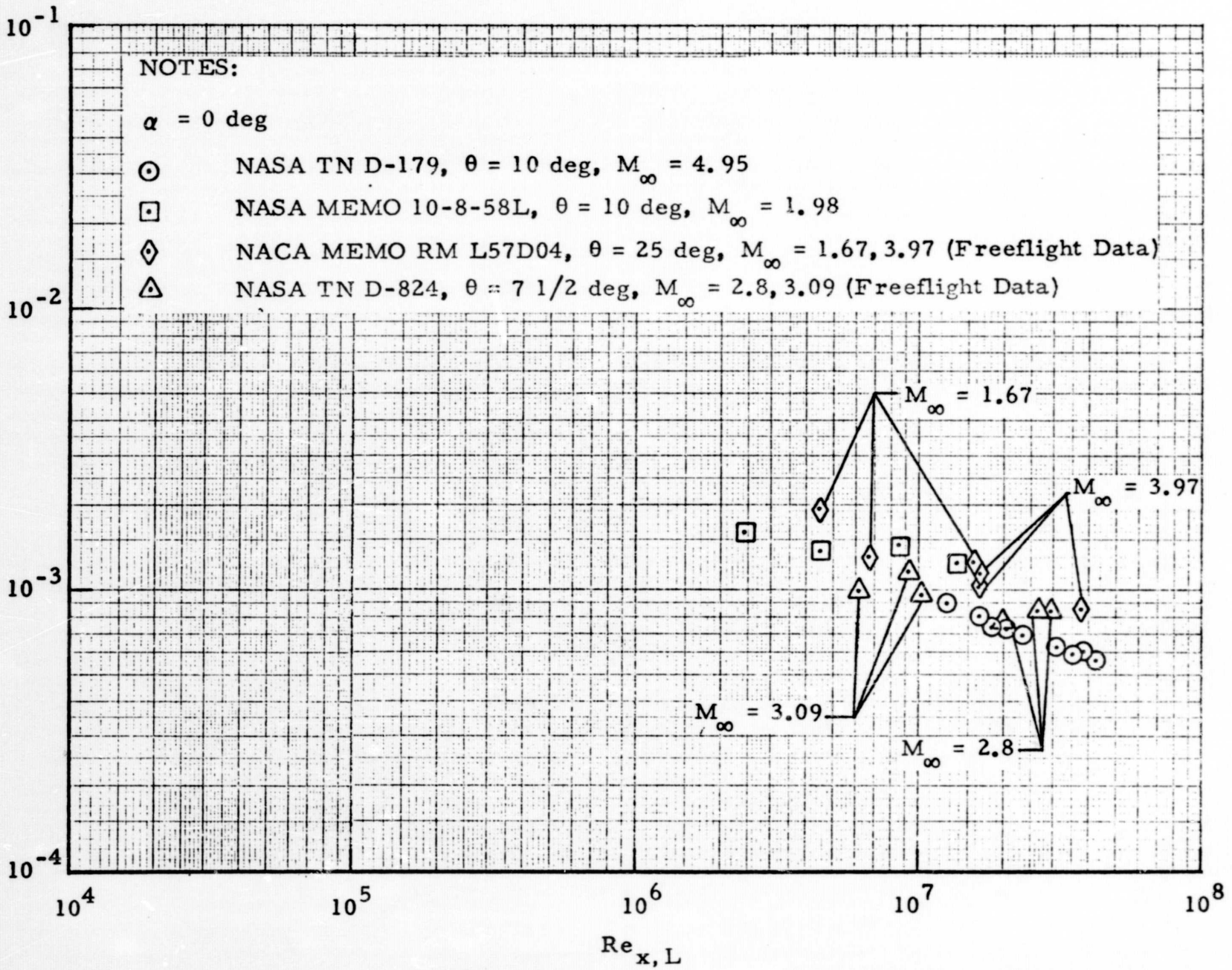

Fig. 3-22 - Local Stanton Number vs Local Reynolds Number for Turbulent Flow over Cones at α = 0 Degrees

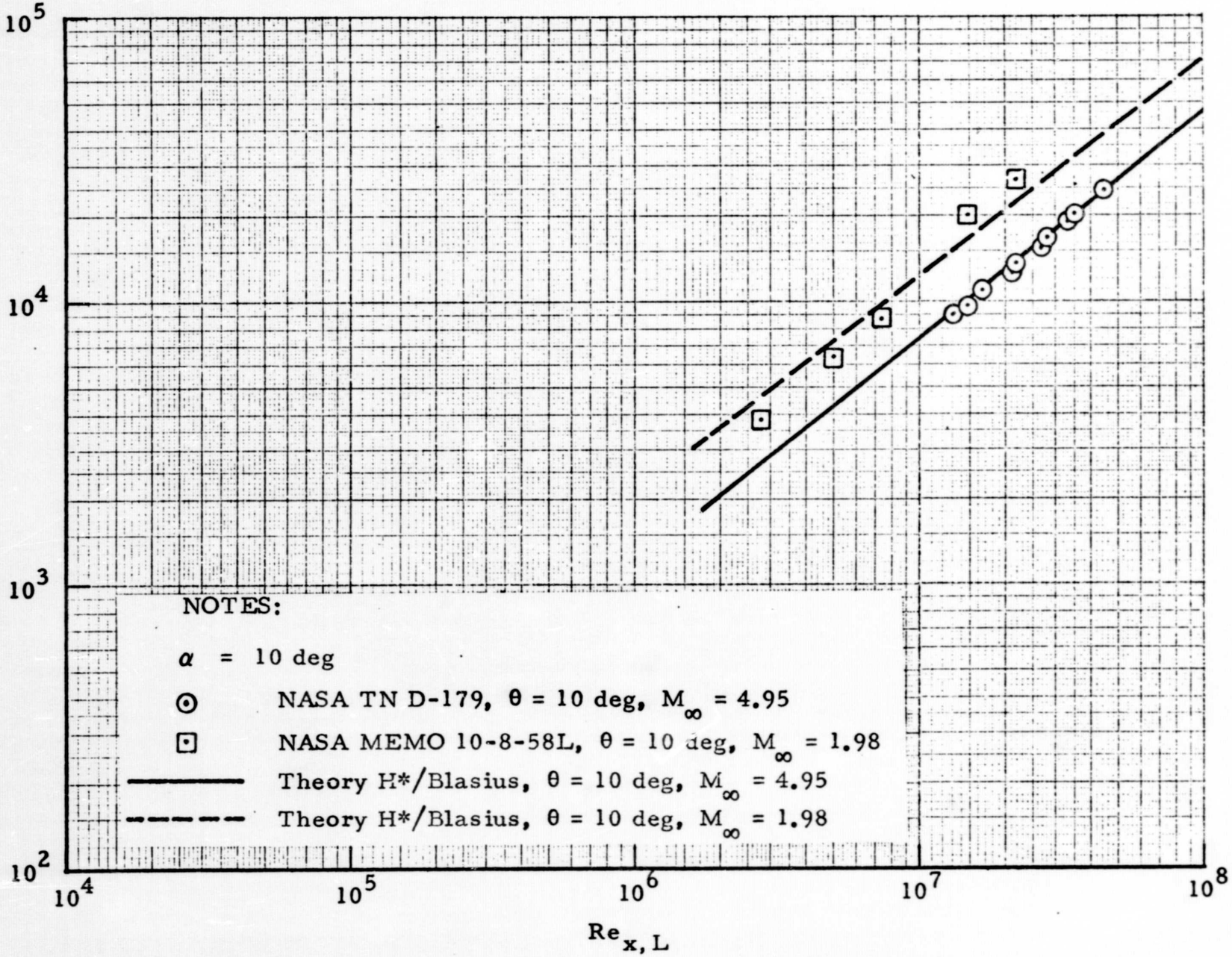

Fig. 3-23 - Local Nusselt Number vs Local Reynolds Number for Turbulent Flow over Cones at α = 10 Degrees

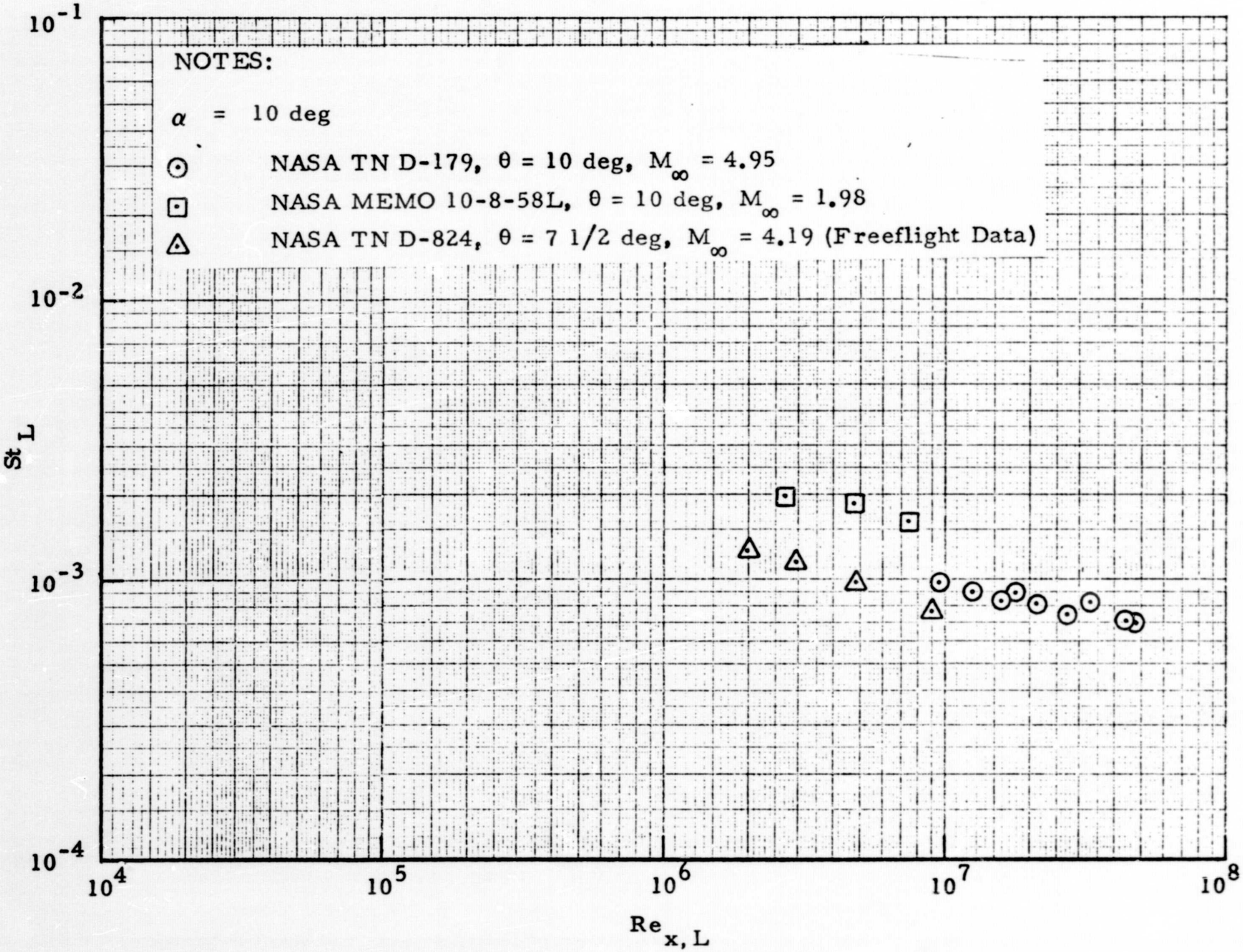

Fig. 3-24 - Local Stanton Number vs Local Reynolds Number for Turbulent Flow over Cones at α = 10 Degrees

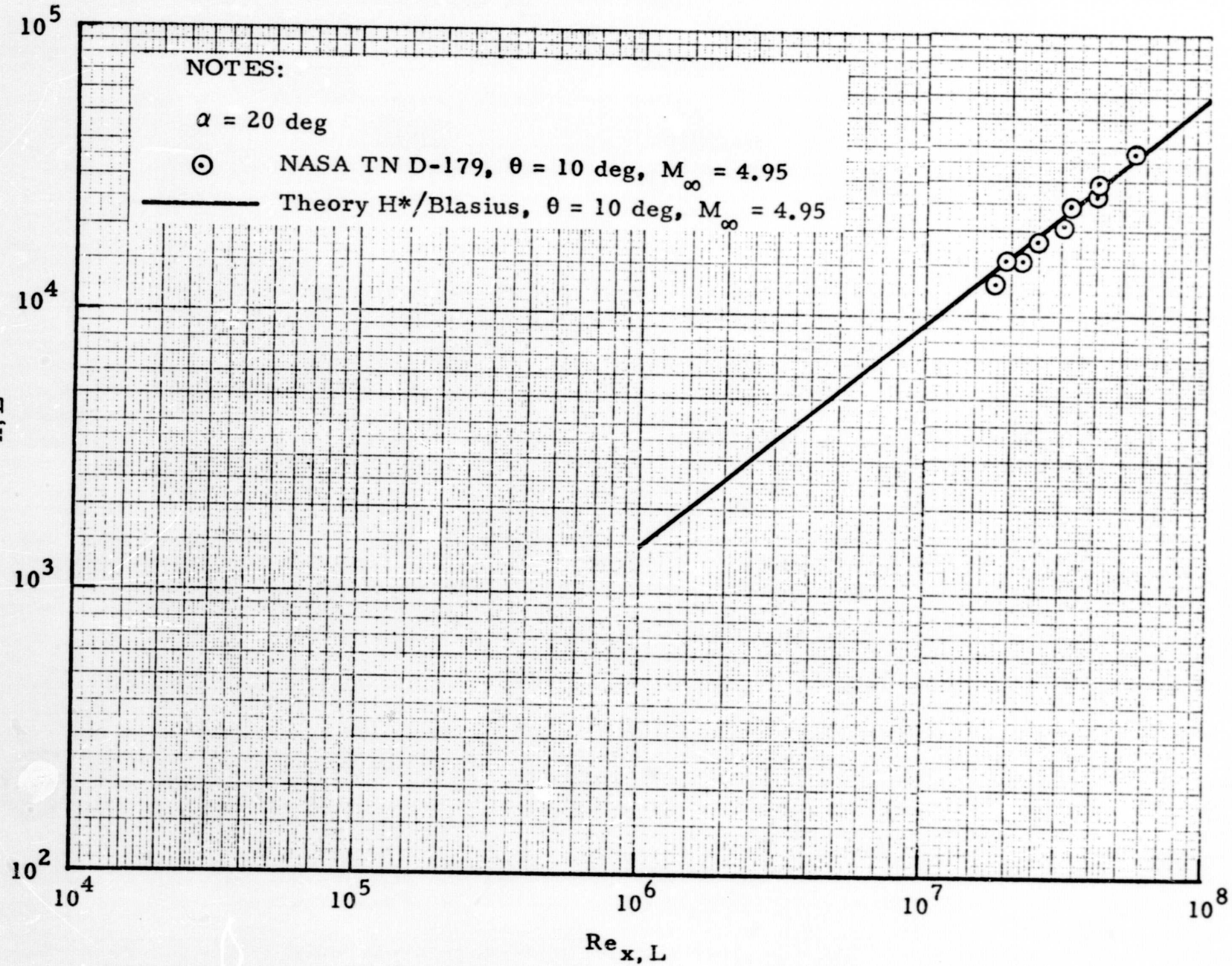

Fig. 3-25 - Local Nusselt Number vs Local Reynolds Number for Turbulent Flow over Cones at α = 20 Degrees

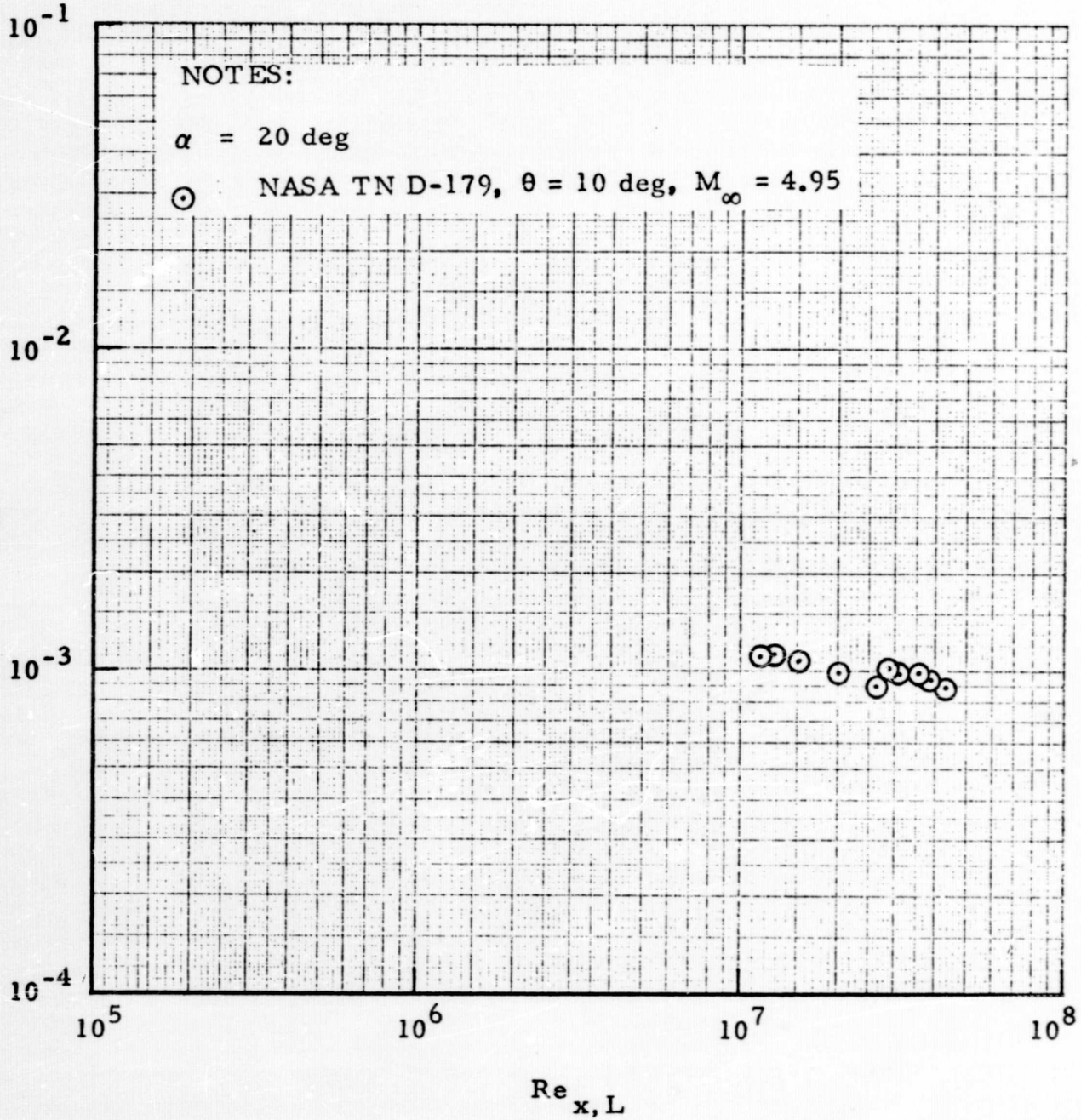

Fig. 3-26 - Local Stanton Number vs Local Reynolds Number for Turbulent Flow over Cones at α = 20 Degrees

Section 4

CONVECTIVE HEAT TRANSFER DESIGN CURVES FOR CONES AND CYLINDERS AT ANGLE OF ATTACK

The purpose of this section is to present the results of the work of Sections 2 and 3 in a form that can be used to determine heating rates to cone and cylinder shapes in freeflight at angle of attack. From the design curves presented, it is possible to obtain windward streamline and off-windward streamline heating for both laminar and turbulent flow. The following sections discuss and explain these design curves. Then, two example problems are given, one for a cylinder and one for a cone. Following this, a discussion of the range of applicability of these "isolated" cone and cylinder curves to composite cone-cylinder-flare shapes is given.

4.1 HEAT TRANSFER DESIGN CURVES

For the convenience of the user these curves are presented in the following order:

Type Curves	Figure Numbers
I. Cylinders	
A. α = 25 deg, laminar and turbulent, M_∞ = 2 to 12	4-1, 4-2
B. Angle of attack correction factors for $\alpha \neq 25$ deg (except α = 0 deg)	4-3, 4-4
C. α = 0 deg, laminar and turbulent	4-5
D. Circumferential distributions, laminar and turbulent	4-6, 4-7
II. Cones	
A. α = 0 deg, laminar, M_∞ = 2 to 12	4-8 – 4-11
B. α = 0 deg, turbulent, M_∞ = 2 to 12	4-12 – 4-16

Type Curves	Figure Numbers
II. Cones (Continued)	
C. Angle of attack correction factors for $\alpha \neq 0$ deg, M_∞ = 2 to 12, laminar and turbulent	4-17, 4-18
D. Circumferential distribution, laminar and turbulent	4-19, 4-20
III. Flowfield Parameters	
A. Cylinders, M_∞ = 1.5 to 26, α = 5 to 50 deg (altitude = 100,000 ft)	4-21 — 4-23
B. Cylinders, altitude correction factors	4-24 — 4-25
C. Cones, M_∞ = 1.2 to 26, $\alpha + \theta$ = 5 to 50 deg (altitude = 100,000 ft)	4-26 — 4-28
D. Cones, altitude correction factors	4-29, 4-30
E. Viscosity and conductivity of air as a function of temperature and pressure	4-31, 4-32
F. Adiabatic wall temperature	4-33

IV. Range of Applicability

The details of each of these curves are now discussed beginning with the cylinders. Freestream Nusselt number, at α = 25 deg, as a function of freestream Reynolds number is presented for laminar and turbulent flow on Figs. 4-1 and 4-2. It is noted that there is a Mach number effect of these values, therefore, separate curves are shown for M_∞ = 2 to 12. These curves are based on a wall temperature of 560°R. This wall temperature affects the $Nu_{D,\infty}$ value only through the heat transfer coefficient in the Nu definition $\left(h_c D/k_\infty\right)$. Note that the k value used here is the freestream value making Nu a freestream Nusselt number. An angle of attack value of 25 deg was chosen as a "reference" condition for presenting these curves. For angle of attack values other than 25 deg, the curves of Figs. 4-3 and 4-4 are provided — again for laminar and turbulent flow. The curves give the ratio of $Nu_{D,\infty}$ at a given angle of attack to $Nu_{D,\infty}$ at an angle of attack of 25 deg. Since there is a Mach number effect, curves are presented for M_∞ = 2 to 12.

These curves are also presented for a wall temperature of 560°R. Figures 4-3 and 4-4 are for angles of attack down to 5 deg because the Nu based on diameter does not correlate at α values near 0 deg. The correlating parameter near 0 deg is Nu based on x, running length down the cylinder, versus Reynolds number also based on x. Therefore, Fig. 4-5 is given for use at α = 0 deg. Both laminar and turbulent curves are provided.

Circumferential heating distributions on cylinders at angle of attack values of 10 to 50 deg are given for laminar and turbulent flow in Figs. 4-6 and 4-7. Specifically, heat transfer coefficient at an angle ϕ, measured away from the windward streamline to the local point, ratioed to the windward streamline value is shown as a function of ϕ. These figures were derived from the data of Ref. 1 for laminar flow, and from Ref. 8 for turbulent flow.

The cone heating curves are shown beginning with Fig. 4-8. The heating parameters for cones are correlated and presented in a way similar to that used for cylinders. However, there is one additional parameter to be considered, namely the cone angle. Also local rather than freestream properties are used, and the "reference" value of Nu is at α = 0 deg rather than 25 deg. Local Nusselt number at α = 0 deg based on x, the distance from the cone apex to the local point at which heating rates are needed, versus local Reynolds number are shown on Figs. 4-8 to 4-16. Figures 4-8 through 4-11 are for laminar flow while 4-12 through 4-16 are for turbulent flow. Note that a separate figure is given for each Mach number and that varying cone angles are shown.

For cones at angles of attack other than 0 deg, the correction factors of Figs. 4-17 and 4-18 are given for laminar and turbulent flow, respectively. These curves present the ratio of local Nusselt number at a given angle of attack to the local Nusselt number at an angle of attack of 0 deg as a function of angle of attack. These values are given for cone angles of 5, 15 and 25 deg and for Mach numbers of 2 to 12.

These correction factors were generated for a specific altitude of 100,000 ft, however, the altitude correction factor is small for altitudes from sea level to approximately 400,000 ft. These curves appear to be somewhat random which is due to two factors. First is the fact that the shock angle on the cones varies with three parameters, cone angle, Mach number, and angle of attack. The second factor is the erratic behavior of thermal conductivity (Fig. 4-32) with temperature and pressure in the regions covered.

Circumferential heating distributions for cones are presented in Figs. 4-19 and 4-20 for laminar and turbulent flow. As in the case for cylinders, the heat transfer coefficient ratios are presented as a function of ϕ, the angle measured away from the windward streamline. These curves are given as reasonable approximations for use for cone angles up to approximately 25 deg rather than for any specific cone angle value. A scarcity of cone data did not allow a comprehensive determination of the effect of cone angle during the present study. The results shown in Figs. 4-19 and 4-20 are fairings and extrapolations of the data in Refs. 3 and 9 for laminar and turbulent flow, respectively.

4.2 LOCAL FLOWFIELD CURVES FOR CONES AND CYLINDERS

In order to obtain Nusselt numbers, hence heating rates, from the preceding design curves it is necessary to know the local Reynolds number. To assist the user in obtaining these, the curves of this section are presented. First, for cylinders, local static to freestream static temperature, density, and velocity ratios are given in Figs. 4-21, 4-22 and 4-23. These are given as a function of Mach number and angle of attack. Note on Fig. 4-23 that the velocity ratio variation with Mach number is negligible. These figures are for an altitude of 100,000 ft. For different altitudes Figs. 4-24 and 4-25 present correction factors as indicated on each respective curve.

For flow fields on cones, Figs. 4-26, 4-27 and 4-28 give temperature, density, and velocity ratios as a function of Mach number. Here the sum of

angle of attack and cone half-angle has been used rather than angle of attack as in the cylinder curves. Again, these curves are for an altitude of 100,000 ft, and altitude correction factors are given in Figs. 4-29 and 4-30.

Figures 4-31 and 4-32 present viscosity and thermal conductivity for air as a function of temperature and pressure. Viscosity, of course, is needed in determining Reynolds number, and conductivity is needed for determining heat-transfer coefficient from the Nusselt number. Figure 4-33 presents the ratio of adiabatic wall temperature to total temperature, as a function of free-stream velocity. The total temperature used here is defined to be the ideal gas value as follows:

$$T_T = \frac{V_\infty^2}{2 g J C_p}$$

This is the value used to obtain T_{aw} to be used in conjunction with h_c obtained from the Nu to get heating rates. This is illustrated in the following example problems.

4.3 APPLICATION OF DESIGN CURVES

4.3.1 Example Problem No. 1

To illustrate the use of these curves the following example problem is given. Assume a cylinder with a 2-ft diameter flying at the following conditions.

Altitude = 150,000. ft
Velocity = 13,000. ft/sec
Angle of attack = 40. deg
Wall temperature = 560.$^{\circ}$R.

Heating rates are desired on the windward streamline and 45 deg away from the windward streamline. First, the freestream Mach and Reynolds number must be determined.

From the 1962 Standard Atmosphere table, the following are determined

$$M_\infty = 12.1$$

$$\rho_\infty = 1.11 \times 10^{-4} \text{ lb}_m/\text{ft}^3$$

$$T_\infty = 479.0^\circ\text{R}$$

$$P_\infty = 1.34 \times 10^{-3} \text{ atm}$$

From Fig. 4-31 $\mu_\infty = 1.1 \times 10^{-5}$ $\text{lb}_m/\text{ft-sec}$ and from Fig. 4-32 $k_\infty = 3.6 \times 10^{-6}$ Btu/ft-sec-$^\circ$R.

From these values

$$\text{Re}_{D,\infty} = \frac{\rho_\infty V_\infty D}{\mu_\infty} = 2.62 \times 10^5$$

At this Reynolds number, the flow should be laminar, therefore from Fig. 4-1

$$\text{Nu}_{D,\infty,\,\alpha=25\text{ deg}} = 8.6 \times 10^2 .$$

Then from Fig. 4-3,

$$\frac{\text{Nu}_{D,\infty,\,\alpha=40\text{ deg}}}{\text{Nu}_{D,\infty,\,\alpha=25\text{ deg}}} = 1.68 \approx 1.7$$

and

$$Nu_{D,\infty,\alpha=40\ deg} = 8.6 \times 10^2 \times 1.7 = 14.6 \times 10^2$$

The heat transfer coefficient is now found from

$$h_c = \frac{Nu\, k_\infty}{D} = \frac{14.6 \times 10^2 \times 3.6 \times 10^{-6}}{2} = 2.63 \times 10^{-3}\ \frac{Btu}{ft^2\text{-sec-}^oR}$$

From Fig. 4-33 (at $\frac{T_{aw}}{T_T} = 0.85$ for laminar flow)

$$T_{aw} = 12{,}700^oR$$

and from

$$\dot{q} = h_c (T_{aw} - T_w)$$

$$\dot{q} = 2.63 \times 10^{-3} (12{,}700. - 560.)$$

$$\dot{q} = 32.0\ Btu/ft^2\text{-sec}$$

This is the heating rate on the windward streamline.

For the point at 45 deg away from the windward streamline, Fig. 4-6, is used, where

$$\frac{h_{\phi = 45\ deg}}{h_{\phi = 0\ deg}} = 0.66$$

Therefore,

$$\dot{q}_{\phi = 45\ deg} = 0.66\,(32.0) = 21.1\ \frac{Btu}{ft^2\text{-sec}}$$

4.3.2 Example Problem No. 2

As a second example, assume we have a cone with a half-angle of 15 deg. Heating rates are desired at a point on the windward streamline 10 ft aft of the apex and at a point at this same axial distance but at 30 deg away from the windward streamline. The cone is flying at the following conditions:

Altitude = 50,000. ft
Velocity = 10,000. ft/sec
Angle of Attack = 20. deg
Wall Temperature = 560.$^{\circ}$R

The following values are taken from an atmosphere table:

T_∞ = 390.$^{\circ}$R
$P_\infty = 1.14 \times 10^{-1}$ atm
$\rho_\infty = 1.16 \times 10^{-2}$ lb_m/ft^3
M_∞ = 10.3

At M_∞ = 10.3 and $\alpha + \theta$ = 35 deg,

$\frac{T_2}{T_1}$ = 8.2 from Fig. 4-26 (at 100,000. ft)

$\frac{\rho_2}{\rho_1}$ = 6.2 from Fig. 4-27 (at 100,000. ft)

$\frac{V_2}{V_1}$ = 0.785 from Fig. 4-28 (at 50,000. ft)

For the altitude correction for $\frac{T_2}{T_1}$ and $\frac{\rho_2}{\rho_1}$ refer to Figs. 4-29 and 4-30 from which

$$T_{CF} = 0.99 \quad \text{for 50,000 ft}$$

$$\rho_{CF} = 1.01 \quad \text{for 50,000 ft}$$

Therefore, for 50,000 ft

$$\frac{T_2}{T_1} = 0.99(8.2) = 8.12$$

$$\frac{\rho_2}{\rho_1} = 1.01(6.2) = 6.46$$

and

$$T_2 = 8.12(390.0) = 3160.0^{\circ}R$$

$$\rho_2 = 6.46(1.16 \times 10^{-2})$$

$$= 7.28 \times 10^{-2} \ \frac{lb_m}{ft^3}$$

$$V_2 = 0.785(10{,}000) = 7{,}850 \text{ ft/sec}$$

From Fig. 4-31, $\mu_2 = 3.9 \times 10^{-5} \ \frac{lb_m}{ft\text{-}sec}$

From Fig. 4-32, $k_L = 1.5 \times 10^{-5} \ \frac{Btu}{ft\text{-}sec\text{-}^{\circ}R}$

From which

$$Re_{x,L} = \frac{\rho_2 V_2 x}{\mu^2} = 14.6 \times 10^7$$

At this Reynolds number it can be safely assumed that turbulent flow exists. From Fig. 4-16,

$$\left.\begin{array}{l} Nu_{x,L} \\ \alpha = 0 \text{ deg} \\ M_\infty = 10 \text{ deg} \end{array}\right] = 4.2 \times 10^4$$

For an angle of attack of 20 deg and $M_\infty = 10$

$$\frac{Nu_{x,L,\alpha=20\text{ deg}}}{Nu_{x,L,\alpha=0\text{ deg}}} = 1.9 \quad \text{from Fig. 4-18}$$

and

$$Nu_{x,L,\alpha=20\text{ deg}} = 1.9\ (4.2 \times 10^4) = 7.97 \times 10^4.$$

From this, the following results:

$$h_c = \frac{\left(Nu_{x,L,\alpha=20\text{ deg}}\right)(k_L)}{x} = 1.2 \times 10^{-1}$$

From Fig. (4-33)

$$T_{aw} = 8000.^{\circ}R \quad \text{at} \quad \frac{T_{aw}}{T_T} = 0.9$$

and

$$\dot{q} = h_c (T_{aw} - T_w) = 890. \frac{Btu}{ft^2\text{-sec}}$$

on the windward streamline at a point 10 ft from the apex.

Now for the heating at a point also 10 ft from the apex but at 30 deg away from the windward streamline, refer to Fig. 4-20. At ϕ = 30 deg, α = 20 deg

$$\frac{h_{c_{\phi = 30\ deg}}}{h_{c_{\phi = 0\ deg}}} = 1.11$$

from which

$$\dot{q}_{\phi = 30\ deg} = 1.11(890) = 980. \frac{Btu}{ft^2\text{-}sec}$$

4.4 REGIONS OF APPLICABILITY OF ISOLATED BODY DESIGN CURVES

When using the preceding design curves on composite shapes such as a cone-cylinder-flare, it is desirable to know how close to a junction the curves apply. Two cases are considered here, downstream of an expansion corner, and upstream of a compression corner. Data for these regions are limited in that instrumentation locations are usually too widely spaced in the corner region to give a distribution. However, the curves of Fig. 4-34 are given as an approximate means for determining the distance downstream of an expansion corner at which the cylinder curves become applicable. Figure 4-34 presents x/D, the distance downstream-to-cylinder diameter ratio, as a function of freestream Mach number for various angles of attack. This curve is for laminar flow only. However, indications are that when there is turbulent flow ahead of a corner, it goes laminar downstream in the expansion region. Therefore, this curve should give a reasonable approximation. On the cone upstream of the expansion corner, the isolated cone design curves should apply all the way to the corner.

In compression corner regions, the available heating data were not consistent enough to allow the development of a set of curves similar to Fig. 4-34. In lieu of this, the following equations from Ref. 21 are offered as a means for

handling problems in these regions. Upstream of a compression corner, the isolated cylinder curves apply up to the separation point. The problem is then to define where separation will occur. This can be estimated by defining a critical pressure coefficient at which separation will occur. The relationships are:

For laminar flow:

$$CP_{critical} = \frac{2.03\,(M_2^{\,2} - 1)^{-0.306}}{\left(Re_{x,L}\right)^{0.25}}$$

For turbulent flow:

$$CP_{critical} = \frac{2.2}{\left(Re_{x,L}\right)^{0.1}}$$

Separation should not occur if CP is less than $CP_{critical}$ where CP is defined by

$$CP = \frac{P_d - P_u}{\frac{1}{2}\rho_u V_u^2}$$

where P_d is the static pressure downstream of the corner, and P_u is the static pressure upstream of the corner. If separation occurs, the following expressions can be used to estimate the location of separation:

For laminar flow:

$$\frac{d_u}{\delta_u} = 570.0\, M_u^{-2.92} \left[\frac{P_d}{P_u} - 1\right]^{1.056}$$

where d_u is the distance upstream of the corner to the separation point and δ_u is the boundary layer displacement thickness upstream of the corner, M_u is the local Mach number upstream of the corner.

For turbulent flow:

$$\frac{d_u}{\delta_u} = 1.1 \times 10^6 \left[M_u^{-1.67} \left(\frac{P_p}{P_u} - 1 \right) \right]^{8.55}$$

where P_p is defined by the expression:

For laminar flow:

$$\frac{P_p - P_u}{\frac{\gamma}{2} M_u^2 P_u} = \frac{1.56 (M_u^2 - 1)^{-0.262}}{Re_{x,u}}$$

where $Re_{x,u}$ is the local Reynolds number upstream of the corner.

For turbulent flow:

$$\frac{P_p - P_u}{\frac{\gamma}{2} M_u^2 P_u} = \frac{1.91 (M_u^2 - 1)^{-0.309}}{\left[Re_{x,u} \right]^{0.2}}$$

For estimating the location of reattachment on the cone downstream of the corner, the following relations are recommended:

For laminar flow:

$$\frac{d_d}{\delta_u} = \frac{\left[Re_{x,u} \right]^{0.5}}{M_u \left(\frac{P_d - P_p}{P_u} \right)^{0.188}}$$

where d_d is the distance downstream of the corner to the reattachment point.

For turbulent flow:

$$\frac{d_d}{\delta_u} = \frac{\left(Re_{x,u}\right)^{0.2}}{M_u^{5.78}\left(\frac{P_d - P_p}{P_u}\right)^{3.175}}$$

To estimate the increase in heating at the point of reattachment, the following relations are used:

For laminar flow:

$$\frac{h_{c,\text{ at reattachment}}}{h_{c,u}} = 5.0 \times 10^6 \left(\frac{P_d}{P_u}\right)^{0.88} \left[Re_{x,u}\right]^{-0.5} \left[M_u\right]^{-3.7}$$

For turbulent flow:

$$\frac{h_{c,\text{ at reattachment}}}{h_{c,u}} = 32.\left(\frac{P_d}{P_u}\right)^{0.62} \left(Re_{x,u}\right)^{-0.2}$$

where $h_{c,u}$ is the heat-transfer coefficient upstream of separation, and M_u is the local Mach number upstream of separation.

Also, for estimating the average heating in the separated region the following expressions can be used:

For laminar flow:

$$\frac{h_{c,\text{in separated region}}}{h_{c,u}} = 0.42$$

For turbulent flow:

$$\frac{h_{c,\text{in separated region}}}{h_{c,u}} = 0.84$$

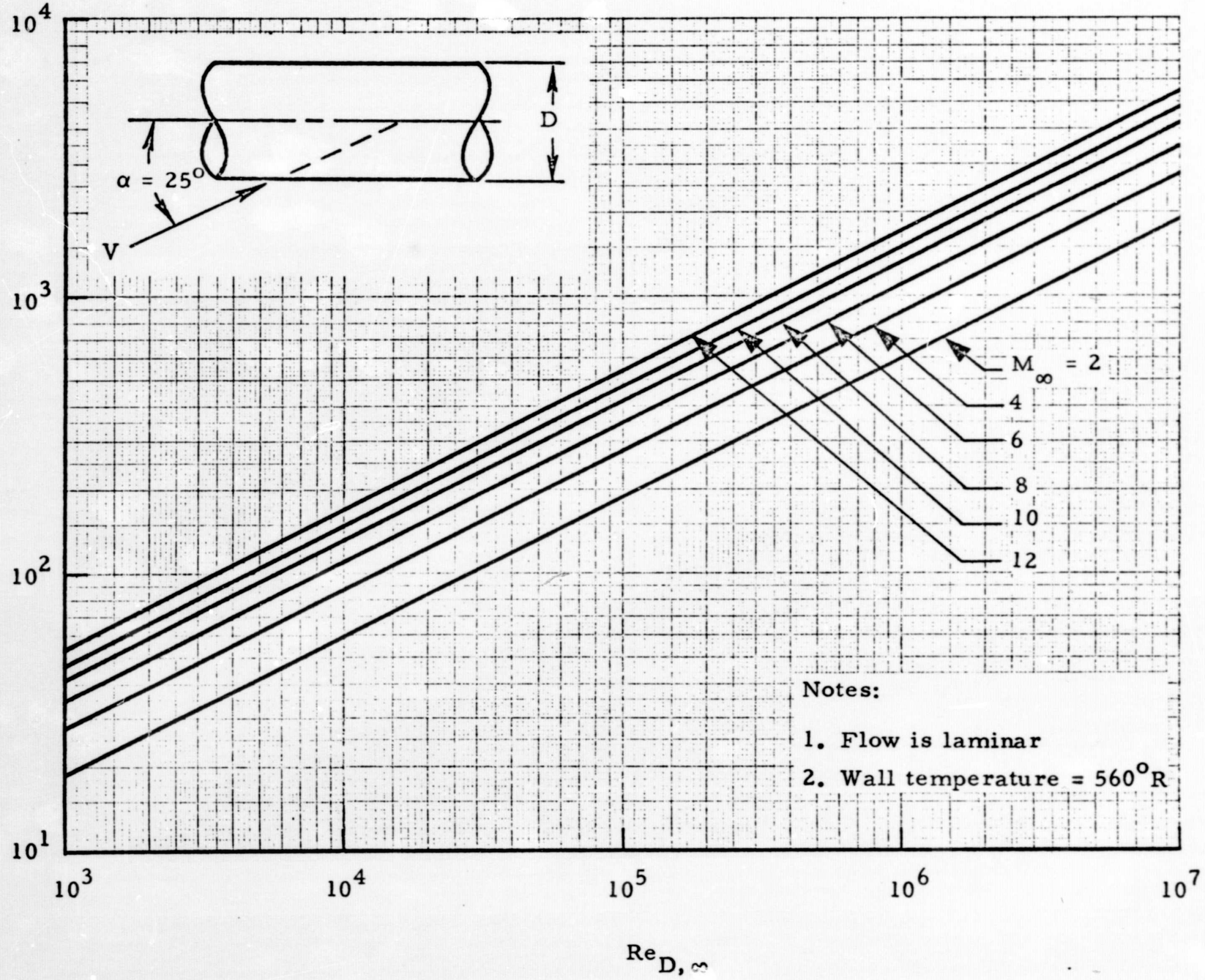

Fig. 4-1 - Reference Freestream Nusselt Number vs Freestream Reynolds Number for Laminar Flow over Cylinders at α = 25 Degrees

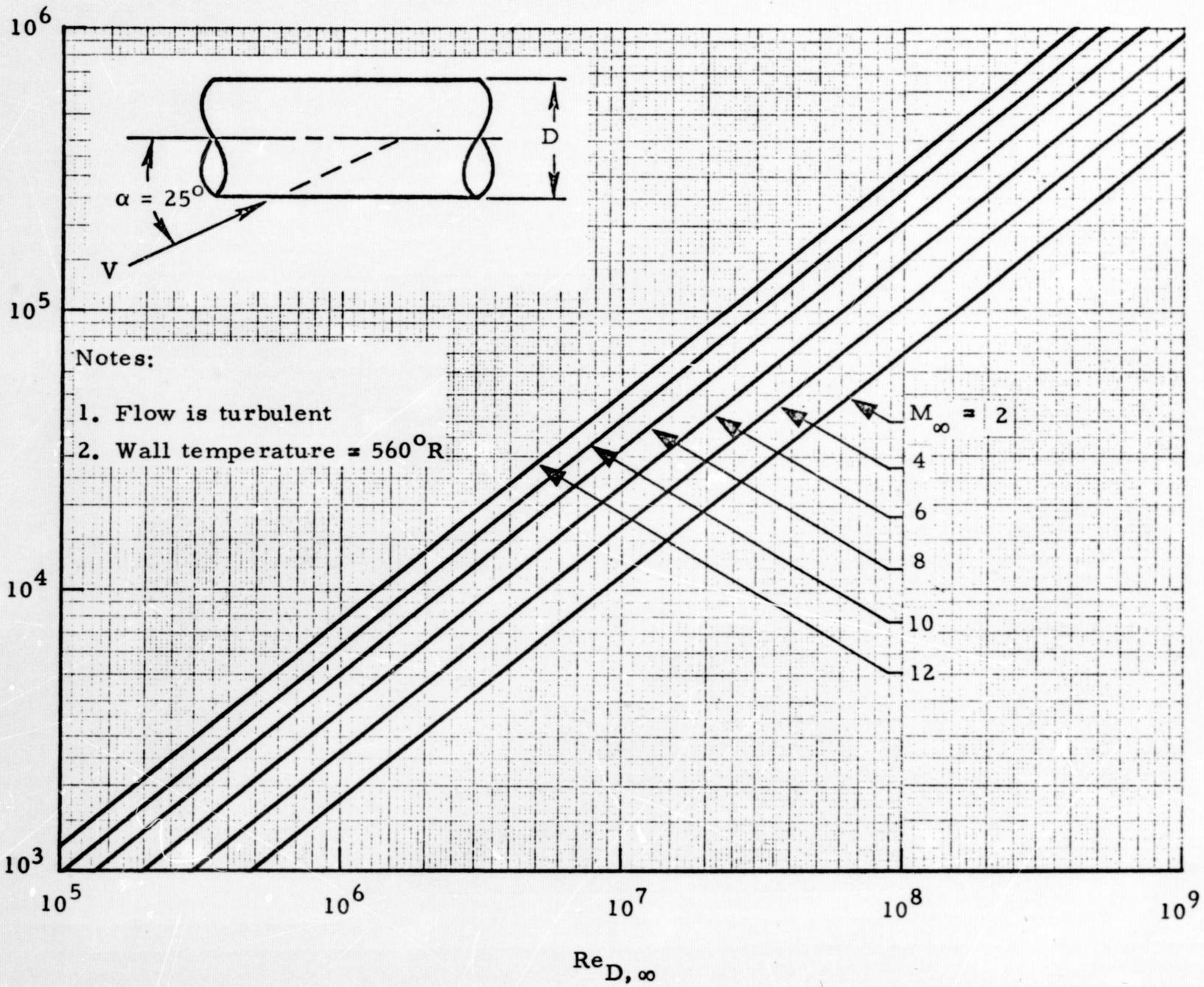

Fig. 4-2 - Reference Freestream Nusselt Number vs Freestream Reynolds Number for Turbulent Flow over Cylinders at α = 25 Degrees

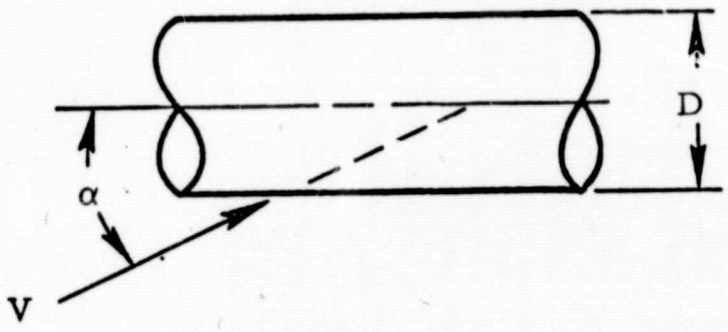

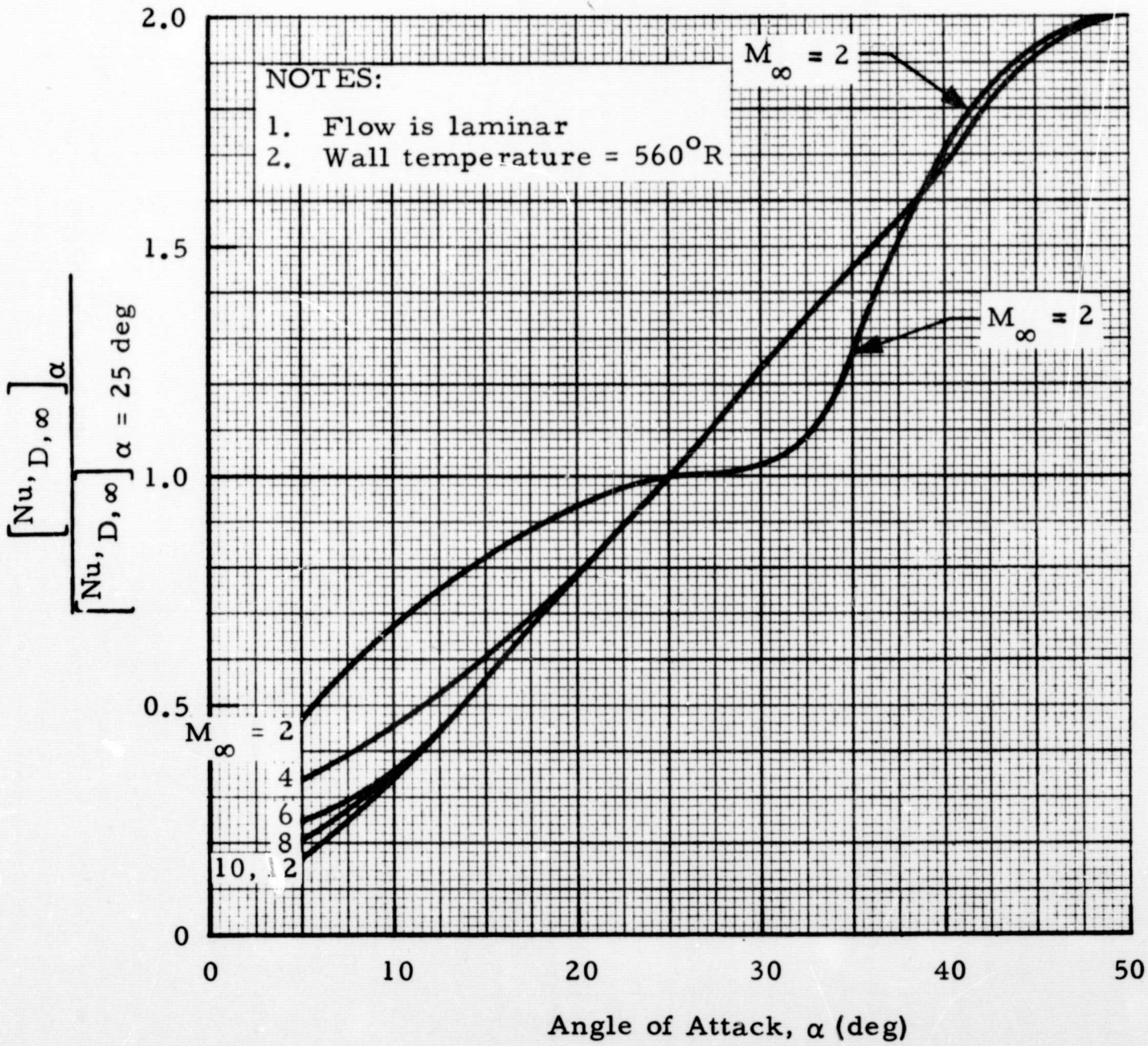

Fig. 4-3 - Angle of Attack Correction Factor for Laminar Flow over Cylinders

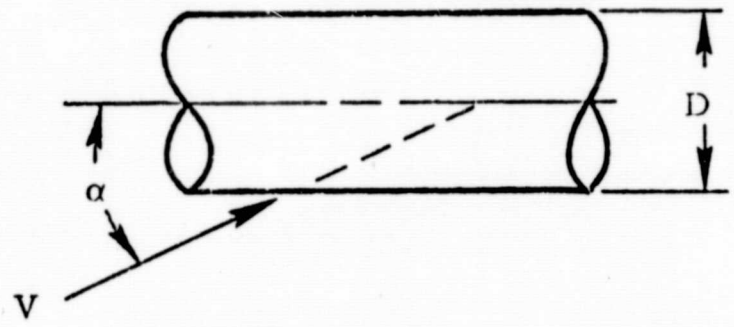

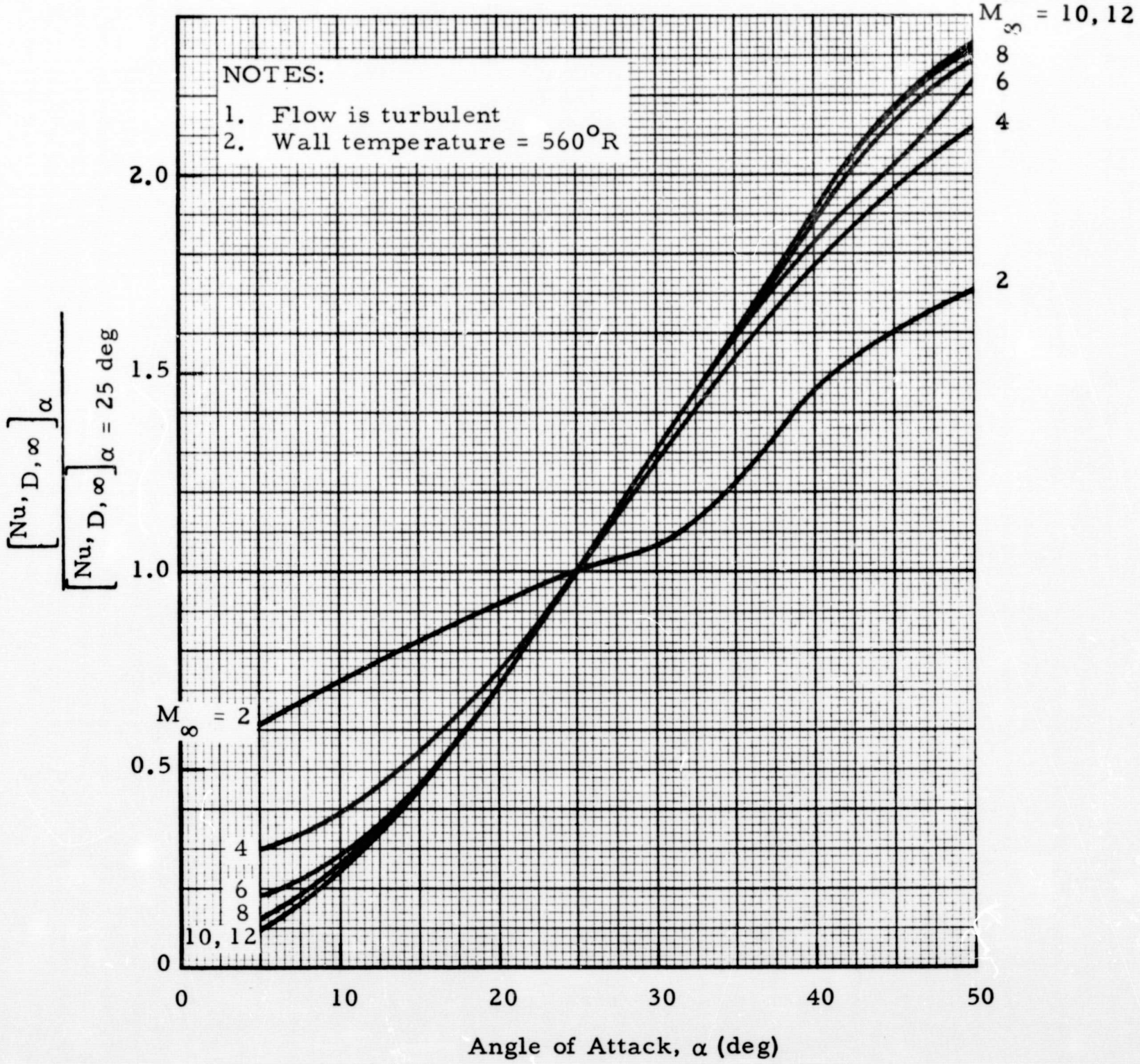

Fig. 4-4 - Angle of Attack Correction Factor for Turbulent Flow over Cylinders

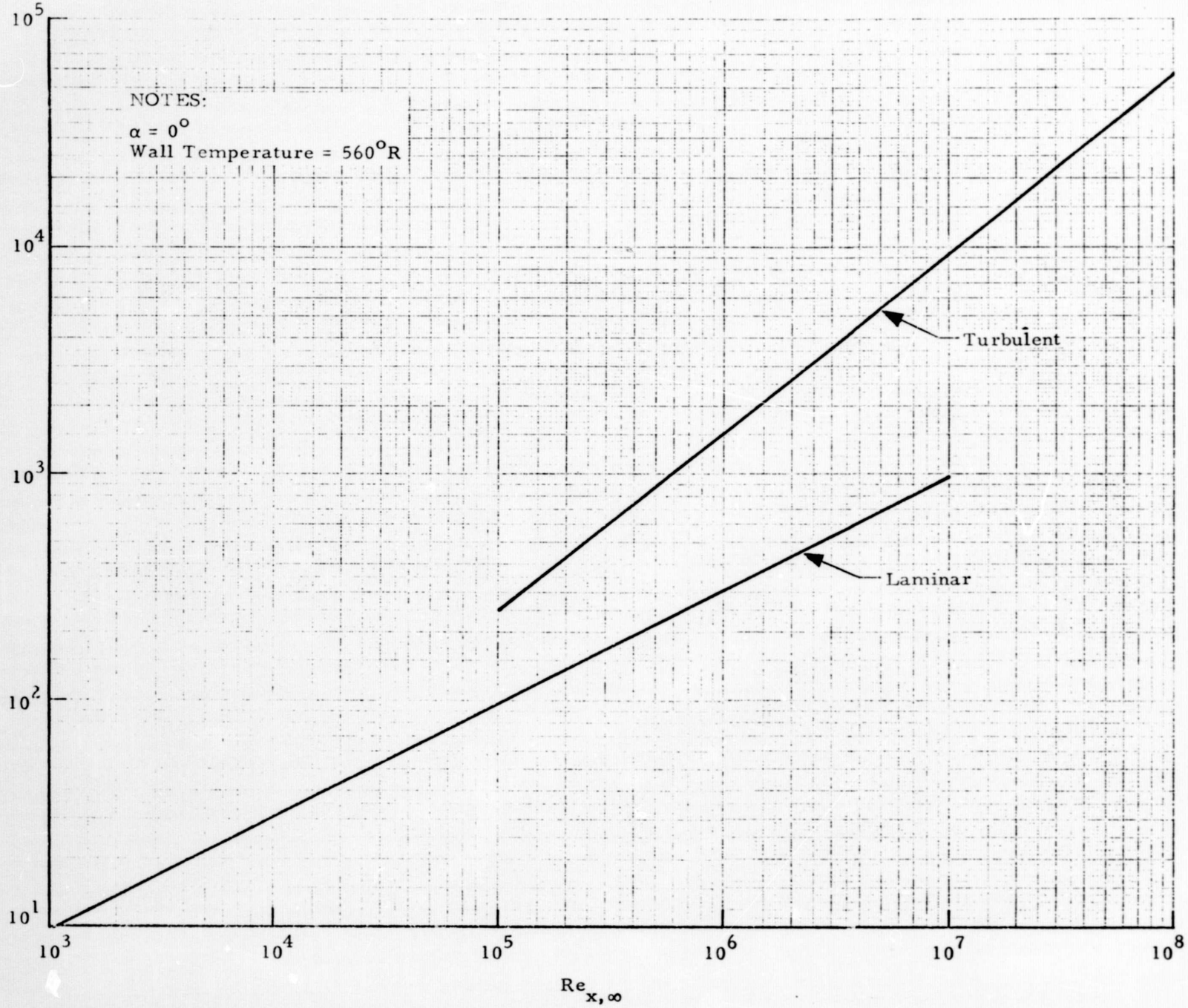

Fig. 4-5 - Freestream Nusselt Number vs Freestream Reynolds Number for Laminar and Turbulent Flow over Cylinder at α = 0 Degrees

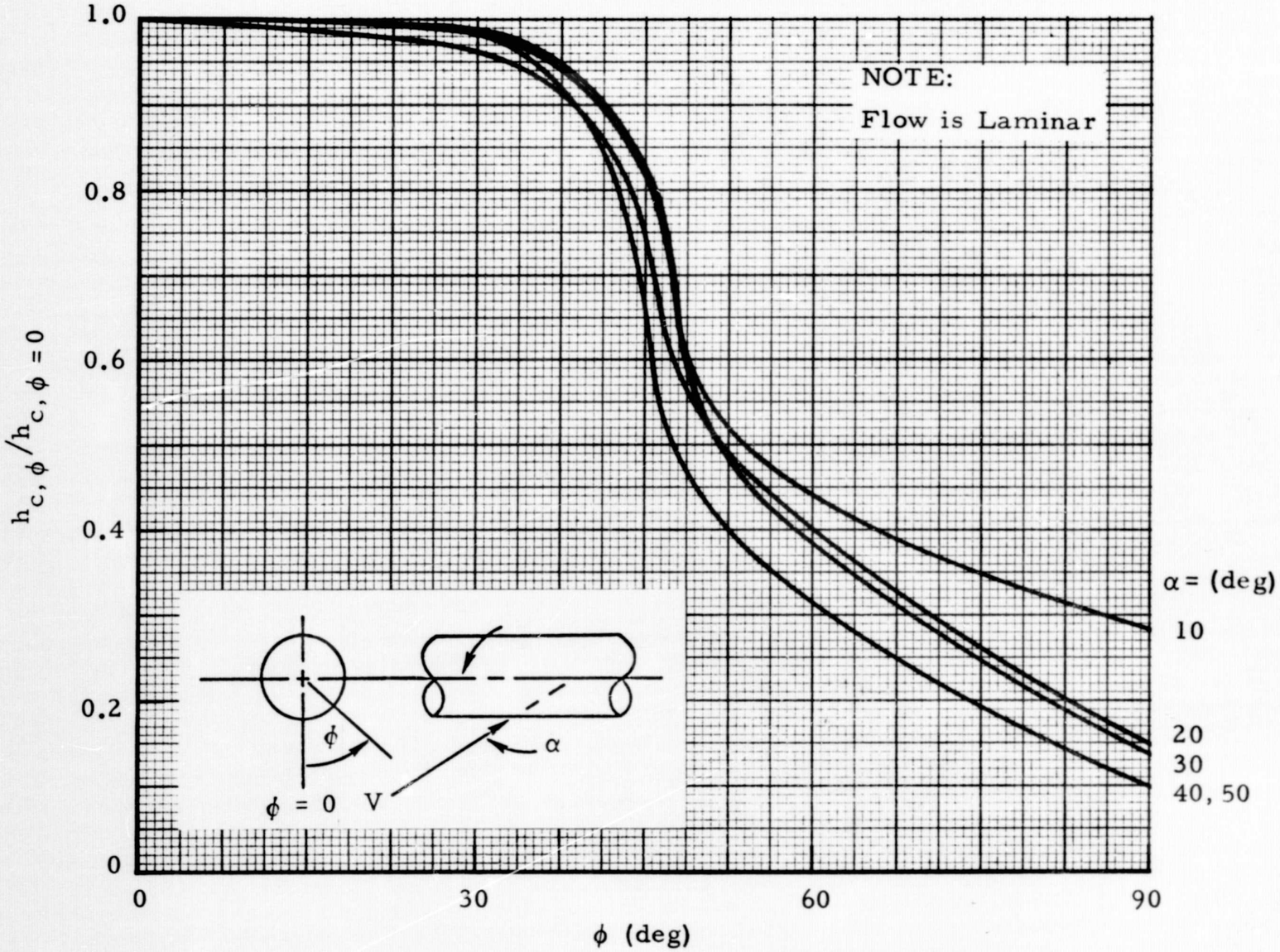

Fig. 4-6 - Circumferential Heat Transfer Coefficient Distribution for Laminar Flow over Infinite Swept Cylinder

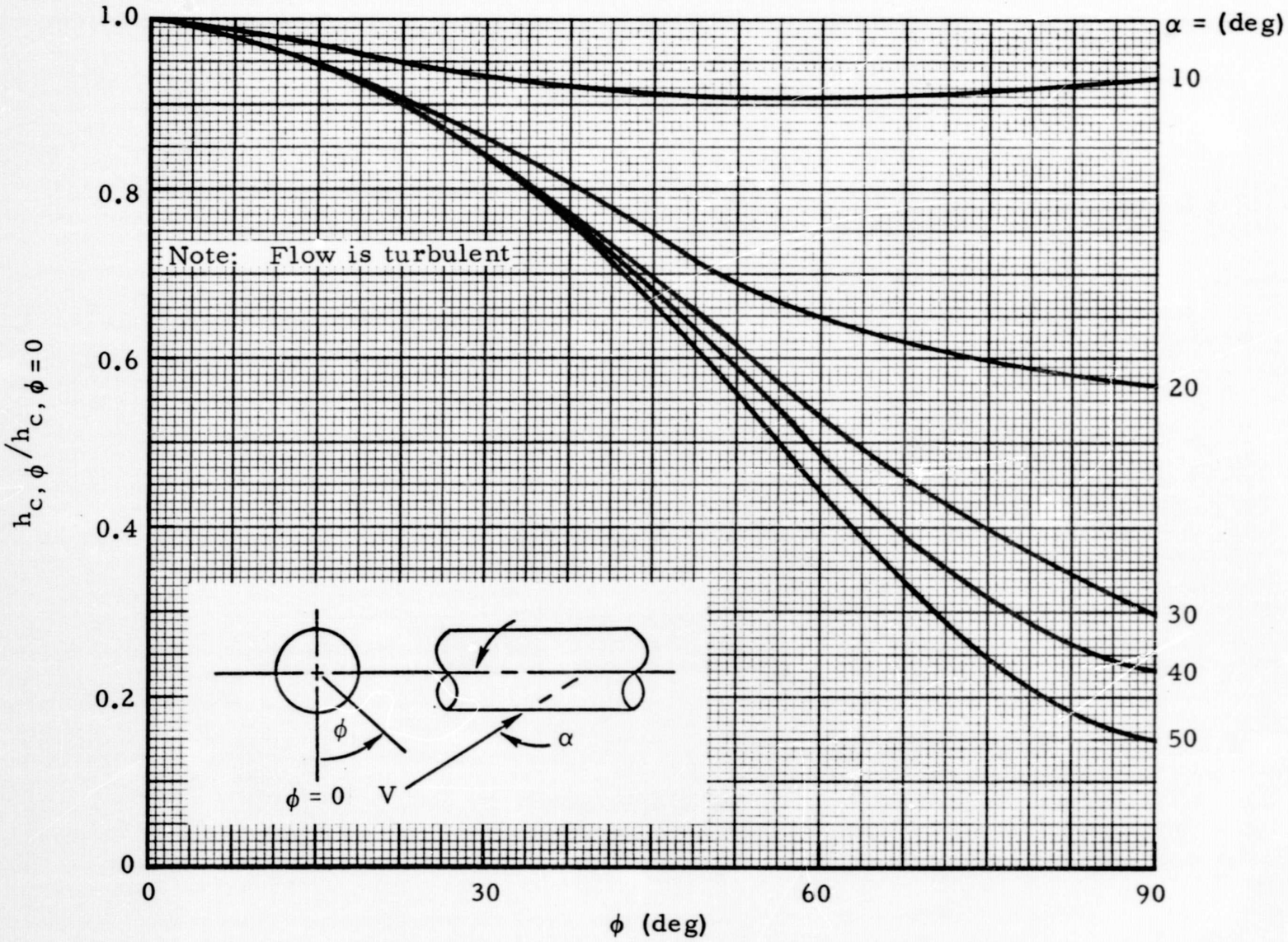

Fig. 4-7 - Circumferential Heat Transfer Coefficient Distribution for Turbulent Flow over Infinite Swept Cylinders

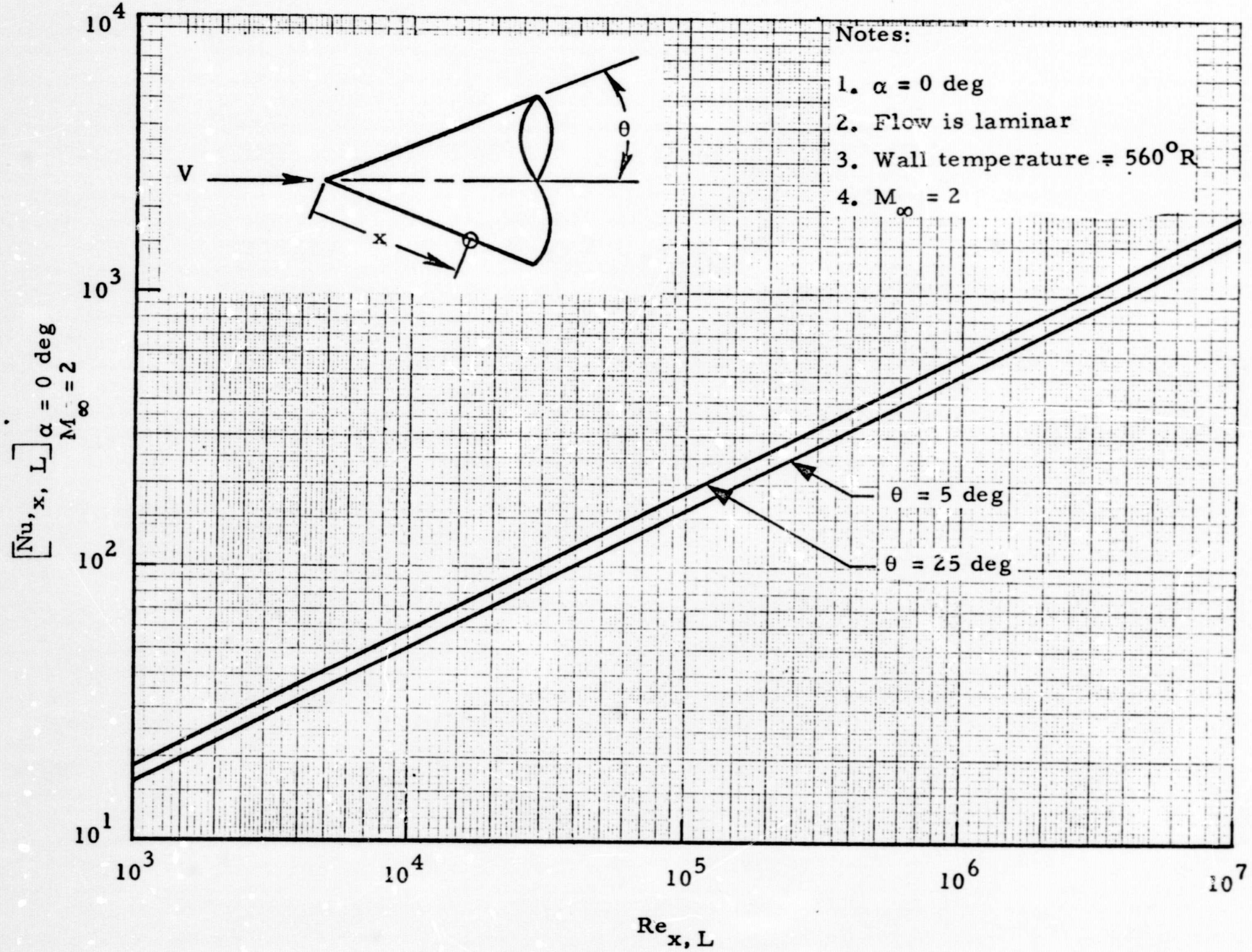

Fig. 4-8 - Local Nusselt Number vs Local Reynolds Number for Laminar Flow over Cones at α = 0 Degrees, $M_\infty = 2$

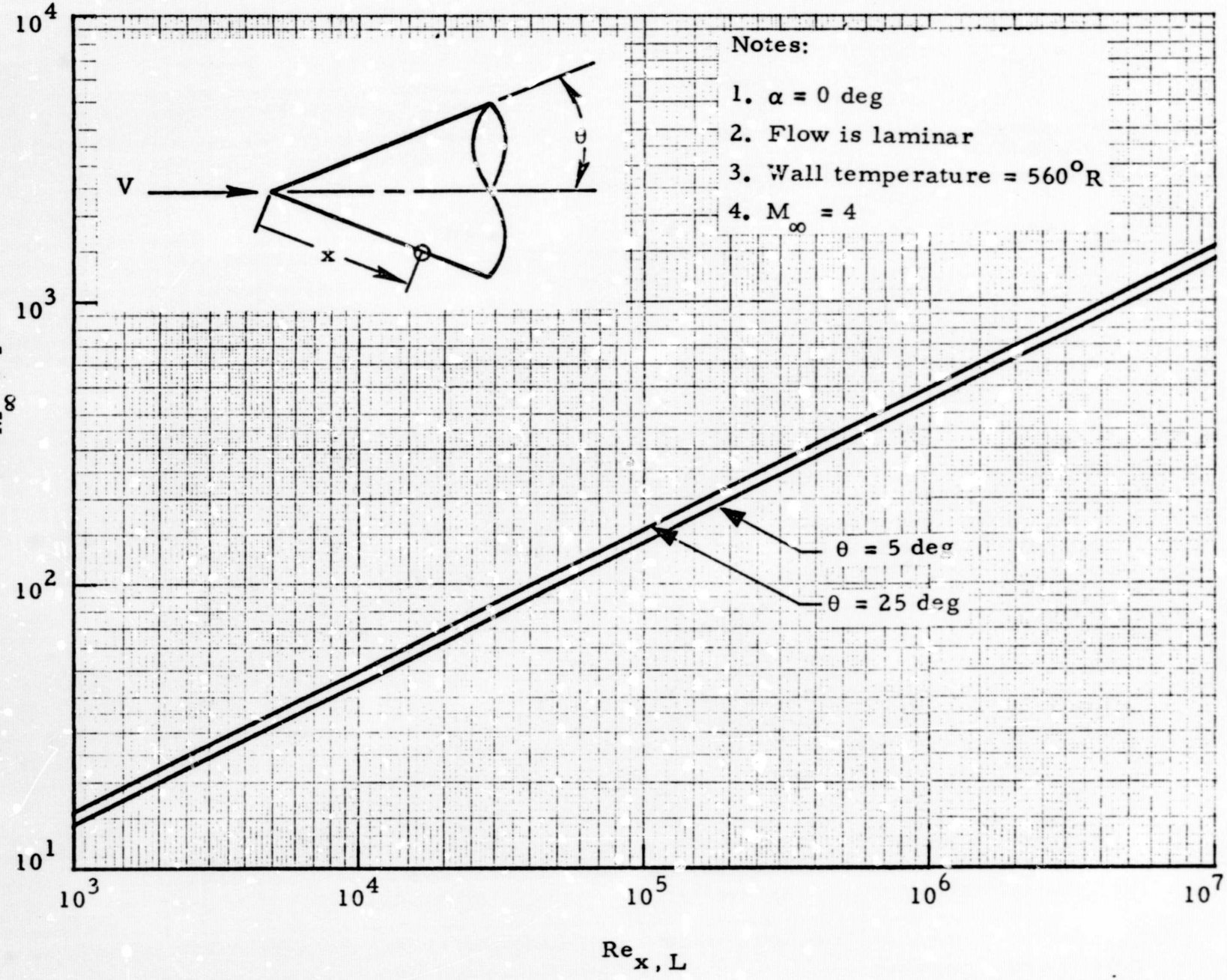

Fig. 4-9 - Local Nusselt Number vs Local Reynolds Number for Laminar Flow over Cones at α = 0 Degrees, M_∞ = 4

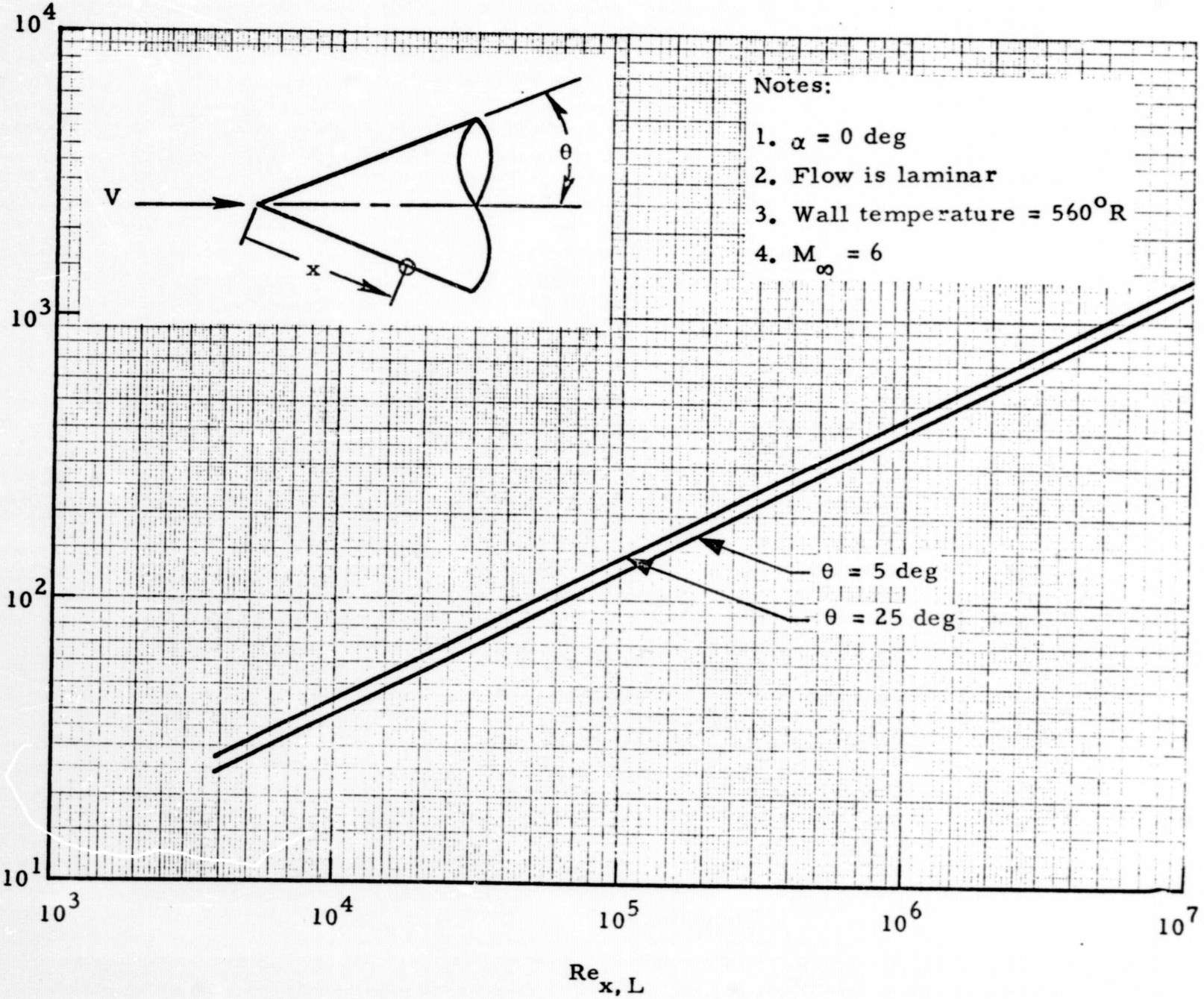

Fig. 4-10 - Local Nusselt Number vs Local Reynolds Number for Laminar Flow over Cones at α = 0 Degrees, M_∞ = 6

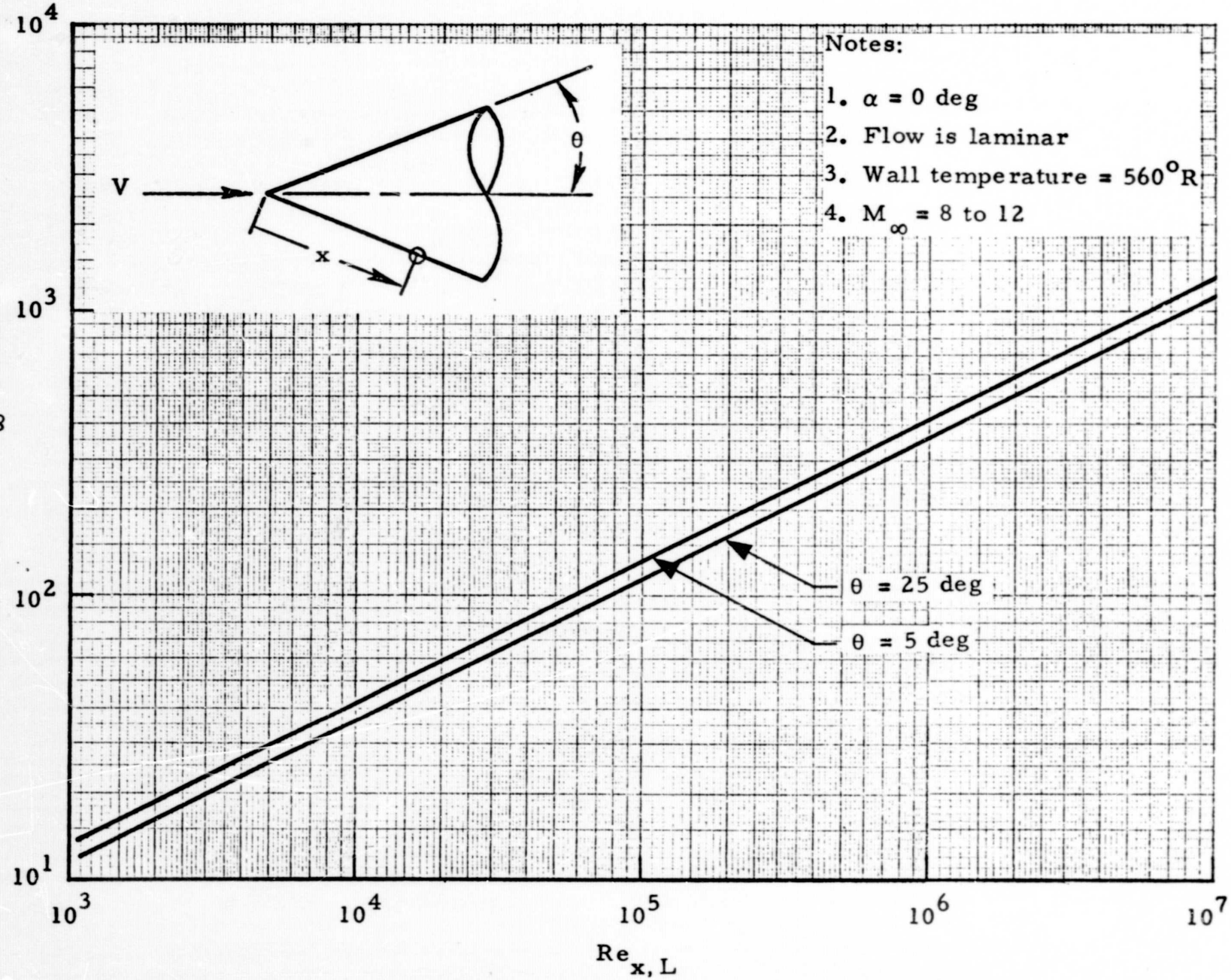

Fig. 4-11 - Local Nusselt Number vs Local Reynolds Number for Laminar Flow over Cones at α = 0 Degrees, M_∞ = 8 to 12

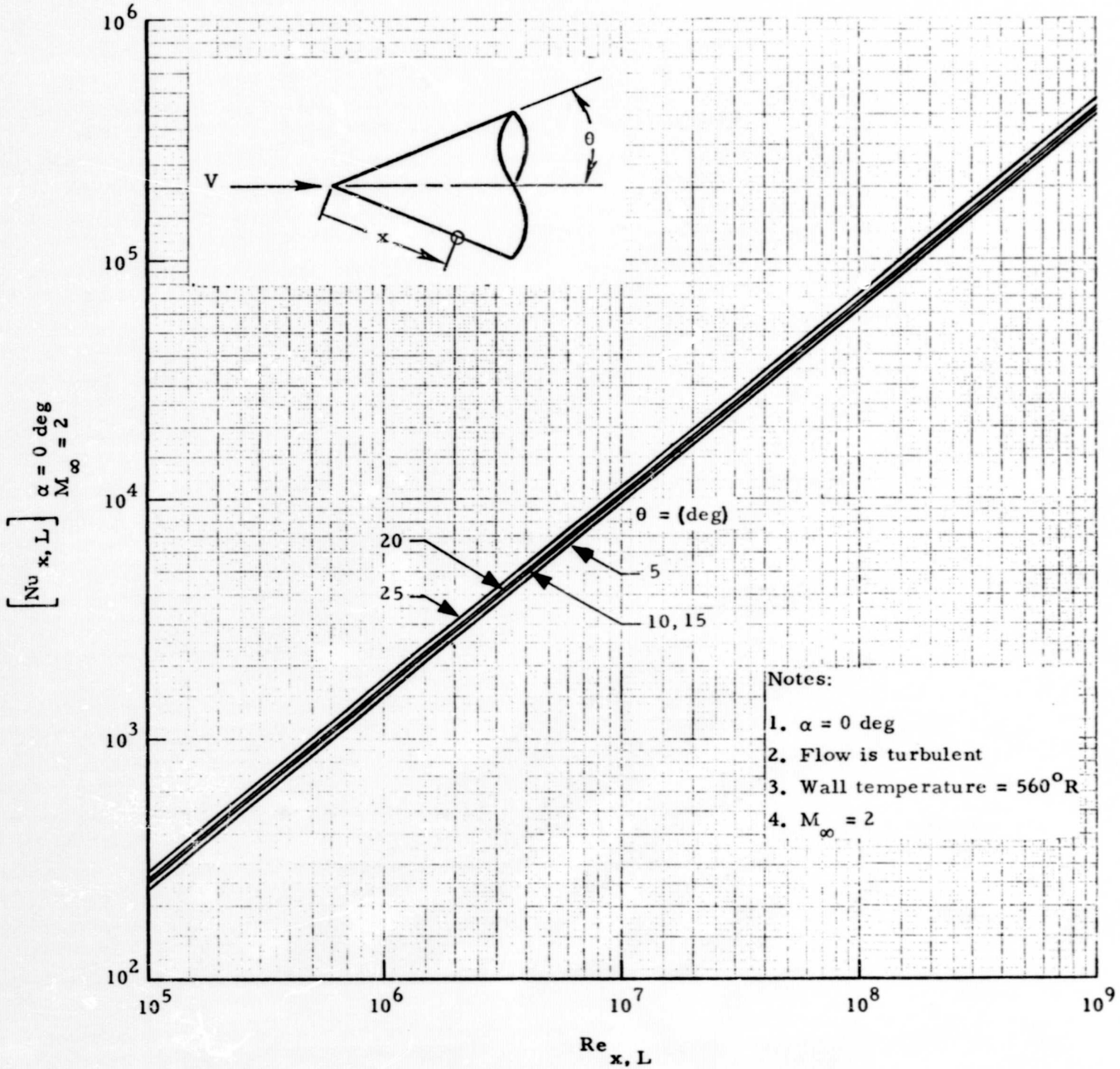

Fig. 4-12 - Local Nusselt Number vs Local Reynolds Number for Turbelent Flow over Cones at α = 0 Degrees, M_∞ = 2

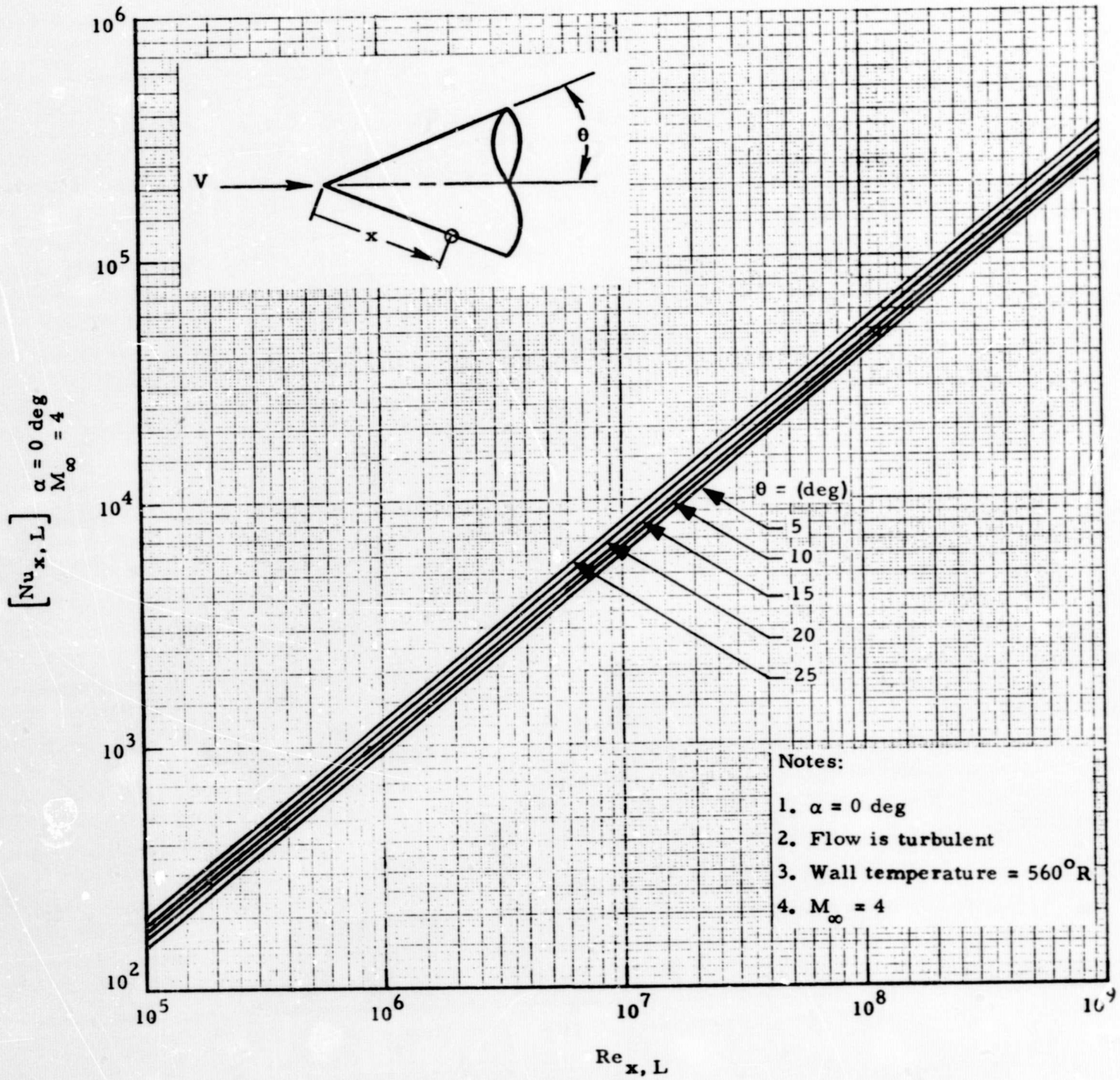

Fig. 4-13 - Local Nusselt Number vs Local Reynolds Number for Turbulent Flow over Cones at α = 0 Degrees, M_∞ = 4

Fig. 4-14 - Local Nusselt Number vs Local Reynolds Number for Turbulent Flow over Cones at α = 0 Degrees, M_∞ = 6

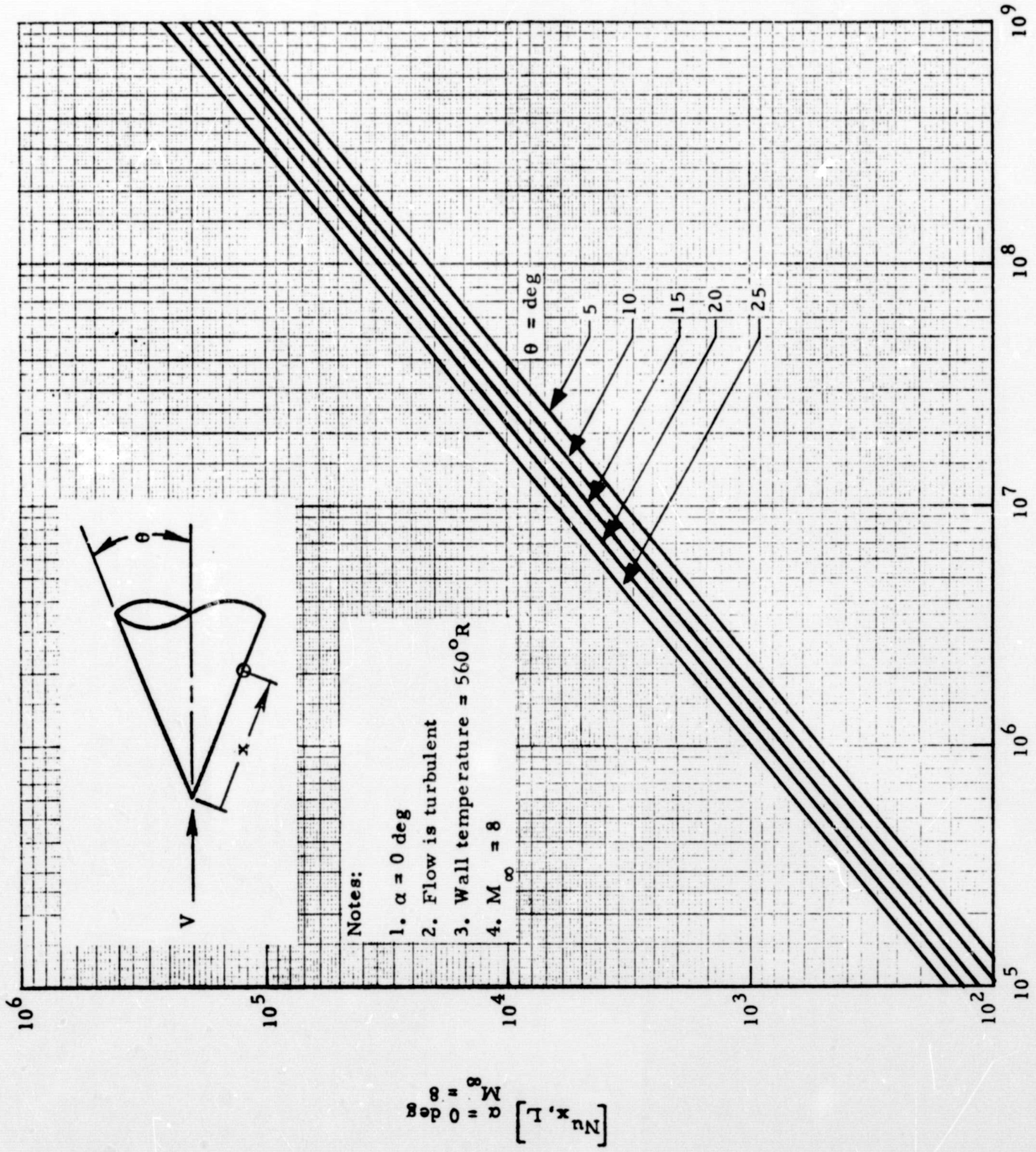

Fig. 4-15 - Local Nusselt Number vs Local Reynolds Number for Turbulent Flow over Cones at α = 0 Degrees, M_∞ = 8

Fig. 4-16 - Local Nusselt Number vs Local Reynolds Number for Turbulent Flow over Cones at α = 0 Degrees, M_∞ = 10 and 12

NOTES: 1. Wall Temperature = 560°R
2. Altitude = 0 to 400,000 feet

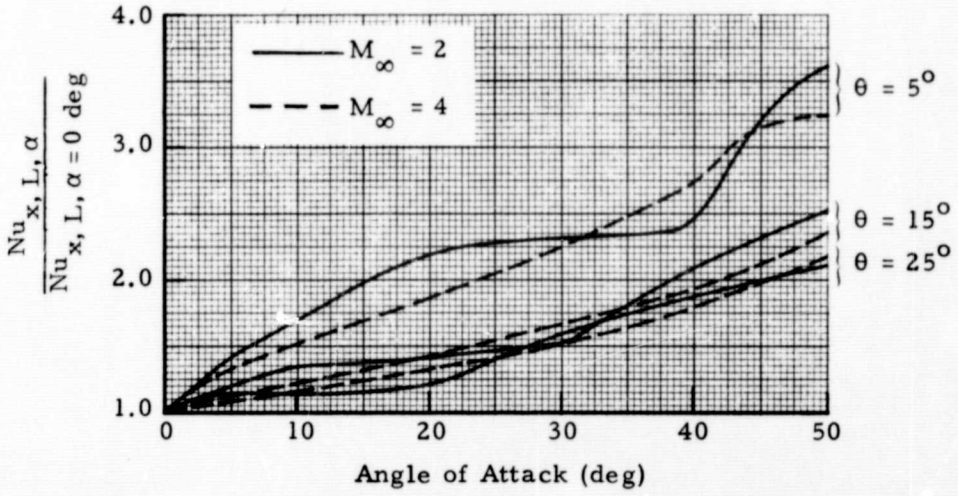

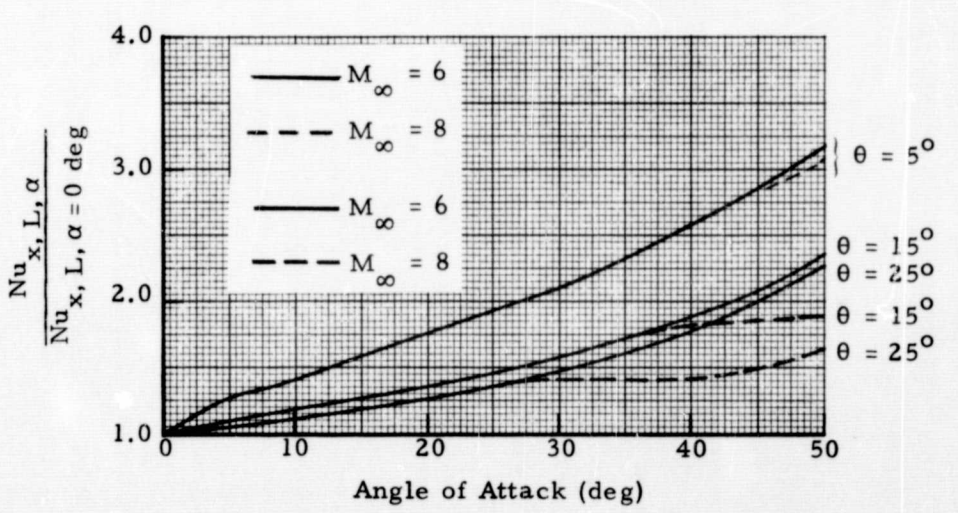

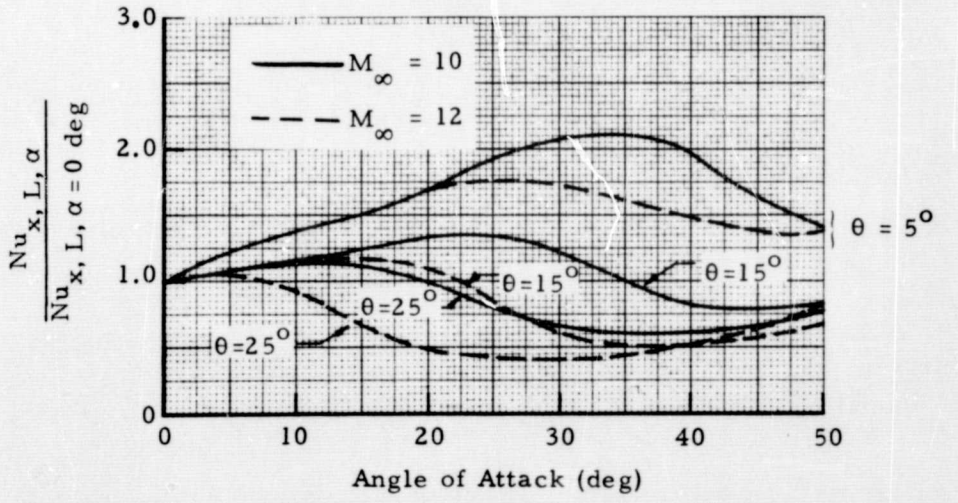

Fig. 4-17 - Angle of Attack Correction Factor for Laminar Flow over Cones for M_∞ = 2, 4, 6, 8, 10, 12

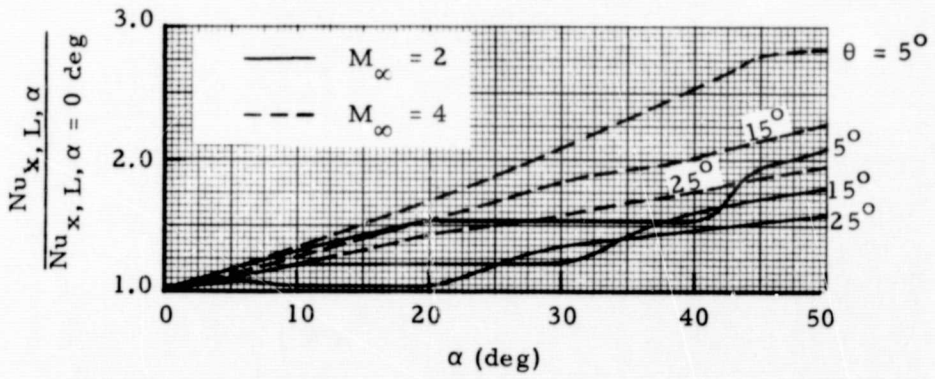

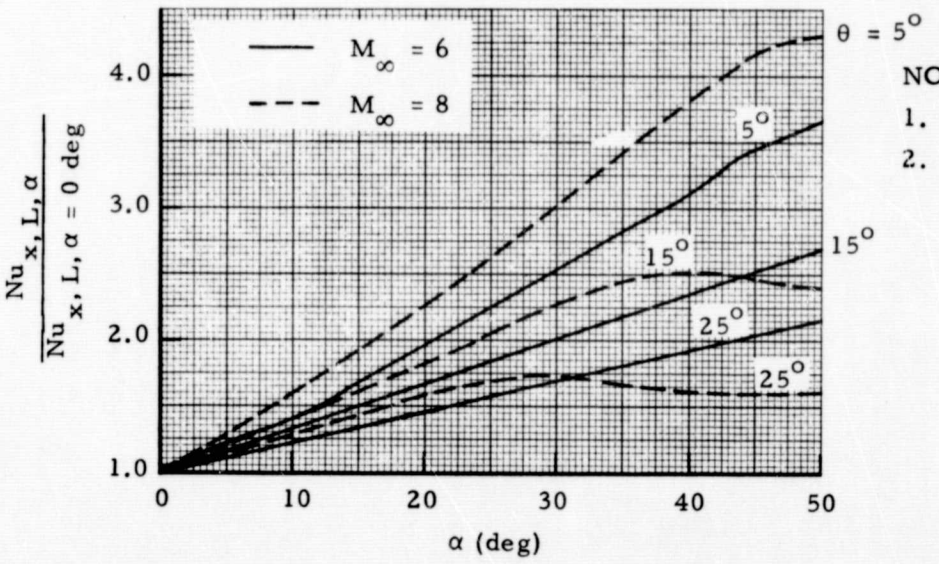

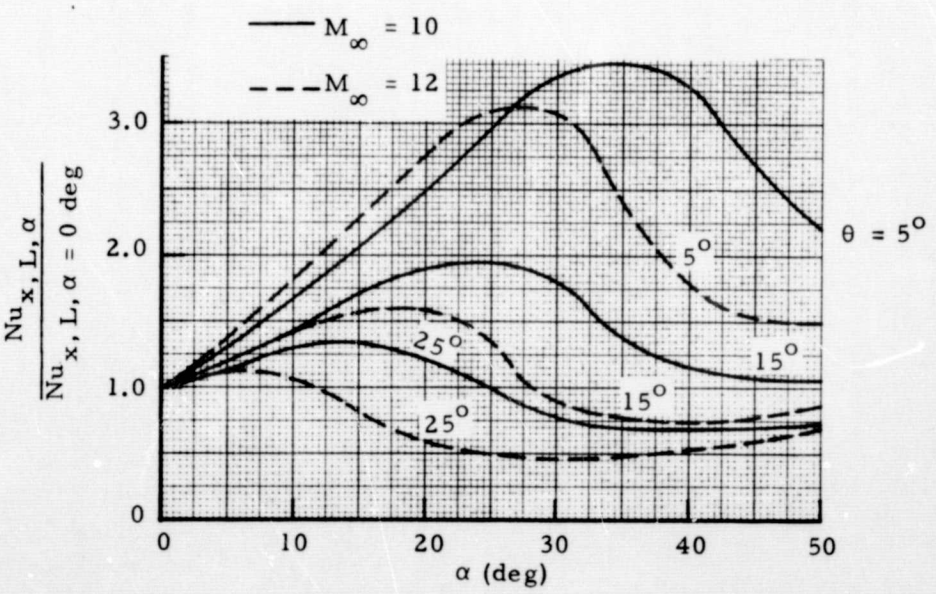

NOTES:

1. Wall Temperature = 560°R
2. Altitude = 0 to 400,000 ft.

Fig. 4-18 - Angle of Attack Correction Factor for Turbulent Flow over Cones for M_∞ = 2, 4, 6, 8, 10, 12

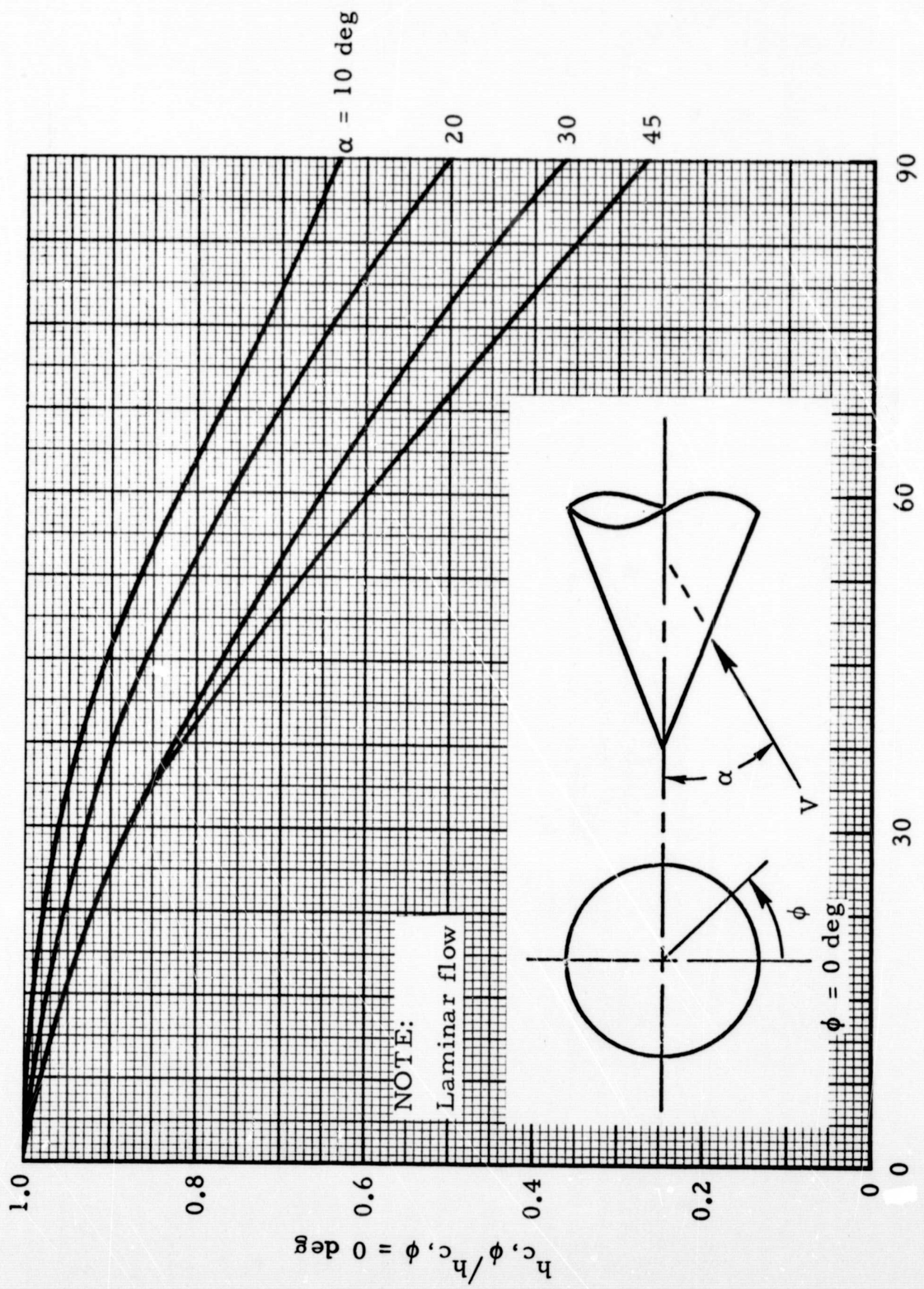

Fig. 4-19 - Circumferential Heat Transfer Coefficient Distribution for Laminar Flow over Cones

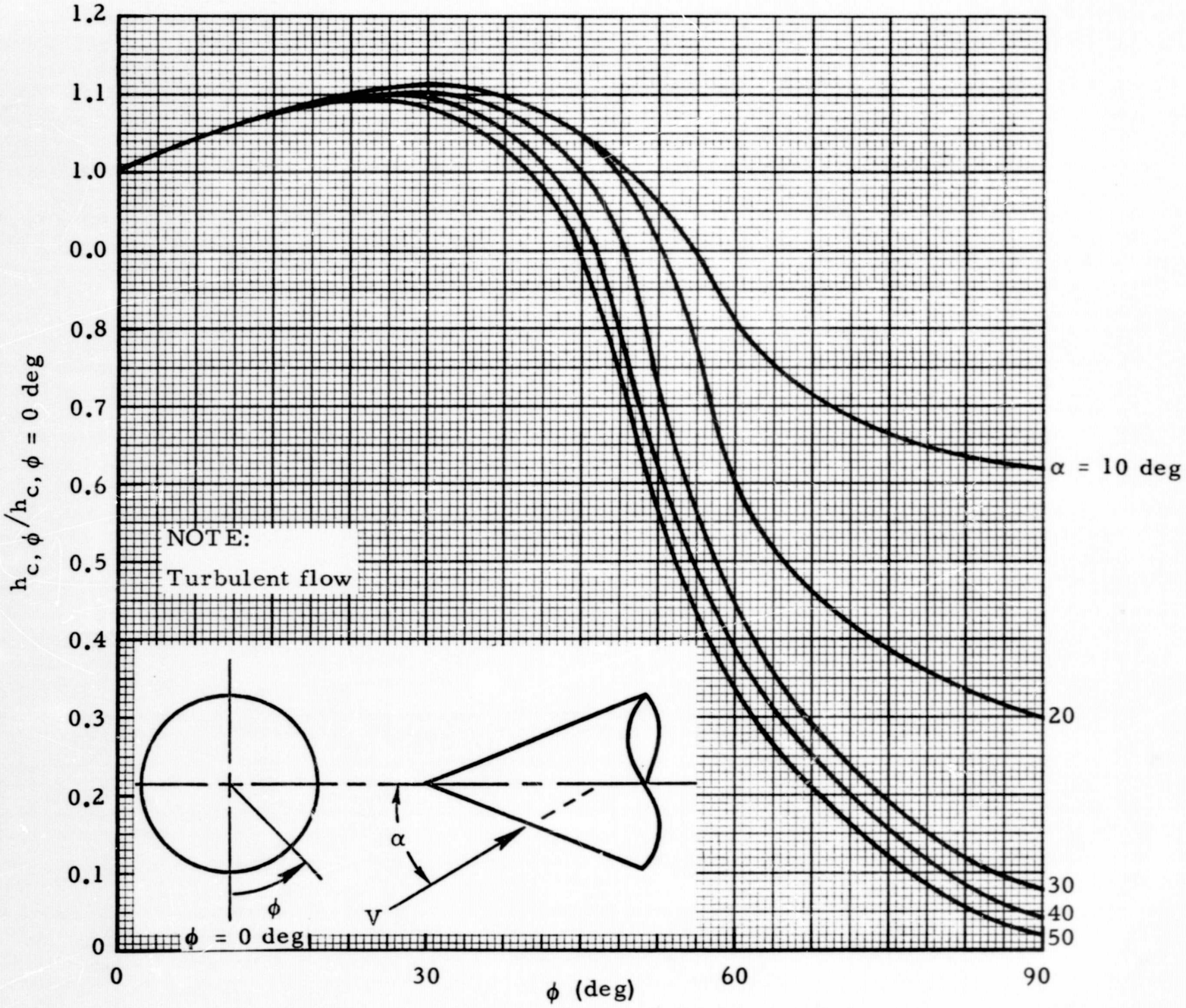

Fig. 4-20 - Circumferential Heat Transfer Coefficient Distribution for Turbulent Flow over Cones

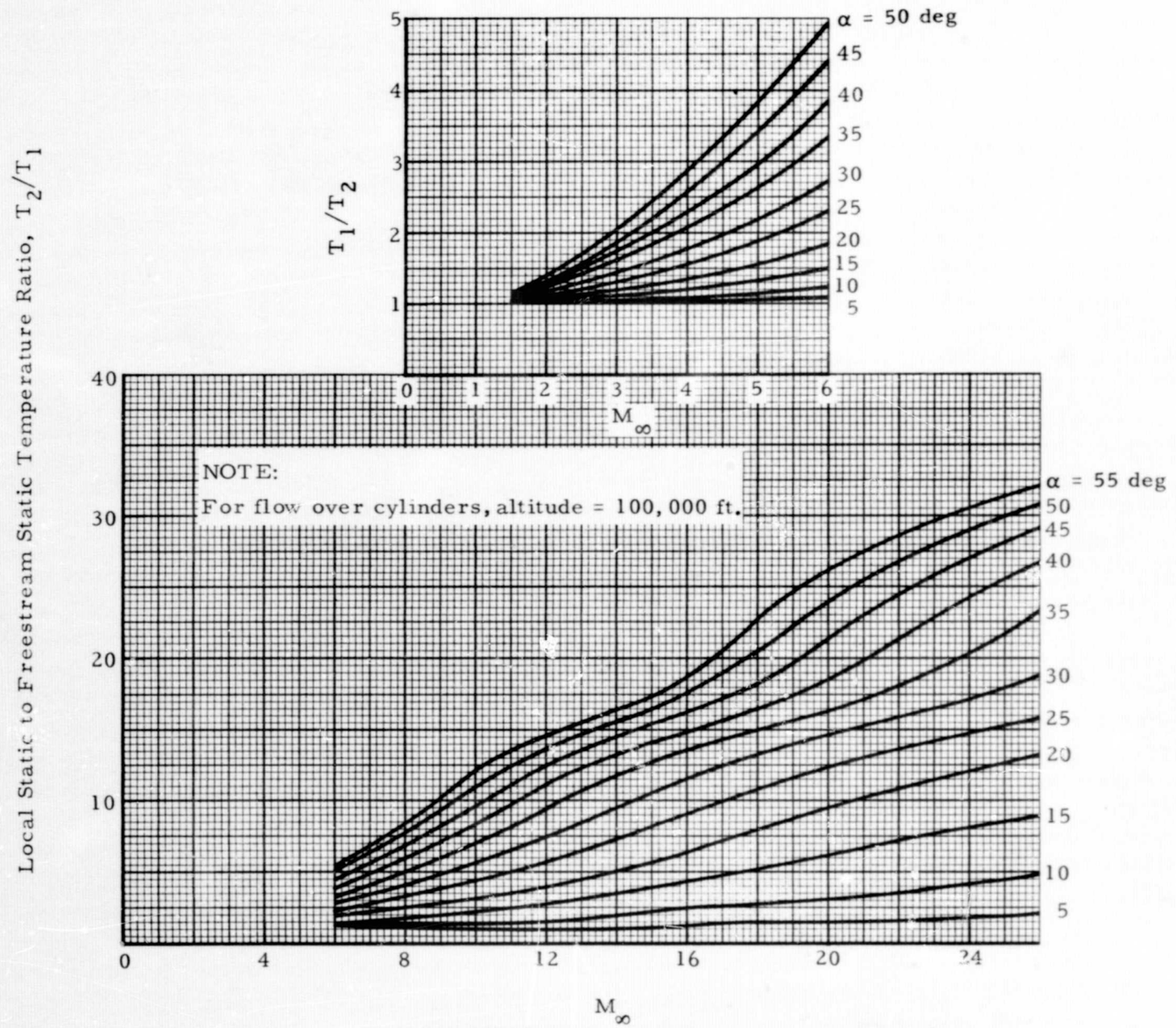

Fig. 4-21 - The Ratio of Local Static Temperature on Cylinder to Freestream Temperature vs M_∞

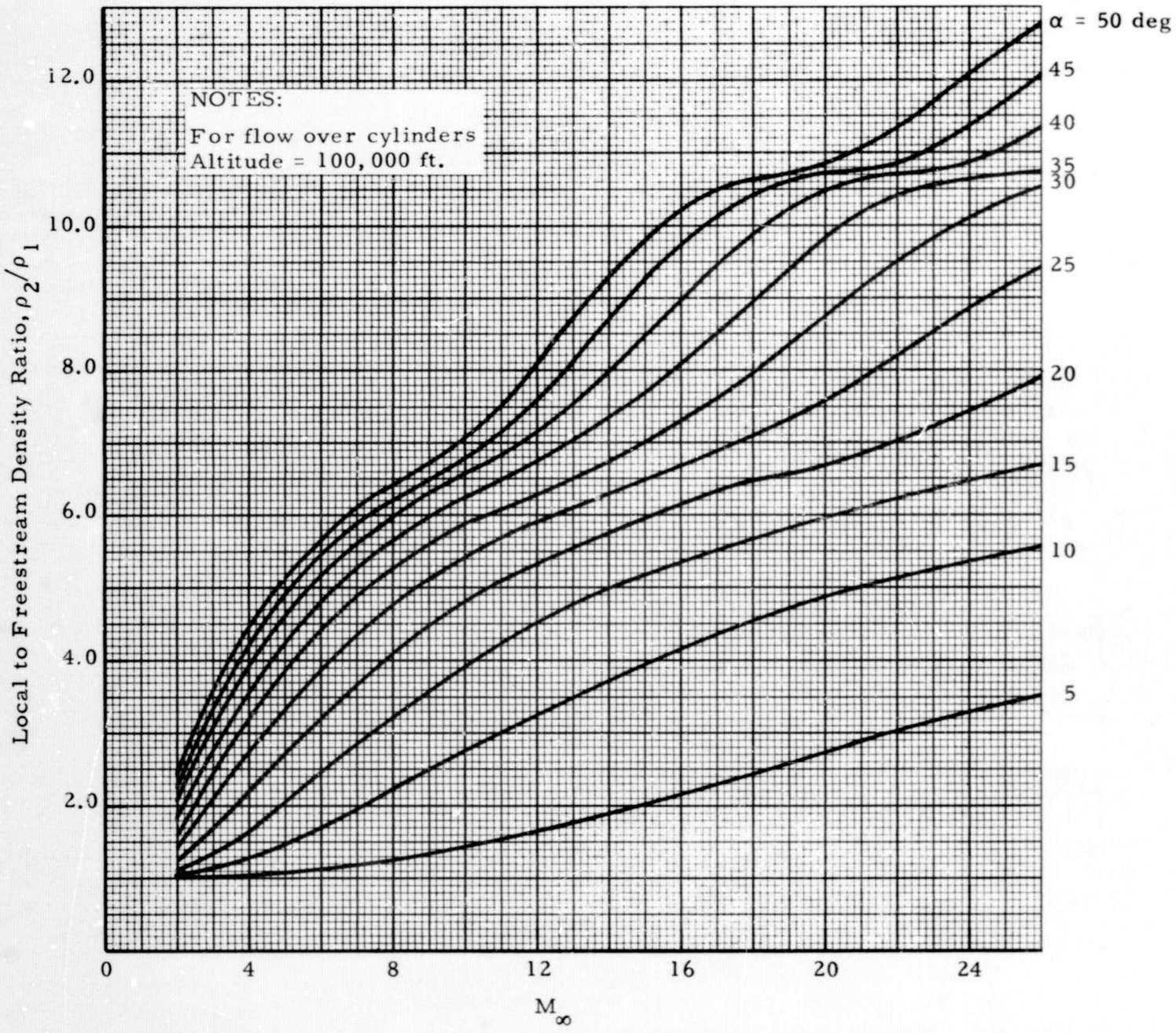

Fig. 4-22 - The Ratio of Local Density on Cylinder to Freestream Density vs M_∞

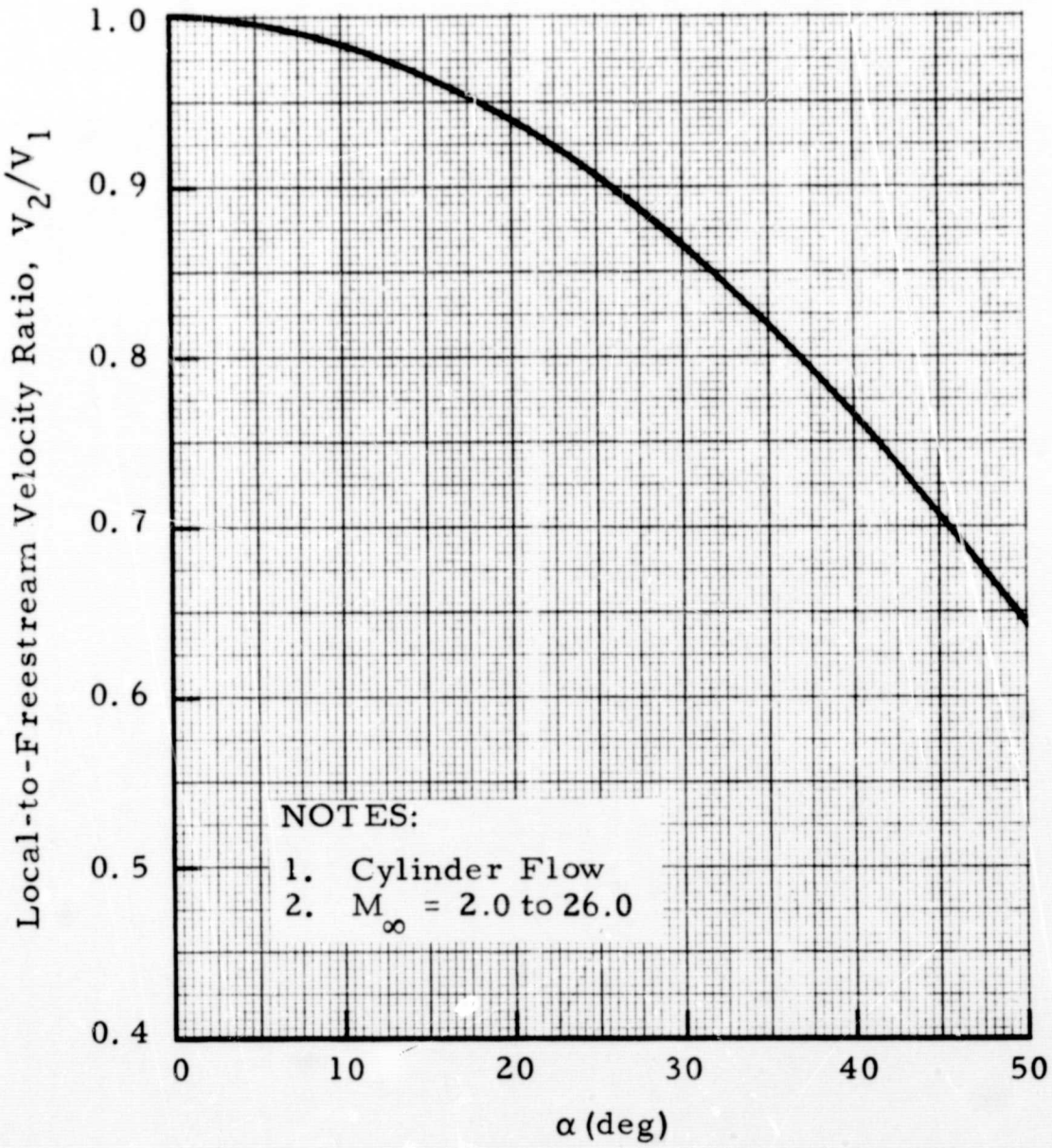

Fig. 4-23 - The Ratio of Local Velocity on Cylinder to Freestream Velocity vs α

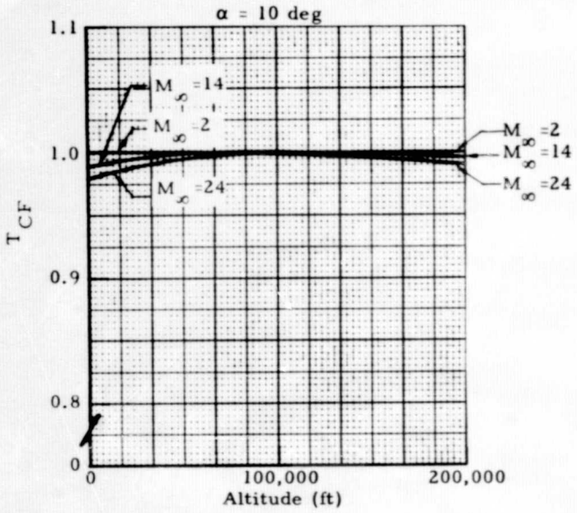

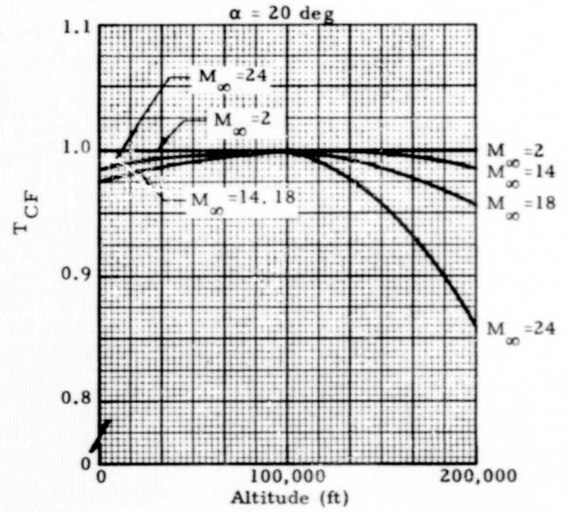

NOTES:

1. $T_{CF} = \dfrac{\left[\dfrac{T_2}{T_1}\right] \text{ at Altitude}}{\left[\dfrac{T_2}{T_1}\right] \text{ at Altitude = 100,000 feet}}$

2. For Flow over Cylinders

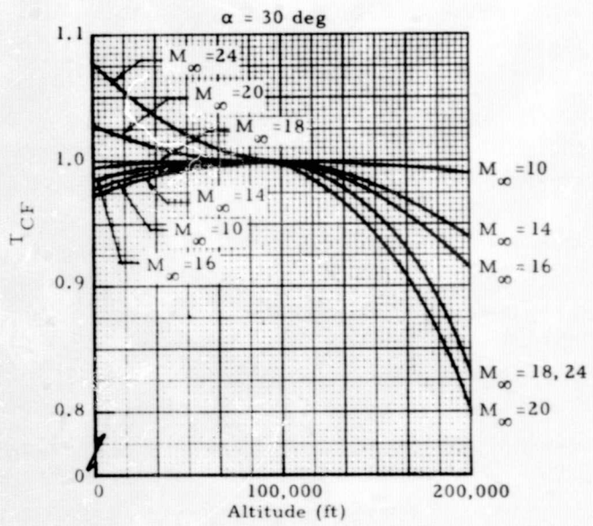

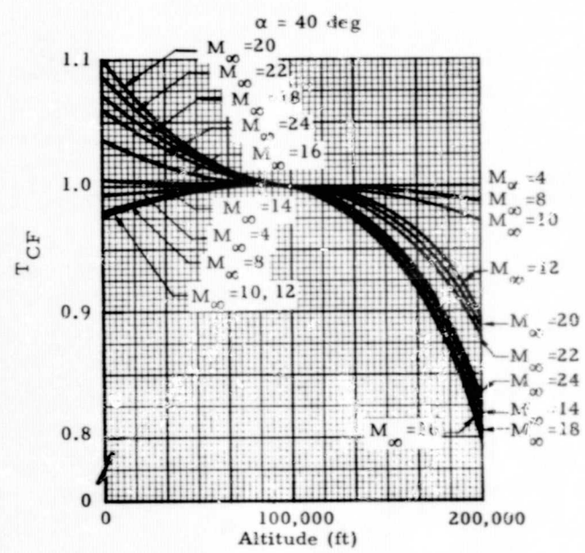

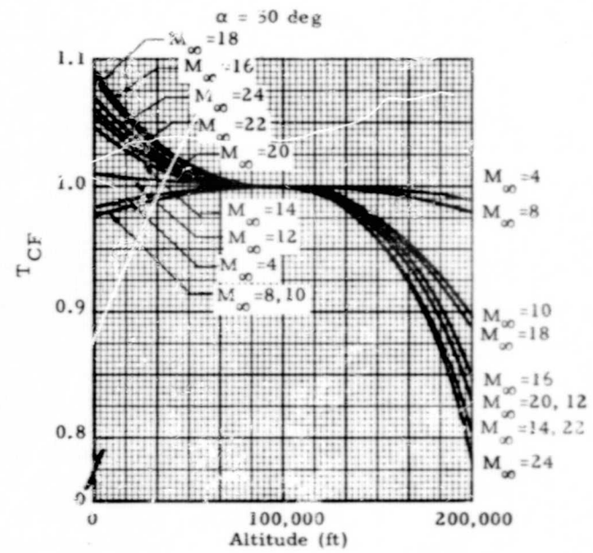

Fig. 4-24 - Altitude and Mach Number Correction Factors for Static Temperature Ratios on Cylinders

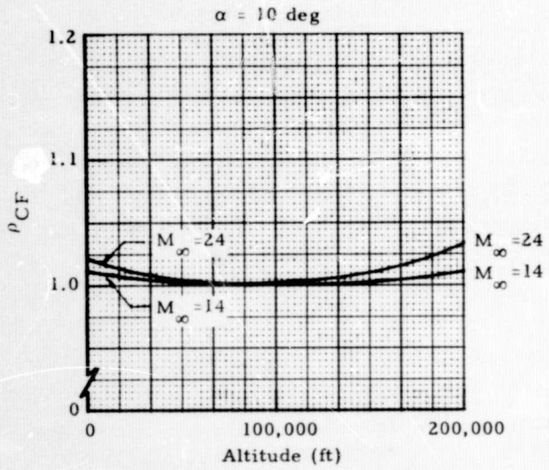

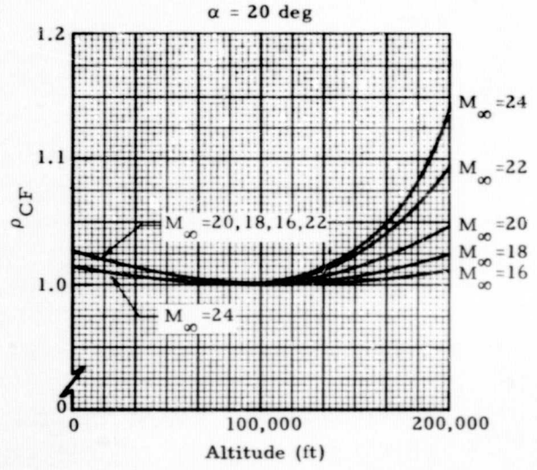

NOTES:

1. $\rho_{CF} = \dfrac{\left[\dfrac{\rho_2}{\rho_1}\right] \text{ at Altitude}}{\left[\dfrac{\rho_2}{\rho_1}\right] \text{ at Altitude = 100,000 ft}}$

2. For Flow on Cylinder

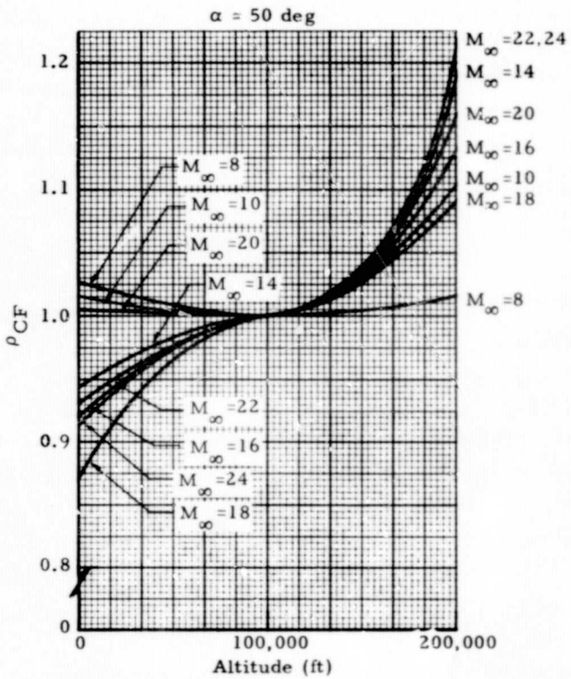

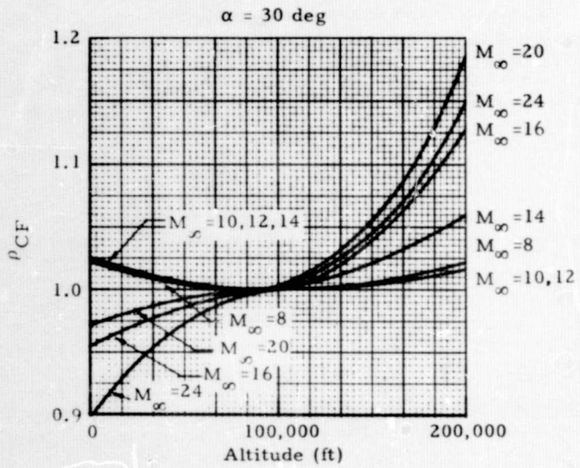

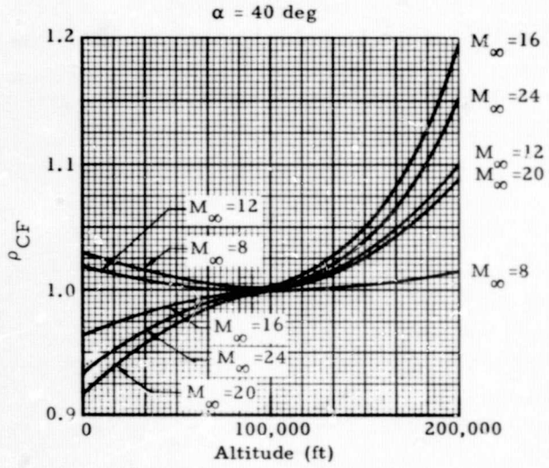

Fig. 4-25 - Altitude and Mach Number Correction Factors for Density Ratios on Cylinders

Fig. 4-26 - The Ratio of Local Static Temperature on Cones to Freestream Static Temperature vs M_∞

Fig. 4-27 - The Ratio of Local Density on Cones to Freestream Density vs M_∞

Fig. 4-28 - The Ratio of Local Velocity on Cones to Freestream Velocity vs M_∞

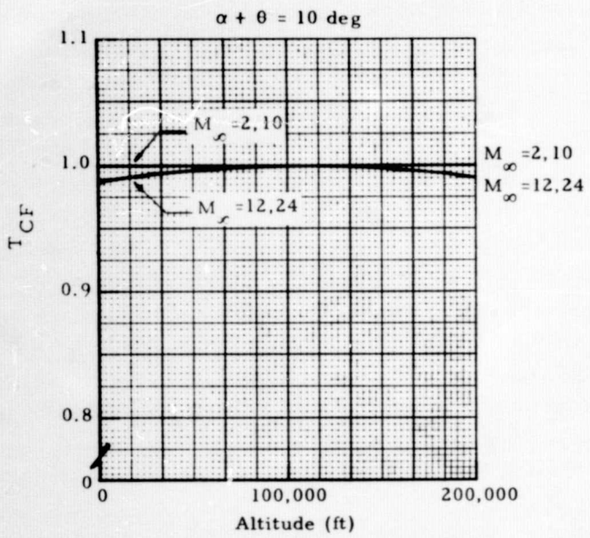

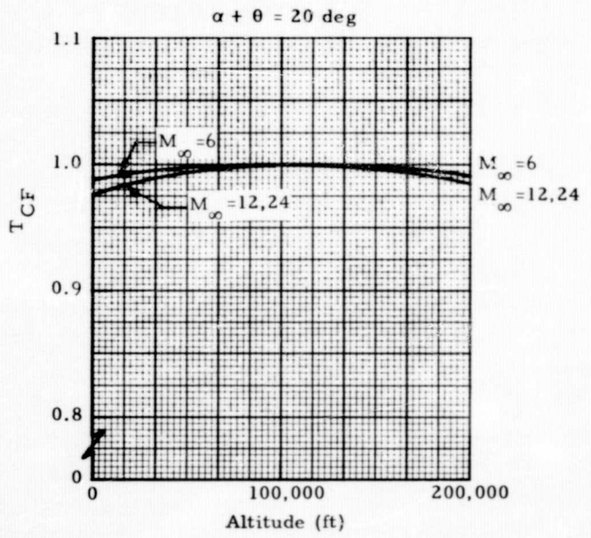

NOTES:

1. $T_{CF} = \dfrac{\left[\dfrac{T_2}{T_1}\right]_{\text{at Altitude}}}{\left[\dfrac{T_2}{T_1}\right]_{\text{at Altitude = 100,000 feet}}}$

2. For Flow on Cones

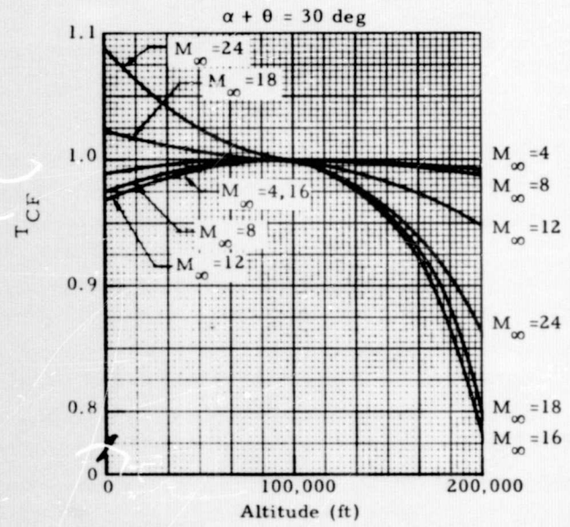

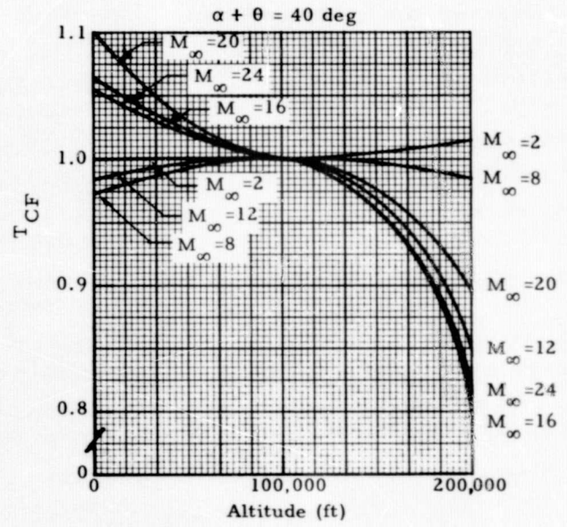

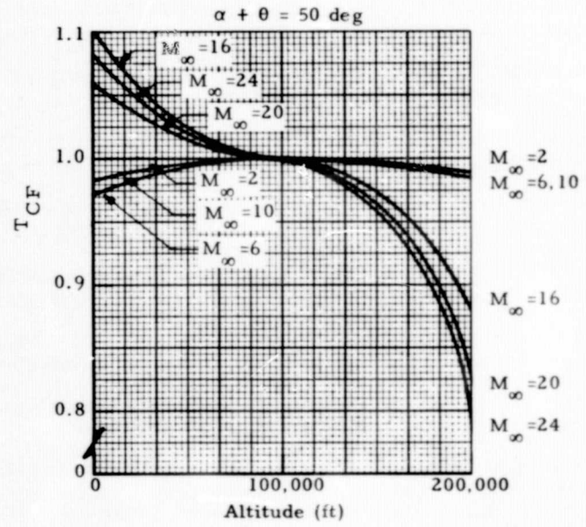

Fig. 4-29 - Altitude and Mach Number Correction Factors for Static Temperature Ratios on Cones

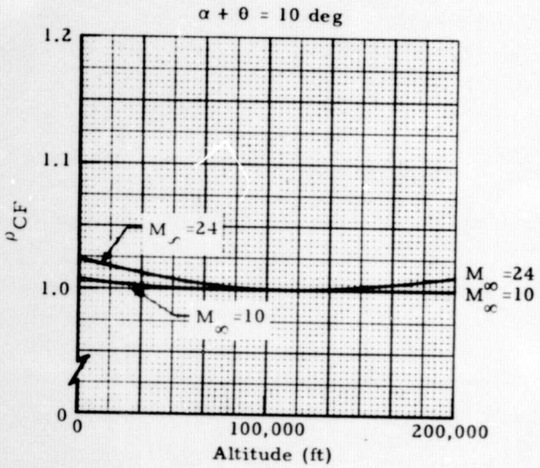

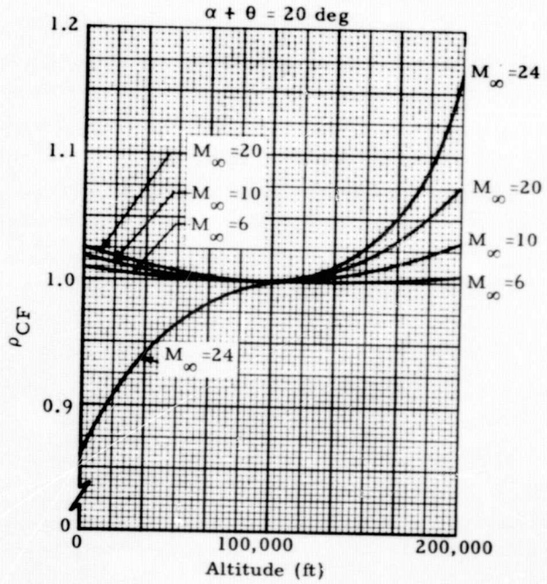

NOTES: 1. $\rho_{CF} = \dfrac{\left[\dfrac{\rho_2}{\rho_1}\right] \text{at Altitude}}{\left[\dfrac{\rho_2}{\rho_1}\right] \text{at Altitude = 100,000}}$

2. For Flow over Cones

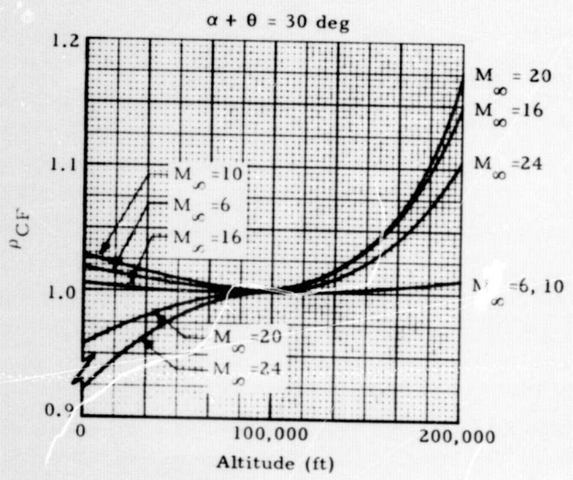

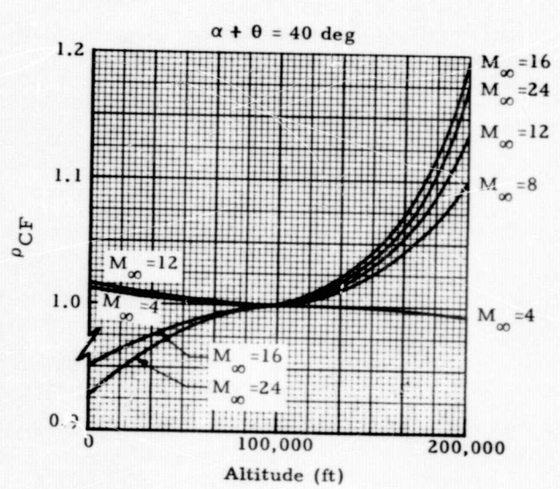

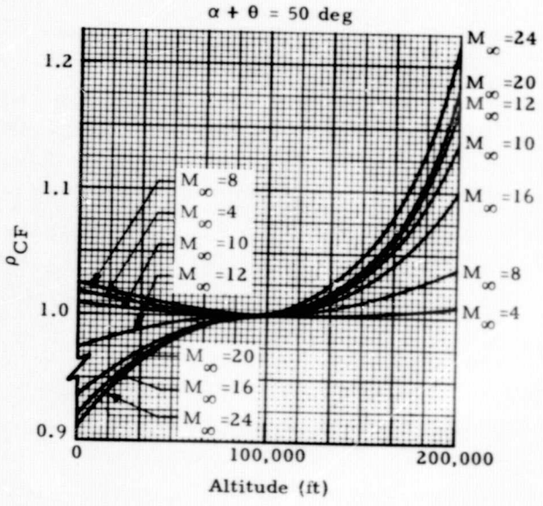

Fig. 4-30 - Altitude and Mach Number Correction Factors for Density Ratios on Cones

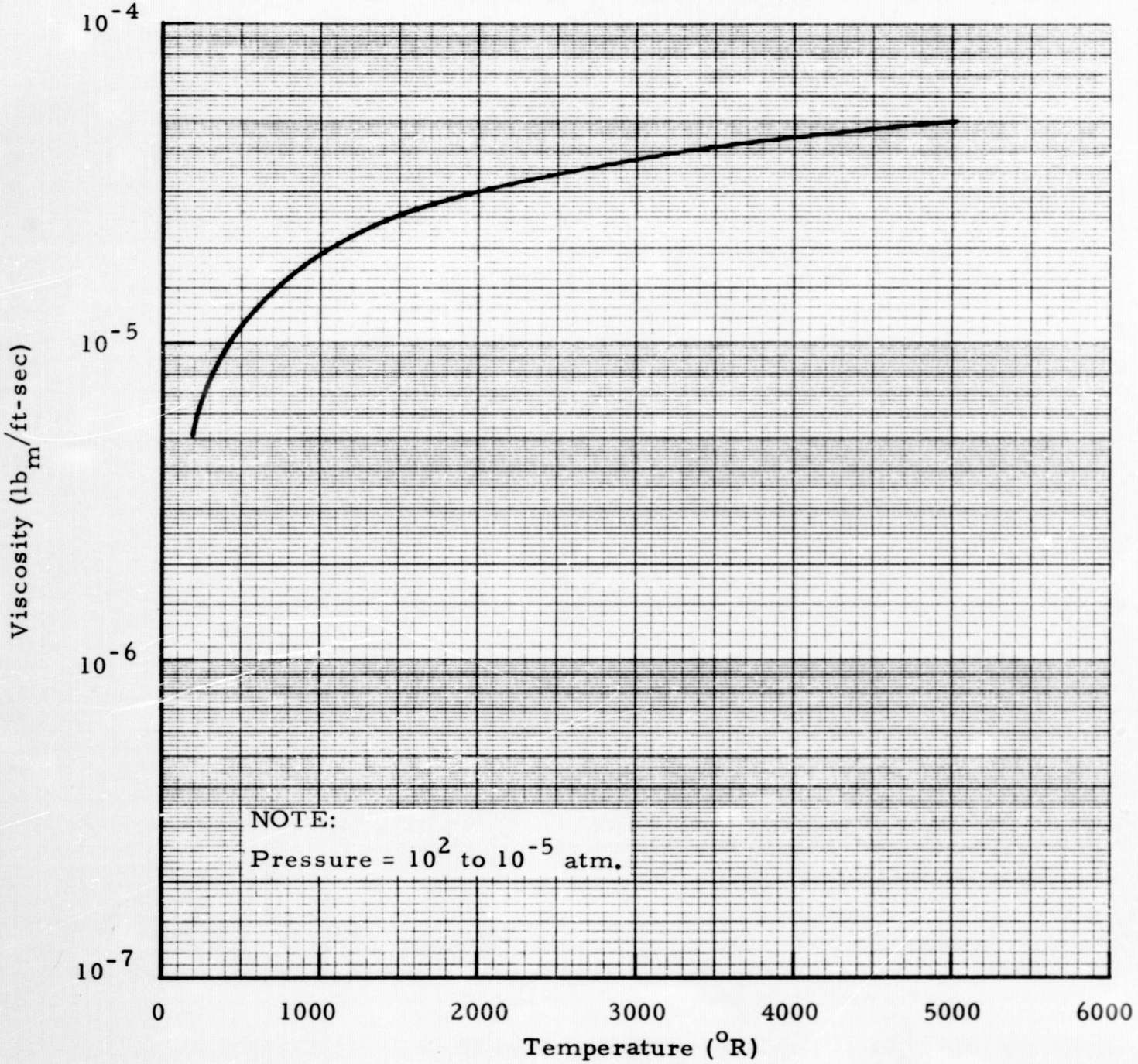

Fig. 4-31 - Viscosity vs Temperature for Air

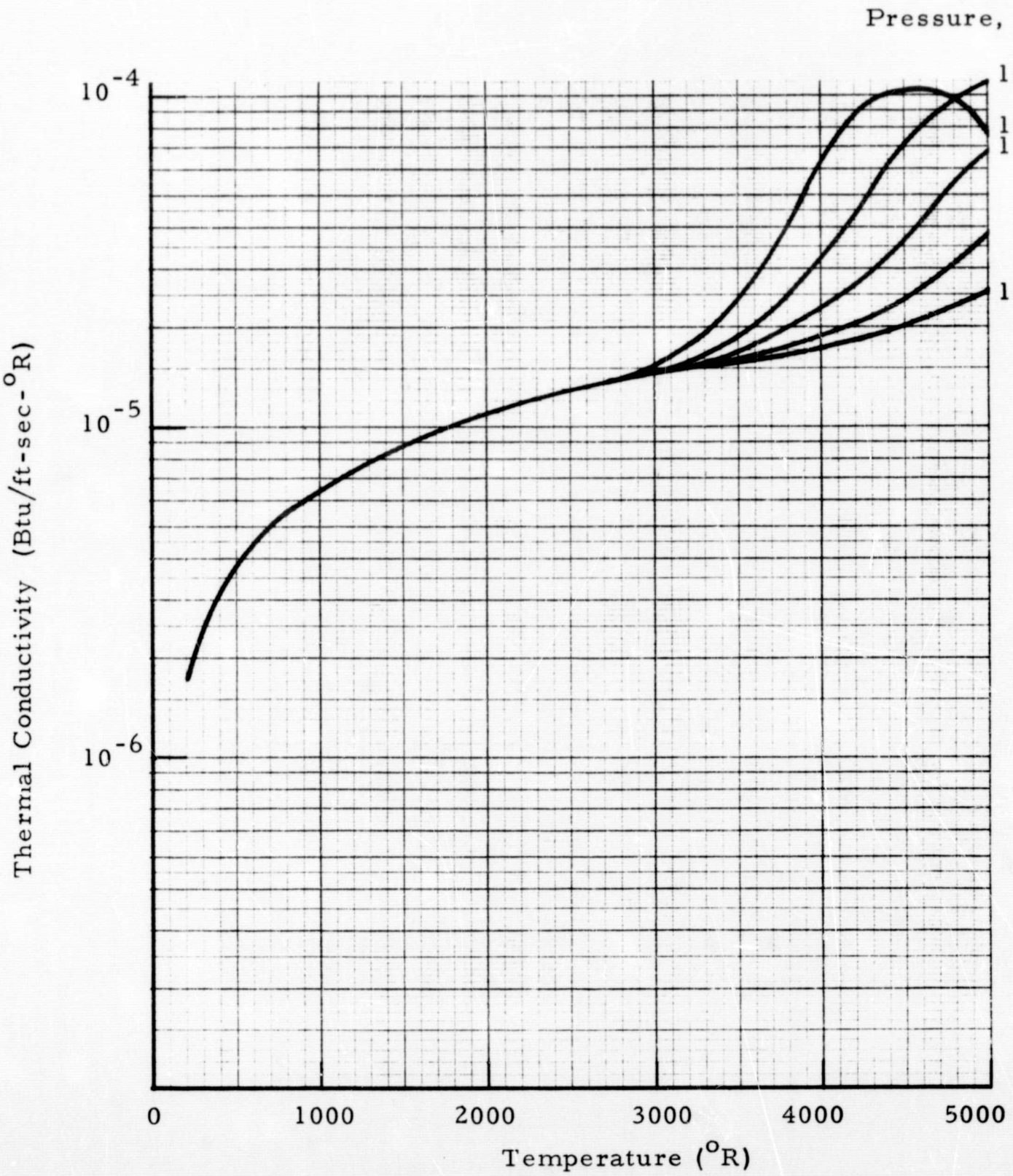

Fig. 4-32 - Thermal Conductivity vs Temperature for Air

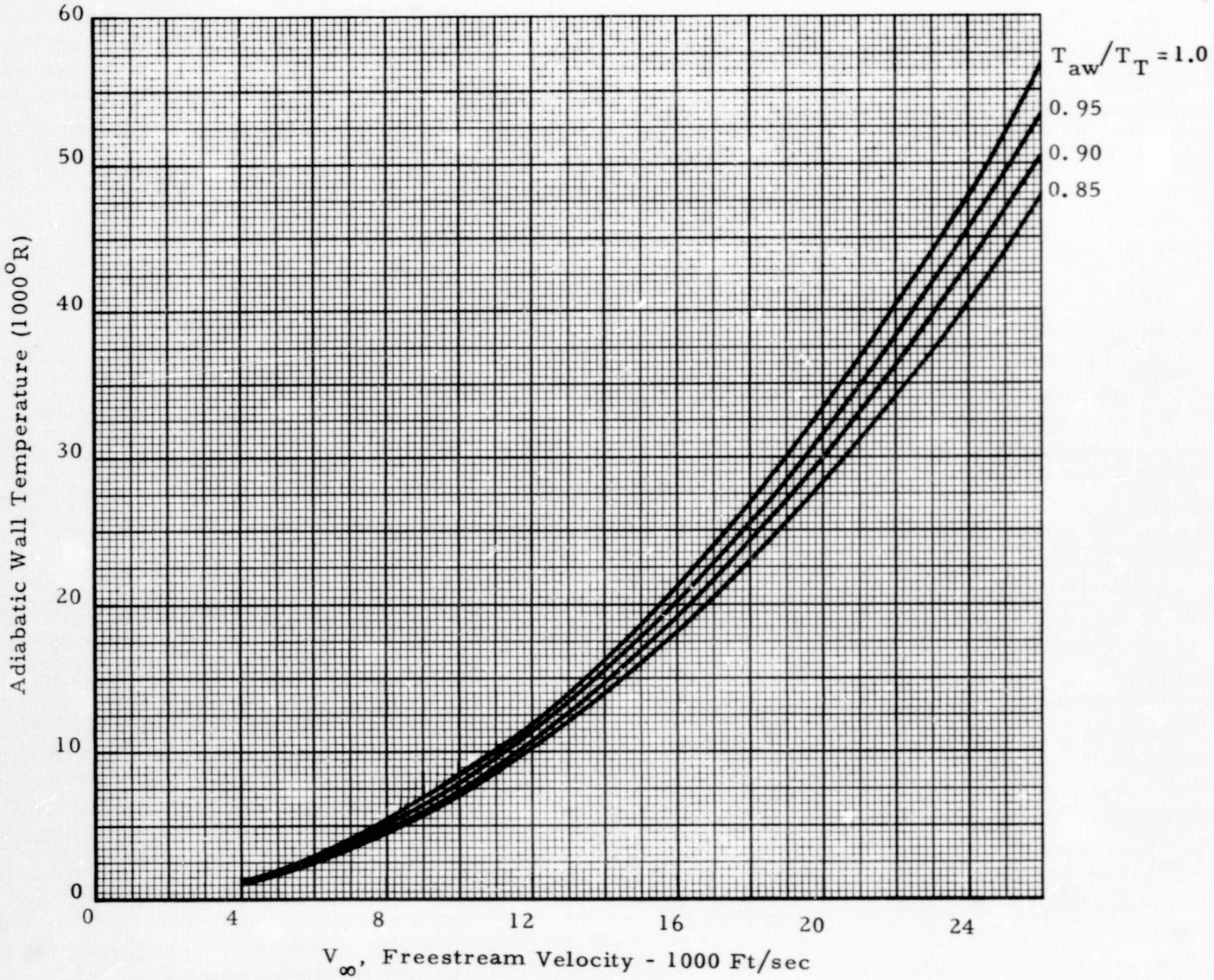

Fig. 4-33 - Adiabatic Wall Temperature vs Freestream Velocity

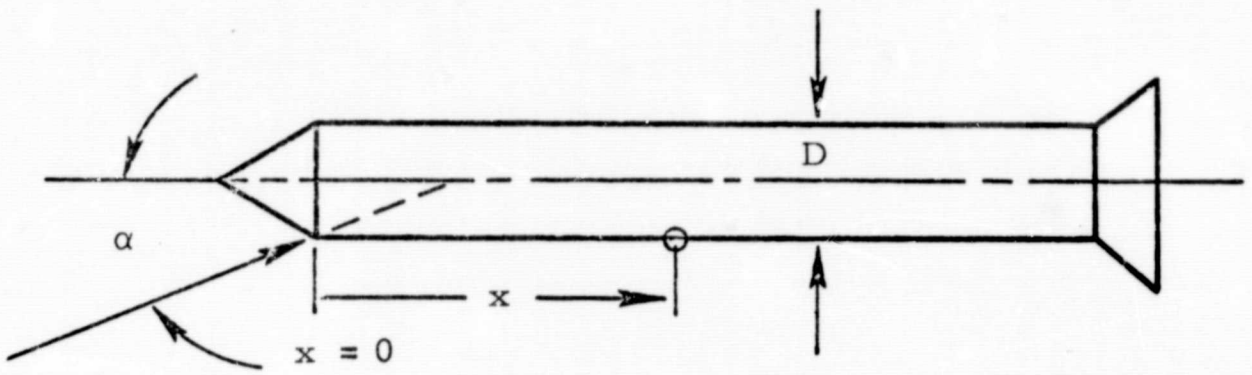

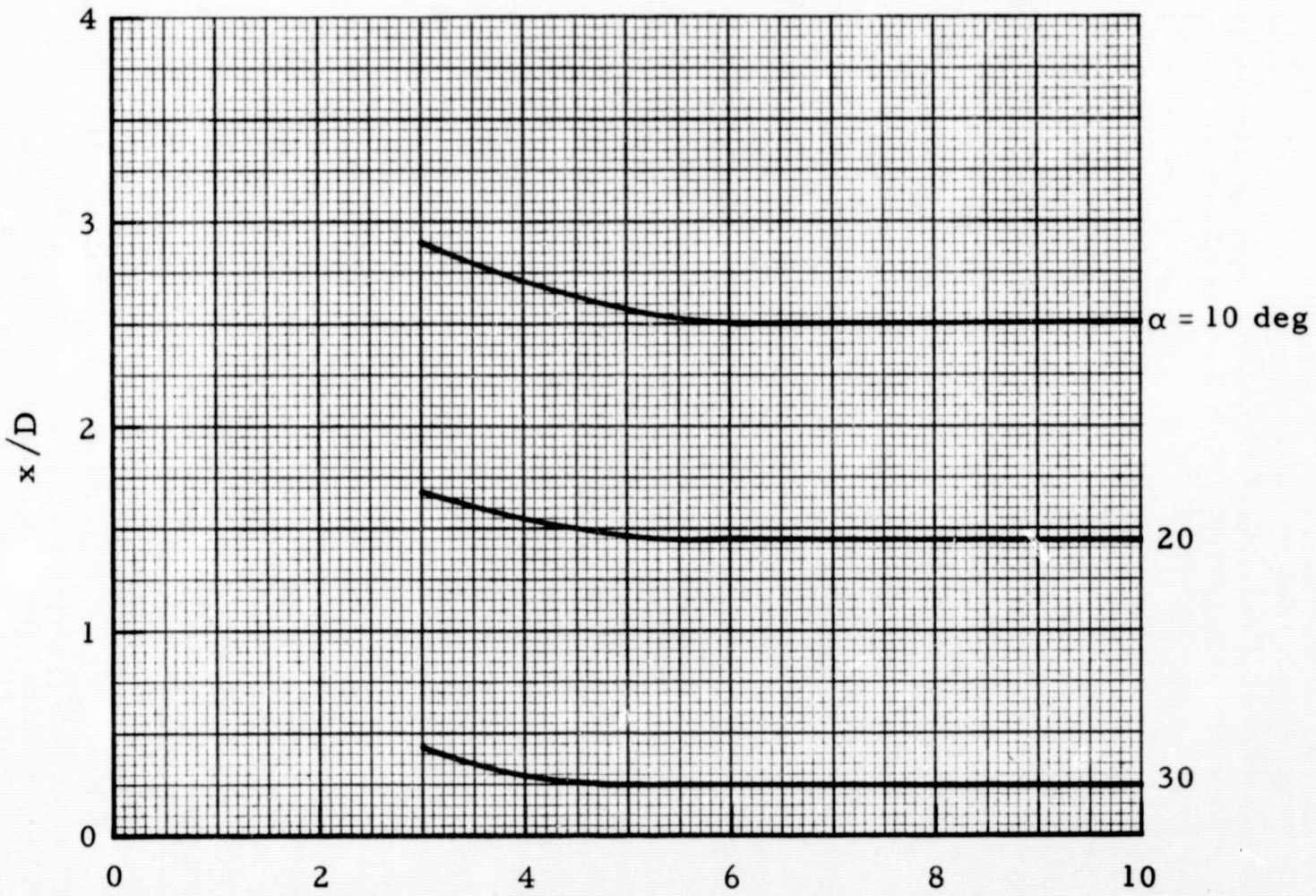

Fig. 4-34 - Approximate Region of Applicability (Upstream of a Compression Corner) of Isolated Cylinder Nusselt Number Curves

Section 5
CONCLUSIONS

The cylinder test data correlated well when plotted in the form of free-stream Nusselt number versus freestream Reynolds number. The effects of Mach number were considerable and were predicted well by the theory. Laminar convective heating rates to cylinders at zero degree angle of attack were well-predicted by flat plate theory. For cylinders at angle of attack, yawed infinite cylinder theory applied. The laminar stagnation line heating rates were well predicted by the method of Kemp, Rose and Detra (Ref. 15). The turbulent stagnation line heating rates were well predicted by the method of Beckwith and Gallagher, Ref. 8.

The cone test data correlated best when plotted in the form of local Nusselt number versus local Reynolds number. The effects of Mach number were more pronounced for turbulent flow than for laminar flow. The heating rate results were well predicted by Streamline Divergence theory.

Much more useful test data are needed especially for turbulent flow over yawed cylinders and cones. Also, more test data are needed on circumferential heating rate distributions for a wide range of Mach numbers and cone half-angles and for turbulent flow over cylinders. The use of a consistent method for obtaining local flow properties on cones helped considerably in obtaining good data correlations. Extrapolation of ground test data to flight conditions is a crucial step. Generally ground test data are obtained at low stagnation temperatures, such that real gas effects are not important. It is felt that the use of theories for extrapolation of data to flight conditions is meaningful.

REFERENCES

1. Laden, G. M., J. R. Dennis and J. C. Liskovec, "The Effects of Angle of Attack on the Ascent Phase Aerodynamic Heating of Agena Vehicles," LMSC-A838943, Lockheed Missiles & Space Company, Sunnyvale, Calif., 9 February 1967.

2. Dearing, David J., "Laminar Heat Transfer Distributions for a Blunted-Cone, Cone-Frustum Reentry Configuration at Mach 10," NASA TN D-5146, April 1969.

3. Bushnell, D. M., R. A. Jones and J. K. Huffman, "Heat Transfer and Pressure Distributions on Spherically Blunted 25° Half-Angle Cone at Mach 8 and Angles of Attack up to 90°," NASA TN D-4792, October, 1968.

4. Goodwin, G., M. O. Creager and E. L. Winkler, "Investigation of Local Heat-Transfer and Pressure Drag Characteristics of a Yawed Circular Cylinder at Supersonic Speeds," NACA RM A 55H31, 24 January 1956.

5. English, R. D., "Effects of Yaw on the Heat Transfer to a Blunt Cone-Cylinder Configuration at a Mach Number of 1.98," NASA Memo 10-8-58L, November 1958.

6. Burbank, P. B., and B. L. Hodge, "Distribution of Heat Transfer on a 10° Cone at Angles of Attack from 0° to 15° for Mach Numbers of 2.49 to 4.65 and a Solution to the Heat-Transfer Equation That Permits Complete Machine Calculations," NASA Memo 6-4-59L, June 1959.

7. Chauvin, L. T., and K. C. Speegle, "Boundary Layer Transition and Heat Transfer Measurements from Flight Tests of Blunt and Sharp 50° Cones at Mach Numbers from 1.7 to 4.7, NACA Memo RML57D04, 18 April 1957.

8. Beckwith, I. E., and J. J. Gallagher, "Local Heat Transfer and Recovery Temperatures on a Yawed Cylinder at a Mach Number of 4.15 and High Reynolds Numbers," NASA TR-R-104, 1961.

9. Julius, J. D., "Measurements of Pressure and Local Heat Transfer on a 20° Cone at Angle of Attack Up to 20° for a Mach Number of 4.95," NASA TN D-179, December 1959.

10. Rumsey, C. B., and D. B. Lee, "Measurements of Aerodynamic Heat Transfer on a 15° Cone-Cylinder-Flare Configuration in Free Flight at Mach Numbers up to 4.7," NASA TN D-824, May 1961.

11. Bergquam, J. E., "Aerodynamic Heating Investigations of Cylindrical Configurations in AEDC Tunnel C (R-128), LMSC-805538, Lockheed Missiles & Space Company, Sunnyvale, Calif., November 1965.

12. Vaglio-Laurin, Roberto, "Laminar Heat Transfer on Blunt-Nosed Bodies in Three-Dimensional Hypersonic Flow," WADC TN 58-147, May 1958.

13. Vaglio-Laurin, Roberto, "Turbulent Heat Transfer on Blunt-Nosed Bodies in Two-Dimensional and General Three-Dimensional Hypersonic Flow," J. Aerospace Sci., January 1960, pp. 27-36.

14. Savage, R. T. and C. L. Jaeck, "Investigation of Turbulent Heat Transfer at Hypersonic Speeds," AFFDL-TR-67-144, December 1967.

15. Kemp, N. H., P. H. Rose, R. W. Detra, "Laminar Heat Transfer Around Blunt Bodies in Dissociated Air," J. Aerospace Sci., July 1959.

16. Beckwith, Ivan E., "Similar Solutions for the Compressible Boundary Layer on a Yawed Cylinder with Transpiration Cooling," NASA TR R-42 (1959).

17. Hansen, C. F., "Approximation for the Thermodynamic and Transport Properties of High Temperature Air," NASA TR-R-50 (1959).

18. "Normal and Oblique Shock Characteristics at Hypersonic Speeds," McDonnell Douglas Aircraft Co., ARDC TR-57-184, 31 December 1957.

19. Prozan, R. J., and E. M. Authement, "An Approximate Conical Flow Solution by the Method of Characteristics," (paper submitted to AIAA J., 1966).

20. Ames Research Staff, "Equations, Tables and Charts for Compressible Flow," NACA RE 1135, (1953), pp. 52-53.

21. Popinski, Z., and C. F. Ehrlich, "Development of Design Methods for Predicting Hypersonic Aerodynamic Control Characteristics," AFFDL TR-66-85, September 1966.